

23109095



LIBRARY
Michigan State
University

This is to certify that the

thesis entitled
AN EXPERIMENTAL INVESTIGATION OF SINGLE-MODE MICROWAVE
HEATING OF SOLID NONREACTIVE MATERIALS IN A CYLINDRICAL
RESONANT CAVITY

presented by

Edward Benjamin Manring

has been accepted towards fulfillment of the requirements for

M.S. degree in Electrical Engineering

Major professor

Date November 11, 1988

O-7639

MSU is an Affirmative Action/Equal Opportunity Institution

PLACE IN RETURN BOX to remove this checkout from your record. TO AVOID FINES return on or before date due.

DATE DUE	DATE DUE	DATE DUE
JUN 1 1 1997		

MSU Is An Affirmative Action/Equal Opportunity Institution

AN EXPERIMENTAL INVESTIGATION OF THE MICROWAVE HEATING OF SOLID NON-REACTIVE MATERIALS IN A CIRCULAR CYLINDRICAL RESONANT CAVITY

by

Edward Benjamin Manring

A THESIS

Submitted to
Michigan State University
in partial fulfillment of the requirements
for the degree of

MASTER OF SCIENCE

Department of Electrical Engineering and System Science

ABSTRACT

AN EXPERIMENTAL INVESTIGATION OF SINGLE-MODE MICROWAVE HEATING OF SOLID NONREACTIVE MATERIALS IN A CIRCULAR CYLINDRICAL RESONANT CAVITY

by

Edward Benjamin Manring

This thesis presents an experimental investigation of single-mode resonant cavity microwave heating of solid nonreactive materials. It includes a brief review of the literature of the past few years on single-mode heating, detailed descriptions of both seven inch diameter and six inch diameter variable length variable coupling 2.45 GHz resonant cavities, heating experiments on rod shaped materials, and the design considerations involved in the construction of a larger 915 MHz cavity. Heating experiments were performed with materials of various dielectic constants and loss factors, including teflon, nylon, silicone rubber, wet wood, and water. On-line measurements of the dielectric constants and coupling efficiencies were taken during heating using perturbation methods, demonstrating coupling efficiencies of 50%-95%. The drying efficiency for wet wood was also measured at values of 55%-66%, corresponding to Specific Consumptions of 1.33 kWh/kg - 1.1 kWh/kg. In order to heat larger materials an aluminum 18 inch diameter 915 MHz cavity was designed and built. Included in the design proceedure are mode charts for 17, 18, and 19 inch cavity diameters, cavity construction material considerations, and special cavity features, such as a removeable bottom, input power coupling ports, and observation windows in the cavity wall. A photograph of the finished 18 inch cavity is also included.

To my parents

O Lord my God, You are
very great;
You are clothed with honor
and majesty,
Who cover Yourself with
light as with a garment,
Who stretch out the heavens
like a curtain ...
May the glory of the Lord
endure forever.

Psalm 104

ACKNOWLEDGMENTS

I offer my sincerest thanks to Dr. Jes Asmussen for his guidance, encouragement, and hard work during the course of these experiments and the writing of this thesis. Thanks is also due to Mr. Haw-Hwa Lin without whose help many of these experiments could not have been performed. I would also like to express my gratitude to Mr. Ron Fritz whose helpful suggestions, technical assistance, and Christian friendship eased my burden at every step. Finally I would like to thank my wife for her patience, perseverance, and emotional support during the course of this work.

This research was supported in part by grants from Darpa (U.S. Army Grant DAAG46-85-K-0006) and the Navy University Research Initiative administered by the University of Illinois.

TABLE OF CONTENTS

LIST OF	TAE	BLESv	ii
LIST OF	FIG	gures vi	ii
CHAPTER	1	INTRODUCTION	1
CHAPTER	2	BACKGROUND	
		2.1 Introduction	5
		2.2 Perturbation Applications	6
			14
		2.4 Electric Field and Material Load	
			17
			20
CHAPTER	3	EXPERIMENTAL SYSTEMS AND RESULTS	
		3.1 Introduction	22
			23
		3.3 Experimental Microwave System For	
			27
			27
			29
			29
			35
			36
			44
			70
		3.6 System Configuration For The Six	. •
			73
			73
			74
			75
CHAPTER	4	A CAVITY DESIGN EXAMPLE	
		4.1 Overview	84
			85
			91
			94
			94
			94
			98
			98

CHAPTER 5	CONCLUSIONS AND RECOMMENDATIONS	
	5.1 <u>Conclusions</u>	
APPENDIX A	CALCULATING THE DIELECTRIC CONSTANT OF A ROD COAXIALLY SUSPENDED IN A CIRCULAR CYLINDRICAL RESONANT CAVITY EXCITED IN	
	THE TM _{Opq} MODE	103
REFERENCES		108

LIST OF TABLES

Table	3.1	Resonant Lengths and Quality Factors For	
		The Seven Inch Cavity With Collars At 2.45 GHz	38
Table	3.2	Frequency Shift For Coaxially Loaded Nylon 66	48
Table	3.3	Frequency Shift For Coaxially Loaded Teflon	48
Table	3.4	Perturbation Calculation Of Dielectric Constant	
		For Coaxially Loaded Rods Of Length Equal To Ls	50
Table	3.5	Empty Cavity Measurements of Ls and Q For Several	
		Modes In The Six Inch Cavity	77
Table	3.6	Perturbation Calculation Of Permittivities Of	
		Nylon And Teflon For TM011 And TM012 Modes	81
Table	4.1	Summary Of Cavity Material Properties	97
Table	A.1	Values Of Bessel Functions Used In The Perturbation	
		Equations For Experiments Presented In This Thesis	109

LIST OF FIGURES

Figure	3.1	Cross-Sectional View Of The Seven Inch Applicator	26
Figure	3.2	Photograph Of The Seven Inch Applicator	27
Figure	3.3	System Configuration	28
Figure	3.4	Oscilloscope Display Of The Absorption	
		Spectrum Near Resonance	32
Figure	3.5	Micro-Coaxial Field Probe, Field Probe Block,	
		And Diagnostic Ports	34
Figure	3.6	Using The Oscilloscope To Measure Q	41
Figure	3.7	Collar Placement In Shorting Plate Holes	42
Figure	3.8	Micro-Coaxial Field Probe Measurements In The	
_		Empty Cavity Excited In The TM012 Mode	44
Figure	3.9	Coaxially Loaded Cavity	46
Figure	3.10	Frequency Shift Versus Sample Height	52
Figure	3.11	Cavity Q Versus Sample Height	52
Figure	3.12	Temperature Probe Placement In Small Cylinders	55
Figure	3.13	Real Dielectric Constant Of Nylon Versus Temperature	57
Figure	3.14	Imaginary Dielectric Constant Of Nylon Versus	
		Temperature	58
Figure	3.15	Real Dielectric Constant Of Nylon Measured	
		With The Coupling Probe Stationary	59
Figure	3.16	Coupling Efficiency Of Nylon Versus Temperature	62
Figure	3.17	Real Dielectric Constant Of Wet Wood Versus Time	63
Figure	3.18	Imaginary Dielectric Constant Of Wet Wood Versus Time	64
Figure	3.19	Coupling Efficiency Of Wet Wood Versus Time	65
Figure	3.20	Real Dielectric Constant Of Water Calculated	
		By Perturbation Methods Versus Temperature	68
Figure	3.21	Imaginary Dielectric Constant Of Water Calculated	
		By Perturbation Methods Versus Temperature	69
Figure	3.22	Real Dielectric Constant Of Silicone Rubber	
		Versus Temperature	71
Figure	3.23	Imaginary Dielectric Constant Of Silicone Rubber	
		Versus Temperature	72
Figure		Cutaway Drawing Of The Six Inch Applicator	74
Figure	3.25	Positioning Of The Temperature Probe In The	
		0.5 Inch Diameter Cavity Length Nylon Rods	. 78
Figure	3.26	Axial Field Patterns Of Nylon Loaded Cavity Excited	
		In The TM012 Mode For Various Input Powers	80
Figure	3.27	Nylon Temperature Versus Time For Input	
		Powers Of 600 mW And 1.00 W	82
Figure	3.28	One Inch Diameter Nylon Rod With Holes For	
		Temperature Cross Section Measurement	83
Figure		Temperature Profile Of One Inch Nylon Rod	84
Figure	3.30	Temperature Measurement Of The Input Power Coupling	
		Probe For 1 Inch Diameter Nylon Load At 5.0 W	86

Figure 4.1	Mode Chart For 17" Diameter Cavity	91
Figure 4.2	Mode Chart For 18" Diameter Cavity	92
Figure 4.3	Mode Chart For 19" Diameter Cavity	93
Figure 4.4	Removeable Bottom Shorting Plate	98
Figure 4.5	Input Port And Coupling Probe	98
Figure 4.6	Photograph Of The 915 MHz Cavity	102

CHAPTER I

INTRODUCTION

This thesis presents an experimental investigation of single-mode resonant cavity microwave heating of solid nonreactive materials. The heating experiments presented were performed using a variable length variable coupling circular cylindrical resonant cavity applicator.

extensively to heating solid materials. Due to rigorous tuning requirements for single-mode applicators and a desire for heating uniformity, most microwave heating applicators in the past have been multi-mode applicators. Since 1971 efforts at Michigan State University have been directed toward the development of single-mode resonant cavity applicators. These 2.45 GHz applicators were originally developed for electrodeless microwave plasma applications. 1-3 Applications of this microwave plasma technology have included electrothermal thrusters for use as rocket engines 4 and ion and plasma sources for use in thin film deposition and processing applications in solid state technology. Solid state technology applications have included ion sources for broad ion beam processing, plasma etching, and plasma assisted oxide growth. 5-8

More recently the single-mode applicator has been used to heat and process solid materials. 9,10 Some of this work is reported in this thesis. The portion reported here includes the results of heating experiments performed with nonreactive rod shaped solid materials excited in single resonant modes. 9 These simple experiments with nonreactive solid materials have been performed in order to gain insight into the

electromagnetic and thermodynamic operation of the loaded single-mode resonant cavity. The experimental principles derived from the nonreactive load experiments have been applied to the curing of reactive epoxy resins with similar results. 10

These experiments have shown that on-line diagnostic measurement of complex permittivity of load materials of simple shape and low dielectric constant may be accomplished by the use of perturbation theory. They have demonstrated repeatablility and controlability for materials of large dielectric constant, such as water. High microwave coupling efficiencies have been achieved even for fairly low loss materials such as nylon. Special experimental techniques have been developed to take on-line measurements of cavity Q, microwave coupling efficiency, and the resonant frequency of material loaded cavities during electromagnetic processing.

1.1 Overview

Chapter 2 of this thesis presents the background for the experiments reported here. In this chapter a brief review of the work done in the past few years on the microwave heating of solid materials will be given. In addition, a few important older papers will be examined.

Chapter 3 contains the experimental system description and results.

Both the seven inch and six inch diameter applicators are described in detail along with the microwave source, the transmission system, and the measurement instruments. Empty cavity experiments were performed to determine empty cavity eigenlengths, quality factors, and coupling probe penetration depth for each mode. These measured parameters calibrated the empty cavity. Two experiments were performed in the loaded seven inch cavity at low power: Dielectric constants of load materials were measured

using perturbation methods, and resonant frequency shift and cavity Q were measured as a function of postition of the load along the cavity axis.

Higher power experiments were performed in the seven inch cavity at input powers of 1 to 8 W. On-line diagnosis of the load permittivity was performed as a function of the load temperature and time. Materials processed in these experiments included nylon 66, water-soaked wood, water, and silicone rubber. In the case of water and water-soaked wood, amounts of water vaporized were measured and heating efficiencies were thereby calculated. By measuring the cavity quality factor, microwave coupling efficiencies were also monitored.

In the six inch cavity low power experiments similar to the ones in the seven inch cavity were performed. Also included in the low power experiments in the coaxially loaded six inch cavity were axial measurements of the square of the radial component of electric field at the wall. Measurements were taken for various input powers when the load had reached a steady state temperature. These experiments demonstrated the axial sine dependence of the TM₀₁₂ mode radial electric field at the cavity wall. This showed that even under heavily loaded conditions the mode field patterns are still clearly defined.

Higher power experiments in the six inch cavity were performed to measure the material load temperature at different points along the radius of the rod shaped load. As expected, higher temperatures were measured at the center than at the surface of the rod where energy losses due to radiation were significant. Temperature measurements of the input coupling probe were also taken to determine if a significant amount of the input power was being absorbed by the coupling probe structure. The temperature of the tip of the coupling probe rose only about 2 °C during

the course of an experiment in the cavity loaded with a 1 inch diameter nylon rod with 5 W of input power. The temperature of the nylon rose almost 30 °C. Rigorous calorimetry analysis was not performed, but the low temperature rise in the coupling probe indicated that the power dissipated in the coupling probe was probably small compared to the power dissipated in the material load.

Chapter 4 is an example of the considerations involved in the design of a circular cylindrical resonant cavity. The design process for a cavity with an intended operating frequency of 915 MHz is presented. The cavity dimensions are discussed, various possibilities for construction materials are considered, and special features of the cavity are examined. The electromagnetic analysis of the distribution of the modes determined that an inside diameter of approximately eighteen inches was best for our requirements. Due to constraints on conductivity, weight, cost, and availability, aluminum was chosen as the construction material. Special features such as a removeable bottom, dual input power coupling ports, and a viewing window are included in the design. A photograph of the finished 18 inch cavity is included in this chapter.

Chapter 5 is the conclusion of the thesis. A summary of the results and recommendations for further work are included. The thesis concludes with an appendix that describes the derivation of the perturbation formulas used for measuring permittivities of rods in cavities excited in TMOpq modes.

BACKGROUND

2.1 Introduction

The heating of solid materials by high frequency electric fields has been observed since the introduction of the radio some ninety years ago. Most early radio engineers regarded rf heating of solids not as a desireable process, but as a nuisance due to the heating of parts of their radio equipment. It was not until the 1940's that the use of rf power was applied to the heating of materials for industrial purposes. For conductors these applications included such things as the annealing of brass and bronze, case hardening of steel, and soldering. For poorer conductors such applications as wood gluing, dehydration of biological materials and fabrics, and pasteurization of milk were developed. 12

These early uses of high frequency electric fields for materials heating did not utilize a resonant structure for the focusing of the fields onto the material. In fact, the low frequencies used, typically less than 100 MHz, would not permit the use of cavity resonant structures of a reasonable size. These early applications were more akin to dc heating, albeit at high frequency, than an application of modern microwave heating technology.

Today, resonant microwave heating technology has not only become a highly productive industrial and scientific field, but the presence of commercial microwave ovens in homes around the world testifies of its practical utility for domestic applications as well. Most industrial and all domestic applications of resonant microwave heating take advantage of

the multimode microwave resonant structure. The nonrigorous tuning and efficiency requirements for the multimode applicator, along with possible advantages in heating uniformity make it suitable for heating materials which vary in size, shape, and dielectric properties. However, multimode heating has limited usefulness in applications which require the understanding of electromagnetic/material interactions, precision control, or very high heating efficiencies.

In all three of these areas single-mode microwave applicators have advantages over multimode applicators. Heating applications with these requirements have been investigated with single-mode cavities during the last 25 years. This chapter is a brief survey of important literature on the subject concentrating for the most part on the most recent publications.

The literature has been divided into four catagories, with some overlap between articles: applications of cavity perturbation techniques to the understanding of electromagnetic/material interactions, exact solutions for some simple cases, electric field and material load temperature measurements, and solutions to the problem of thermal runaway.

2.2 Perturbation Applications

It is somewhat misleading to entitle one section "Perturbation Applications" since nearly all single-mode microwave cavity applications make use of perturbation techniques to understand electromagnetic/material interactions. Almost all of the papers cited in this chapter include some application of perturbation theory; even those concerned with exact analysis have made use of it for the sake of comparison. Appendix A of this thesis may be consulted as an example of the use of perturbation theory for dielectric constant measurement using a resonant cavity.

A formula similar to equations A.14 and A.15 of appendix A was derived by E. F. Labuda and R. C. LeCraw¹³ for the TM₀₁₂ circular cylindrical resonant cavity. Citing problems with material placement in the cavity for materials which either filled the entire lower part of a cavity, a disk load, or which extended the entire cavity length, a rod load, they used a shorter rod shaped material suspended by nylon thread to make dielectric constant measurements. The effects at the ends of the rod were neglected since the electric field was low in those regions of the cavity.

The excitation frequency was 9.400 GHz with cavity diameter 1.278 inches and cavity length 1.904 inches. Coupling to the cavity was not discussed. The sample sizes were 0.05 inches in diameter and 0.95 inches long. Holes in the ends of the cavity permitted the insertion of the rods. The accuracy of ϵ' measurement was reported at 3% while r" less that 0.001 could not be measured due to uncertainties. Figures were not given for larger loss factors. Labuda and LeCraw claimed that better accuracy in ϵ " measurement could be obtained with slightly larger sample sizes.

Using the results of Labuda and LeCraw, N. L. Conger and S. E. Tung ¹⁴ made perturbation measurements of the dielectric constants of powder materials at 9.400 GHz using a cavity of the same dimensions as Labuda and LeCraw. These powder materials were held in quartz tubes. The added perturbation effects of the tubes were roughly considered by measuring the dielectric constants of solids both by suspending the solids themselves and by suspending them in a quartz tube. For a tube of 3 mm i.d. and 0.5 mm wall thickness with materials of $2 < \epsilon_r' < 8$ and $0.2 < \epsilon_r'' < 1.0$ the effects of the presence of the tube on the real dielectric constant were no more than 5% and no more that 2% for the imaginary part.

Conger and Tung 14 also measured the real parts of the dielectric constants of powders of NaCl, KCl, Corning 7740 glass, fused quartz, and Corning 7900 Vycor and compared the results with the theoretical formulas of Lorentz, Bruggeman, and Böttcher. Agreement within 4% using the Böttcher formula and within 6% using the Bruggeman formula was found. Perhaps one of the more generally useful sections of their work is the description of the circuit they used to mark points on an oscilloscope display in order to measure frequency. A circuit to provide frequency markers can also be found in the Handbook of Microwave Measurements, M. Sucher, J. Fox ed. 15.

An application not requiring marker circuitry is found in a paper by Maria A. Rzepecka. ¹⁶ She measured the dielectric constants of chemical compounds of well known dielectric constant such as carbon tetrachloride, amyl alcohol, nitrobenzene, and water as well as the the dielectric constants of several food products using a rectangular cavity in the TE₀₁₃ and TE₀₁₉ modes at 2.45 GHz. Instead of using frequency blanking markers to measure the width of the resonance curve for cavity quality factor calculation, she used a frequency counter and demonstrated that it was at least as accurate as the first method. In 1973, the year her paper was written, frequency marker circuitry was cumbersome. Now, many sweep oscillators have the circuitry built in and the problem is nonexistant. Her paper includes a useful examination of errors associated with the measured parameters used in the perturbation calculation.

For permittivity vs. temperature measurements Rzepecka and others used conventional means to heat the sample under consideration. This was done by Rzepecka using blown hot air. D. Couderc, M. Giroux and R. G. Bosisio 17 used microwave energy to heat samples to high temperatures

(1500 °C) in order to measure the dielectric constant in that temperature region. In order to heat and diagnose simultaneously two resonant modes were used. One mode was used to heat the sample and one was used to diagnose. In their circular cylindrical cavity, the heating mode was the TM_{010} mode at 2.45 GHz while either the TE_{111} mode at 3.1 GHz for spherical samples or the TM_{012} mode at 3.7 GHz for cylindrical samples were used for diagnostic purposes. Two different cavities were used depending on which diagnostic mode was desired. The TE_{111} cavity was 9.177 cm in diameter and 5.936 cm in length. The TM_{012} cavity was 9.144 cm in diameter and 10.668 cm in length.

The heating power was coupled into the cavity via an iris between the cavity and a section of WR 284 rectangular waveguide. The magnetron frequency was varied as much as 1% by a feedback mechanism in order to maintain a high degree of coupling as sample permittivity changed with temperature. Diagnostic modes were coupled into the cavity coaxially while heating frequency signals were discriminated out of the diagnostic system by a high pass filter. The sample was held in place with thin fused silica cylinders and the temperature was monitored using an infrared radiation thermometry system aimed through a small hole in the wall of the cavity.

Perturbation equations similar to A.14 and A.15 were derived for the ${\rm TM}_{012}$ diagnostic mode for cylindrical samples and slightly more complicated formulas were derived for the ${\rm TE}_{111}$ diagnostic mode for the spherical samples. Using these formulas, the dielectric constants of Myclalex, Steatite 302, and Corning 7740 were measured from room temperature to 600 C. At higher temperatures a correction term was introduced into the the perturbation formulas to allow for the increased conductivity of the dielectric test samples.

For permittivity measurements of materials with large dielectric constants, such as foods which contain a large amount of water, Akyel, Bosisio, Chahine, and Bose 18 normalized the standard TM_{010} cylindrical rod perturbation formula for ϵ_r and ϵ_r to the complex permittivity of water. This allowed them to measure complex dielectric constants of freshly mashed banana and freshly mashed potato using perturbation methods.

These measurements, as well as ordinary measurements of the dielectric constant of sunflower oil, which has a relatively low dielectric constant, were made for a number of different temperatures. The temperature was measured in what appears to be a rather inexpensive way using a thermocouple which did not penetrate into the cavity region. The sample was contained in a quartz tube around which was another quartz tube of larger diameter. During heating, nitrogen was passed through the larger tube around the contained sample. The temperature of the nitrogen was measured by the thermocouple located just outside the resonant region. The authors claim that the temperature of the nitrogen did not vary from the temperature of the sample by more than 1 °C at equilibrium.

The measured dielectric constants of sunflower oil, mashed banana, and mashed potato each demonstrated hysteresis effects with temperature. For a given temperature, the real part of the dielectric constant was higher as the temperature was rising and lower as the temperature was falling. The imaginary part of the dielectric constant for a given temperature was lower as temperature increased and higher as temperature decreased. The dielectric constants of some organic compounds were also measured in the TM₀₁₀ cavity and compared to measurements made using Time Domain Spectroscopy (TDS) methods resulting in good agreement.

TDS is a method in which a wave is reflected off of the surface of a dielectric. The reflection coefficient provides information on the dielectric constant. Generally this is done by mounting the sample in a coaxial line. A pulsed signal is applied to the line and propagates in a TEM mode toward the dielectric sample. At the air/dielectric interface, part of the pulse is reflected while the remainder is transmitted through the dielectric until it reaches the rear interface where it is reflected again. The first reflection provides sufficient information to measure the dielectric constant, but if the sample is not long enough, multiple reflections will be measured in the time window during which transient analysis is carried out. Akyel, Bosisio, Chahine, and Bose 18 used short samples and accounted for multiple reflections in their analysis.

In order to determine errors associated with perturbation measurements a detailed error analysis was performed by Shuh-han Chao for dielectric spheres in rectangular and cylidrical cavities. ¹⁹ He includes a review of the use of perturbation theory since the 1940's and derives the perturbation equations for a resonant cavity. The quasi-static approximation to the actual field inside a spherical sample is quoted from Brodwin and Parsons. ²⁰

Chao's error analysis has to do with errors in resonant frequency and cavity quality factor measurement. Errors having to do with the quasi-static approximation to the actual fields inside the sample are not considered. In his analysis he assumes the uniformity of the fields inside the sample, which is valid for small sample size and low dielectric constant. That assumption leads to the conclusion that errors are minimized for the largest possible sample size. He notes that this

conclusion must be balanced by the consideration that errors associated with the quasi-static approximation increase with sample size.

Experimental demonstration of the error analysis was performed by measuring the permittivity of small spheres of silicon in a rectangular cavity in the TE_{103} mode. The dimensions of the cavity were 1.02 cm x 2.29 cm x 6.46 cm with an excitation frequency near 9.5 GHz. The power was coupled in through an iris. Spheres of silicon of radii 0.81 mm, 1 mm, and 1.5 mm were held in a cylindrical styrofoam sample holder while the resonant frequency and quality factor were measured using swept frequency techniques. Using perturbation theory and the results of the error analysis, the complex permittivity of the silicon and associated errors were calculated. For the largest sample, with the smallest calculated error, the real part of ϵ_{r} was found to be 11.21 within 7% while the imaginary part was found to be 0.020 within 24%.

In a manner similar to Akyel, Bosisio, Chahine, and Bose, ¹⁸ Jain and Voss measured the dielectric properties of chicken eggs using a calibrating fluid because of the high water content of the eggs. ²¹ Their method and resonant cavity were based on work done by Risman and Bengtsson²² and Risman and Ohlsson. ²³ The cavity they used was not variable in length or coupling, hence transmission measurements provided the equivalent of cavity quality factor measurements for the determining of the dielectric loss factor. The excitation mode TM₀₁₂ at 2.45 GHz, hence the cavity was similar in size to the cavities used in the experiments reported in chapter 3 of this thesis. To measure the dielectric properties of the eggs over a wide temperature range their cavity was placed in a conventional oven with precision temperature control and allowed to come to equilibrium. It should be noted that this

also avoided the need for specialized temperature measurement instrumentation to be inserted into the cavity.

Some of the work presented in this thesis was previously reported by Asmussen, Lin, Manring, and Fritz. The advantages and disadvantages of the single-mode versus the multimode method was discussed. Then the single-mode seven inch circular cylindrical resonant cavity with variable short length and coupling probe was described in detail. A similar description of the cavity is found in section 3.2 of this thesis. The coupling, matching, and control of single-mode applicators were also discussed in reference to an equivalent circuit of the cavity and power delivery circuit.

The single-frequency cavity Q measurement technique was described along with its use for determining coupling efficiencies. Using perturbation methods, the Q measurements along with resonant frequency measurements made possible the on-line measurement of complex permittivities and coupling efficiencies for materials as they were heated by the electric field. The temperature was measured using a fiber optic probe temperature measurement system which is also described in section 3.3 of this thesis and by Wickersheim. He results of experiments performed in the TM₀₁₂ mode at 2.45 GHz for nylon, wet wood, and water were presented. Finally, it was shown that silicon wafers may be heated in the TE₁₁₁ mode to temperatures of 260 °C in 4 minutes using only 37 W of input power. For higher powers it was noted that temperatures of 900 °C could be achieved.

This work was extended by Jow, Hawley, Finzel, Asmussen, Lin, and Manring to the heating and on-line diagnosis of chemically reactive (epoxy/amine) material loads. 10 The material studied was DER332 resin

activated by the curing agent DDS. In epoxy/resin reactions curing temperature is an essential parameter to the understanding of the reaction. The temperature was monitored in these microwave assisted reactions using the fiberoptic thermometer mentioned above and described by Wickersheim. Using perturbation techniques the complex permittivity of the DER332/DDS mixture was monitored during the cure.

Recently resonant cavities have been used to measure microwave region complex surface impedances of high $T_{\rm c}$ superconducting materials. Sridhar and Kennedy measured the complex surface impedances small disks of $Y_1 Ba_2 Cu_3^0 y \text{ and } La_{1.85} Sr_{0.15} Cu_4 \text{ in a very high Q } (10^4 - 10^{12}) \text{ resonant}$ cavity whose walls were made of Pb and cooled to 4.2 K. Cavity Q was measured by pulsing the cavity and detecting a decay time on a fast scope. Q was then give by Q-27f, where 7 is the decay time.

Coupling was achieved through two ports in the top of the cavity. Inside the ports two 50Ω coaxial lines terminated in loops which did not penetrate into the cavity. The magnetic field lines through the loops "looked into" the cavity. The coaxial lines could be adjusted in order to achieve a match. The excitation mode was TE_{011} to eliminate electric fields at the surface of the cavity. It was decoupled from the TM_{111} mode due to the presence of central pumping and sample insertion holes. It was also interesting to note that TM_{111} itself was decoupled into two TM_{111} modes.

The surface impedance was measured versus temperature from 4.2 to 200 K using perturbation theory. Since the electric fields inside the cavity were very low, the sample was heated externally through the saphire rod on which it was mounted while the cavity walls were maintained at 4.2 K.

2.3 Exact Solutions for Simple Cases

The electromagnetic problem for a rod shaped load in a circular cylindrical cavity resonator has been solved for a limited number of cases by several authors. 26-30 None of these "exact" solutions has considered how coupling has been achieved to provide the fields inside the cavity. Furthermore, all of the solutions which are for loads of length less than the cavity length make use of the mode matching technique first proposed by Hahn 31 which requires an infinite number of terms to be considered in order to be truly exact. Each of the papers 26-28 truncates the infinite series when convergence is achieved, or at a point where numerical calculation in a reasonable amount of time is possible. More importantly, none of these mode matching solutions are for materials with a nonzero dielectric loss factor.

Bolle 26 considered a circular cylindrical cavity loaded with a lossless dielectric situated in the center. The modes he considered were ${
m TM}_{010}$ and a ${
m TM}_{012}$. Given the dielectric constant, the cavity size, and the material size, Bolle was able to calculate the resonant frequency for the ${
m TM}_{010}$ case with a $10{
m x}10$ matrix for the material lengths $16{
m x}$ of the cavity length. For the ${
m TM}_{012}$ case a $10{
m x}10$ matrix approximation was capable of predicticting the resonant frequency for pieces of length only $1{
m x}$ of the cavity length. The dielectric constants of the materials were presumably low.

Zaki and Atia²⁷ in the interest of developing high quality dual mode bandpass filters also made exact calculations of resonant frequencies for a symmetrically loaded rod in a resonant cavity. On either end of the rod inside the cavity was a dielectric of variable permittivity and around the rod was a dielectric of a different permittivity. They solved for the

resonant frequency given the dimensions of the cavity and the rod, and the permittivities of the rod and other dielectrics. This was done using a mode matching technique.

Their primary contribution was that these solutions were for hybrid, nonaxially symmetric modes as well as for axially symmetric TM and TE modes. Materials of high dielectric constant can also be measured with their solution. However, the solution is only for perfect dielectrics, ie. the lossless case.

Vigneron and Guillon²⁸ have extended the work of Zaki and Atia to the case for asymmetric positioning of the load in the cavity. Their work also considers hybrid modes and they also include mode charts for given load conditions. Unfortunately there are a large number of typographical errors in their mathematical equations and care must be taken if one wishes to follow their development in arriving at the characteristic equations. The characteristic equations appear to be correct despite the typographic errors elsewhere. Similar to Zaki and Atia, Vigneron and Guillon consider only the lossless case.

An exact method which does not rely on mode matching is given by Roussy and Felden. 29 In order to avoid the difficulty encountered in mode matching, Roussy and Felden considered only the case where the length of the material was equal to the cavity length. However, they also included losses in the sample and the consideration of a second layer of material on the outside of the first. The outside layer in most applications would represent the wall of a tube used to contain the material under testing. The errors in their experimental results for low permittivity materials were due mainly to uncertainty in the dimensions of the tube. No

measurements on materials with higher dielectric constants than 9-j0.2 were reported.

A similar problem is solved by Li, Akyel, and Bosisio³⁰ for which results for high complex permittivity materials such as water show good agreement with known values. In their treatment the authors not only solve the two layer cavity-length load problem, but also correct for the holes in the cavity used to introduce the load materials. The correction to the "exact" solution is done using perturbation methods. The limitation to their work is that it is only for the TM₀₁₀ mode.

2.4 Electric Field and Material Load Temperature Measurements

The measurement of the electric fields inside a resonant cavity or waveguide is a significant problem for most heating applications.

Conducting electric field measurement probes inserted into resonant or transmission structures radically alter the field patterns making almost all direct electric field strength measurements impossible. The only exception is for measurements taken at a conducting wall when the probe does not need to be inserted very far.

The method of measuring electric field patterns at cavity walls using a microcoaxial field probe was described by Rogers¹ and has been used extensively in work done at Michigan State University.^{5,9,10,32} This method is also described in section 3.3 of this thesis. In these applications only electric field strengths relative to a low power empty cavity field strength have been necessary. Absolute calculations were not made.

A similar electric field strength measurement at a conducting boundary is described by Burkhart. 33 He was interested in absolute

measurement of the normal electric field at the wall of an evacuated resonant cavity or waveguide. The coaxial field probe he describes does not protrude into the cavity, but is flush with the cavity wall. A theoretical analysis of the amount of power coupled out versus field strength was in good agreement with his experiments. The measurements reported were for very high powers, 100 MW, in 8.5 cm diameter circular waveguide operating in the TM_{O1} mode at 7.0 GHz.

Another method for the measurement of electric field strength inside a resonant cavity is the bead-pull technique. This method was first used by Maier and Slater ³⁴ in the early 1950's to measure the field strength in resonant cavities by positioning ellipsoidal metallic beads in various regions of the cavity and measuring the resulting frequency shift. This method is useful for determining the magnitude of the field, but is not well suited for determining the field direction.

Using the single bead-pull technique Bernier, Sphicopoulos, and Gardiol describe an automated system for electric field strength measurement. 35 They used a small lossless dielectric bead to perturb the fields. Since the frequency shifts were very small when the bead was in regions of low electric field, the microwave power source was phase-locked to provide accurate measurements of the resonant frequency. A feed back system was used to control the source to provide resonance at all bead positions. The resonant frequency was recorded as a function of the position of the bead which was mechanically driven. The position of the bead was automatically recorded on the x-axis of an x-y recorder while y-axis corresponded to the frequency shift. The frequency shift was related to the magnitude of the square of the electric field by a perturbation calculation.

In the interest of gaining insight into the direction of the fields and not only their magnitude, Amato and Hermann developed what they refer to as a multiple bead-pull technique. ³⁶ In resonantors used for charged particle acceleration knowledge of the direction of the electric fields is essential. The passing of a charged particle through the resonator will often excite modes in the resonator besides the acceleration mode. Therefore knowledge of the field directions at frequencies higher than the fundamental frequency is important.

The frequency shift for a metallic needle perturbation depends on the magnitudes of the electric field parallel to the needle, the electric field perpendicular to the needle, the magnetic field parallel to the needle, and the magnetic field perpendicular to the needle. The needle of the equation in terms of coefficients which depend on the needle geometry as $-if/f \approx u_i E(||)^2 + v_i [E(\perp)^2 - H(\perp)^2] - w_i H(||)^2$ where the subscript i refers to the different geometries of the needle. Passing three different sized needles through the resonator gives three equations to solve for the unknown fields. Misalignment errors contribute greatly to the uncertainty of this method. In order to minimize these errors the authors used needles which were suitably different from one another in diameter and calculated v_i and w_i from the more easily measured u_i .

In the measurement of the temperature of materials inside microwave resonators one encounters similar problems to that of measuring the electric field, namely the problem of how to take the measurement without disturbing the fields. Thermocouple devices and conventional thermometers are conductors and therefore cannot be inserted into the cavity without altering the fields. In the past the problem has been solved by using infrared radiation thermometry for high temperature measurements 17 or by

passing a gas around the sample and measuring the temperature of the gas as it exited the field region. The temperature of the gas could be related to the temperature of the sample. 18

Recently, however, fiberoptic thermometry has made direct measurement of sample temperatures possible without disturbing the electric fields. Wickersheim²⁴ describes the 1986 version of the Luxtron fiberoptic thermometer which bases temperature measurements on the decay time of radiation from a phosphor excited by a flash of light. The phosphor is located at the tip of a thin (approximately 1 mm diameter) fiberoptic probe. The perturbation produced by the insertion of the fiberoptic probe is virtually undetectable for most cavity systems.

The phosphor excitation flash is produced by a xenon bulb and travels down the fiberoptic probe to the phosphor. The radiation from the phosphor then travels back through the probe to a detector which measures the decay time. The temperature of the phosphor is then related to the decay time and displayed on a digital readout. It is accurate to $\frac{1}{2}$ 1 °C.

2.5 Thermal Runaway

In microwave heating applications, as opposed to conventional heating, the characteristics of load materials affect the operation of the applicator itself. There is a greater degree of applicator/material interaction in the microwave applicator. Generally this can be related to the changing dielectric constant of the material as it is heated. One of the most common heating problems for solids is the thermal runaway effect, that is the uncontrolled rapid increase of load temperature. This has to do with the change in the lossy part of the permittivity with material temperature.

In most materials the losses increase with increasing temperature. This leads in turn to an increased absorption of microwave energy.

Roussy, Mercier, Thiebaut, and Vaubourg have shown that heat radiation from the material load is sufficient to prevent thermal runaway for materials whose dielectric loss factor as a function of temperature has a negative curvature. The materials with a dielectric loss factor versus temperature with positive curvature the unstable thermal runaway effect can occur. In order to prevent thermal runaway in the heating of EPDM rubber, the authors monitored the temperature and the derivative of the temperature with respect to time. Using these measurements they controlled the output of the microwave power source. In this manner, by reducing the power when the material began to heat rapidly, they prevented thermal runaway.

Another approach to controlling thermal runaway takes advantage of the detuning characteristic of a resonant cavity with change in load permittivity. Huang used this method to prevent the thermal runaway of nylon as it was heated to near melting temperatures in a microwave cavity. By delivering klystron power to a TM₀₁₀ resonant cavity with undercoupled impedance mismatch, Huang was able to prevent thermal runaway of nylon monofilament as it was drawn through the cavity. In undercoupled conditions the mismatch between the cavity and the power source increased with increasing dielectric loss factor of the nylon. As the impedance mismatch increased, power coupled to the nylon decreased allowing the nylon to come to thermal equilibrium without melting.

CHAPTER III

EXPERIMENTAL SYSTEMS AND RESULTS

3.1 Introduction

This chapter describes the systems and the experimental results that were obtained from experiments carried out in a seven inch diameter circular cylindrical applicator and in a similar six inch diameter applicator which was designed for diagnostic electric field measurements. The purpose of these experiments was to demonstrate the experimental viability of the Michigan State University single-mode cavity applicator in the application of heating solid materials.

In this chapter the applicators, the microwave power source, the transmission system, and the measurement apparatus are described. The experiments performed with this equipment are divided into three categories: empty cavity experiments at low powers (less than 100 mW), loaded cavity experiments with coaxially loaded rod shaped materials at low powers (up to 500 mW), and loaded cavity experiments with coaxially loaded rod shaped materials at higher powers (up to 8 W). The rod shaped loads were of two types: rods which extended the entire cavity length and rods of length approximately 25% of the cavity eigenlength. The load materials included nylon 66, teflon, quartz, water-soaked wood, water, and silicone rubber.

Empty cavity experiments included the determination of empty cavity eigenlengths for various modes, empty cavity quality factor, and verification of radial electric field patterns at the cavity wall. Low power loaded cavity experiments provided measurements of resonant

frequency shifts from the empty case and loaded cavity Q for various load materials and load configurations. The frequency shift and change in cavity Q measurements made possible the calculation of the dielectric constant of the load material using perturbation techniques.

Higher power loaded cavity experiments demonstrated the on-line diagnostic capability of the system. At higher powers load material permittivities were monitored as load temperature changed during heating. On-line measurement of cavity Q also provided a means of determining the microwave coupling efficiency. For water and water-soaked wood the amount of water brought to boiling and evaporated was measured yielding a heating efficiency. Finally, for the six inch diagnostic applicator, temperature measurements of the coupling probe during load material heating were made to determine if a significant percentage of the input power was dissipated in the coupling apparatus.

3.2 Seven Inch Applicator Description

The seven inch applicator, which is displayed in the sketch of Figure 3.1 and the photograph of Figure 3.2, is a circular cylindrical resonant cavity with a seven inch inside diameter. It consists of a section of circular waveguide with shorting plates on either end which are perpendicular to the waveguide axis. These components are all made of brass. As shown in Figure 3.1 one of the shorting plates (3) is fixed to the waveguide (1) with silver solder. This shorting plate is referred to as the cavity bottom. The other shorting plate (2) is adjustable and is referred to hereafter as the sliding short. In order for the sliding short to maintain contact with the inner surface of the waveguide (1),

referred to as the cavity wall, it is ringed with silver finger-stock (4) which is under tension against the wall.

The sliding short is rigidly suspended by means of three 0.5 inch diameter threaded rods (9) from a plate (10) which is attached to the top of the waveguide with removeable bolts. On the top of this plate is a gearing mechanism (not shown) which allows for the turning of tapped gears around the threaded rods to raise and lower the sliding short. This gearing mechanism is activated either manually using a knob, or with a reversible electric motor which can be governed by a feedback signal from a control system. The plate (10) and sliding short (2) are removeable allowing for the insertion of materials into the cavity for processing.

There are holes (11) two inches in diameter in the centers of each the cavity bottom, the sliding short, and the top plate. These holes allow for the introduction of experimental materials (5) into the cavity. These holes introduce a deviation from the ideal cavity. Also material rods of diameter less than two inches do not fit tightly against their sides as is required for experiments involving load materials of length equal to the cavity eigenlength. To minimize these problems, brass collars (12) have been constructed to fit inside the two inch holes of the cavity bottom and sliding short. These collars are either solid or have a hole in their centers the same diameter as the load material. Figure 3.7 of section 3.4.1 shows in greater detail the placement and means of securing these collars in the holes.

In order to couple microwave energy into the cavity, an adjustable coaxial probe (8) is inserted through a port (7) in the cavity wall.

Since the probe is generally connected to the microwave source through a 50 Ohm transmission system, the probe is also designed to have a 50 Ohm

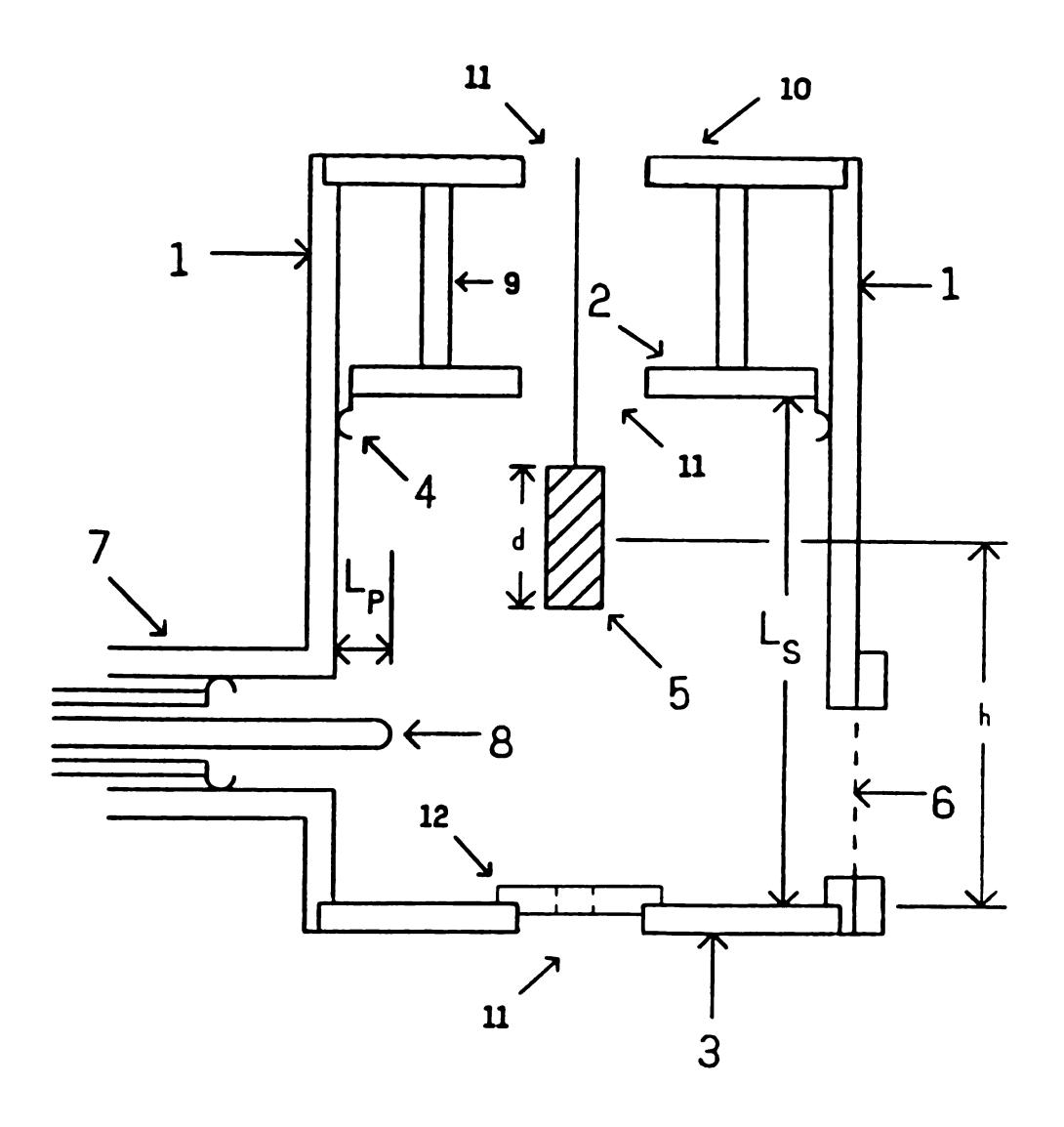


Figure 3.1 Cross-sectional View of the Seven Inch Applicator

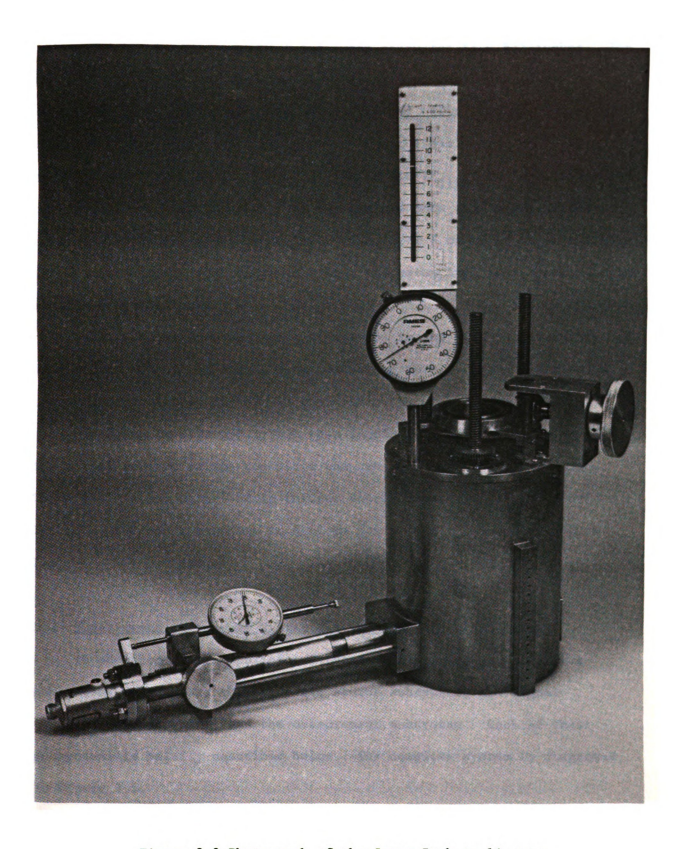


Figure 3.2 Photograph of the Seven Inch Applicator

characteristic impedance. The diameter of the inner conductor is 0.375 inches and the inner diameter of the outer conductor is 0.875 inches. The port (7) is located at approximately one-quarter of the waveguide wavelength (f=2.45 GHz) from the cavity bottom. This location is chosen because it is a good compromise position for the excitation of several resonant modes such as TE₁₁₁, TM₀₁₁, TE₂₁₁, and TM₁₁₁. In fact, referring to Table 3.1 of section 3.4.1, the experiments show that all possible empty cavity modes in the eigenlength range from 6 cm to 16 cm, the limits of the eigenlength range achievable with the seven inch applicator, can be excited from this port.

There is also an observation window (6) in the side of the cavity.

This window is covered with a fine conducting mesh to prevent microwave energy from radiating out of the applicator.

Not shown in Figure 3.1, but seen in Figure 3.2, are precision dial indicators mounted on the top plate and the coupling probe structure. These indicators, described in further detail in section 3.3.3, provided length measurements accurate to 0.01 mm for L_s and L_p , shown in Figure 3.1.

3.3 Experimental Microwave System For The Seven Inch Applicator

In addition to the applicator, the experiment consists of three subsystems. These are the microwave source subsystem, the signal transmission subsystem, and the measurement subsystem. Each of these subsystems is briefly described below. The complete system is diagramed in Figure 3.3.

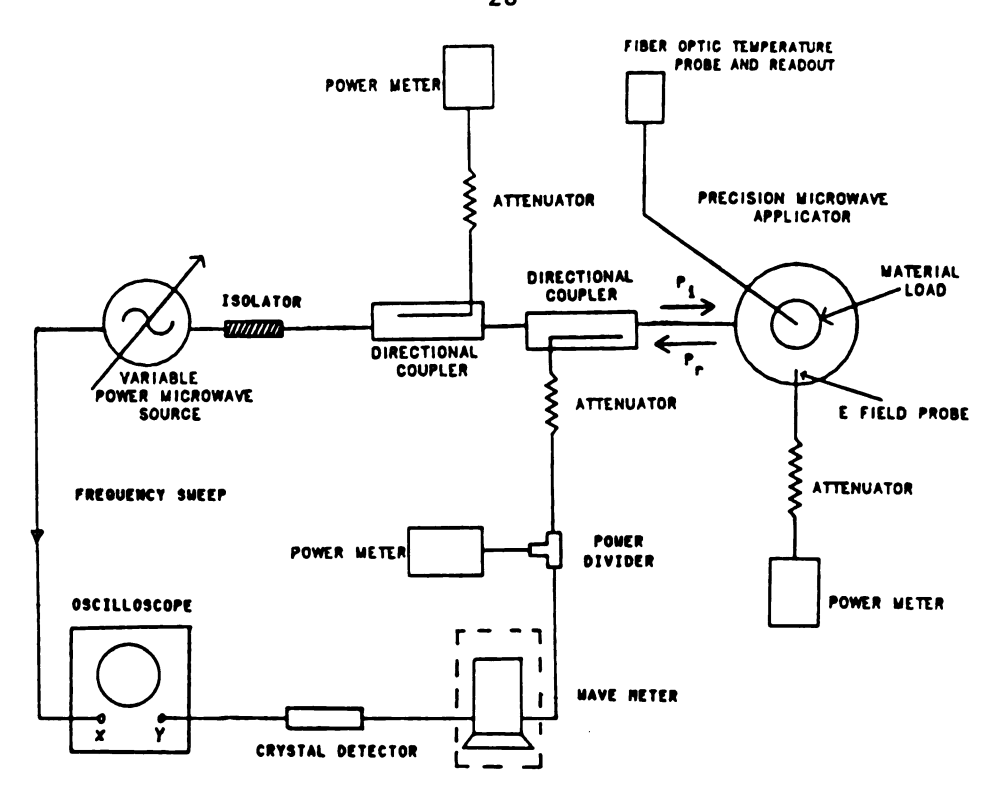


Figure 3.3 System Configuration

3.3.1 The Microwave Power Source Subsystem

In order to make the measurements presented in this thesis, it was necessary to be able to produce both single frequency CW signals at 2.45 GHz and swept frequency signals in a range about 2.45 GHz. The variable power microwave source shown in Figure 3.3 was used for both types of signal generation. The power source was a Hewlett Packard 8350B Sweep Oscillator with an HP 86235A 1.7 - 4.3 GHz RF plug-in unit. In CW mode near 2.45 GHz, this source is stable to within ± 0.3 MHz during periods of a few hours or more over a 0 to 20 mW output power range.

Since processing of the experimental materials often required input powers of more than 20 mW, it was necessary to amplify the signal from the sweep oscillator. A Varian VA-1356 traveling wave tube amplifier (TWT) was used to accomplish this. The sweep oscillator and the amplifier were

connected with a short 50 Ohm coaxial cable. With the amplification, output powers of nearly 30 W could be achieved.

The final component of the microwave power source subsystem was an isolator connected directly to the output port of the TWT. This was used to protect the TWT by dissipating any power which might be reflected from the cavity applicator.

3.3.2 The Transmission Subsystem

P_r.

Referring to Figure 3.3, two coaxial directional couplers were located between the applicator and the microwave power source. These were placed back to back and connected to the output power port of the isolator and the input power port of the applicator coupling probe. The directional coupler connected to the isolator drew off 20 dB of the incident power coming from the TWT and coupled it to a power meter. The reading of this power meter, part of the measurement subsystem, when calibrated for the attenuation due to the attenuator and the coaxial cable between the source and the cavity, was referred to as incident power, ie. power incident on the applicator, and is abreviated P₄.

The second directional coupler was used to sense 10 dB of the power reflected back from the applicator. This output was further attenuated before being fed to the input port of a power divider. One ouput of the power divider was connected to a power meter while the other ouput was connected to a crystal detector as shown in Figure 3.3 and described below in section 3.3.3. The power read on the meter, taking into account the attenuation by the directional coupler, the attenuator, and the power divider, gave the magnitude of the power reflected at the cavity input,

The total power into the cavity is denoted P_{t} and defined by

$$P_{t} = P_{i} - P_{r}. \tag{3.1}$$

3.3.3 The Measurement Subsystem

The experimental measurements made fall into six catagories: cavity length, $L_{\rm g}$, and depth of coupling probe penetration into the cavity, $L_{\rm p}$, both of which are shown in Figure 3.1, signal frequency measurements, measurement of incident and reflected powers, relative power measurements proportional to the square of the normal electric field at the cavity wall, temperature monitoring of materials being processed, and time.

The cavity length and probe penetration were measured using sensitive dial indicator meters accurate to within 0.01 mm, which are mounted on the top plate of the cavity and the coupling probe structure as shown in the photograph of Figure 3.2. Relative differences between separate measurements are then good to ± 0.01 mm. Uncertainties in calibrating the zero point of coupling probe penetration and the cavity length, however, increase the error of absolute measurement by introducing a systematic error of approximately ±0.5 mm. For the coupling probe, the zero point was set by removing the sliding short and looking straight down along the cavity wall on the coupling probe. When it appeared that the coupling probe was just entering the cavity, the coupling probe dial indicator was set to zero. The zero point of the sliding short was set by placing an object of known length inside the cavity and lowering the sliding short until it rested on the object. The sliding short dial indicator was then set to the length of the object on which the short rested.

The signal frequency was measured in one of three ways. For CW mode, the sweep oscillator provided a frequency measurement accurate to 0.1 MHz. Operation in sweep mode required the use of an oscilloscope to display a system characteristic versus input signal frequency. The system characteristic of chief interest with respect to the signal frequency was the reflected power. The sweep generator was capable of producing a low voltage signal proportional to the frequency of the plug-in output microwave signal. This voltage was applied to the X terminal of an X-Y oscilloscope, shown in Figure 3.3, while a voltage proportional to the power reflected at the cavity was applied to the Y terminal. The voltage proportional to the reflected power was produced by a crystal detector connected between one of the ouputs of the power divider, shown in Figure 3.3, and the Y terminal of the oscilloscope.

An example of a swept frequency oscilloscope display is shown in Figure 3.4. The x-axis represents frequency and the y-axis represents reflected power. The inversion of the coordinate system in Figure 3.4 is due to the negative proportionality factor of the crystal detector. The relatively flat nonzero region of the power absorption curve represents frequencies at which all of the power incident on the cavity is reflected. The power absorption dip in the middle of the display represents a frequency at which all the incident power is absorbed into the cavity. At this frequency, an electromagnetic resonance is excited in the cavity and the power is dissipated in the cavity walls and any materials present inside.

In Figure 3.4, the small blank area on the display is a marker produced by the HP 8350 Sweep Oscillator at a frequency which is given by a digital readout to five places on the sweep oscillator display. For

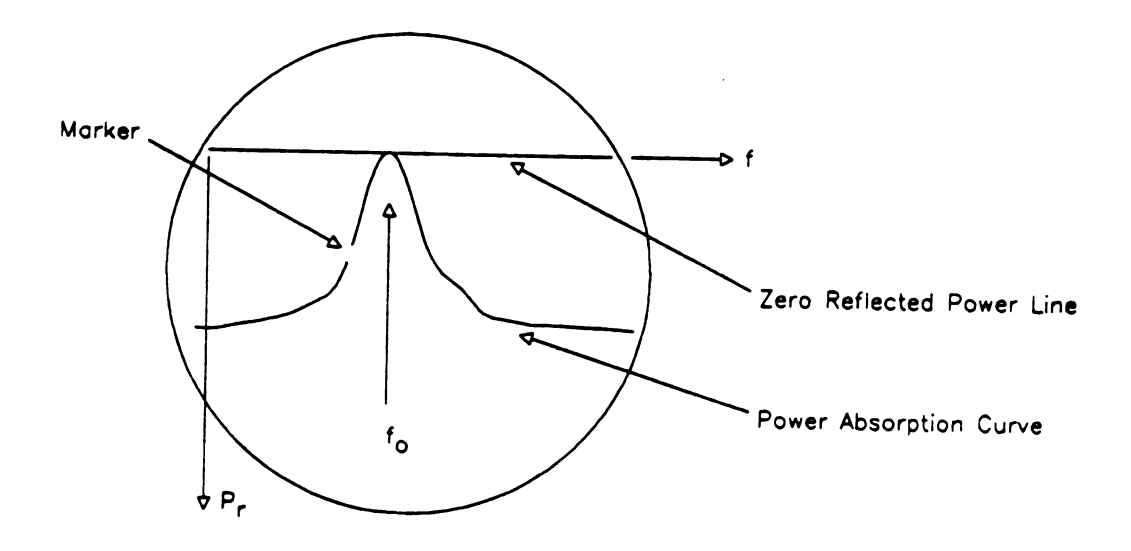


Figure 3.4 Oscilloscope Display of the Absorption Spectrum Near Resonance

some sweep oscillator models no digital readout is available for frequency measurement. In such a case the frequency can be measured by connecting a frequency meter, shown inside the dashed square in Figure 3.3, between the directional coupler and the crystal detector. The frequency meter, which is actually a small, calibrated resonant cavity, places a narrow absorption dip on the oscilloscope display at a frequency which is read on the side of the frequency meter. The absorption dip produced by a frequency meter has a full width half max bandwidth of typically 0.4 MHz and is therefore not as accurate as the HP 8350 Sweep Oscillator markers.

Measurements of absolute input and reflected powers were made using HP 432A power meters with appropriate thermistor power sensors. These power meters were placed in the circuit as described in section 3.3.2

above on the transmission subsystem and shown in Figure 3.3. To prevent damage to the meters and the crystal detector due to excessive input or reflected powers, 10 or 20 dB attenuators were placed at the attenuated output of the directional couplers.

It is desirable to know the electric field intensities at various locations in the cavity for a variety of reasons. Such measurements would provide experimental verification of field patterns for resonant modes, allow for precise quality factor determination, demonstrate the effects on the fields by the introduction of material loads into the cavity, give information on the effect of the coupling probe and other nonidealities on the field patterns, and provide insight into the most effective ways to use various modes for materials processing. Unfortunately it is very difficult to make such measurements without greatly changing the resonant fields in the cavity except at the cavity walls. However, measurements at the cavity walls do provide sufficient information to determine the cavity quality factor and partial resonant mode structure.

In the experiments with the seven inch applicator, measurements of the relative strength of the square of the radial electric field at the cavity wall were made through holes in the cavity wall using a micro-coaxial field probe and a power meter. Figure 3.5 is a detail sketch of the micro-coaxial field probe and field probe "block", also shown in the photograph of Figure 3.2, which was soldered to the outside of the cavity in order to provide good contact between the cavity wall and the outer conductor of the micro-coaxial field probe. Using the cylindrical coordinate system of Figure 3.5 and referring to Figure 3.2, it can be seen that the field probe block is located 90° away from the coupling probe.

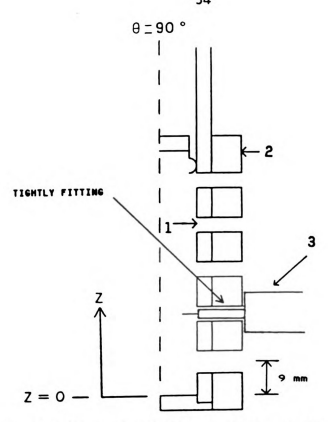


Figure 3.5 Micro-Coaxial Field Probe, Field Probe Block, And Diagnostic Ports

Referring to Figure 3.5, holes (1) which are located in the side of the applicator in a vertical column were used as diagnostic ports for the micro-coaxial field probe measurements. There were 15 holes, each approximately 2 mm in diameter, and spaced 9 mm apart beginning 9 mm from the cavity bottom. A field probe block (2) soldered to the side of the applicator through which the holes were drilled served to make sure that good contact between the applicator wall and the outer conductor of the micro-coaxial field probe was maintained, and to keep unattenuated radiation from being transmitted through the holes. When the micro-coaxial field probe was inserted into one of the diagnostic holes, the inner conductor of the micro-coaxial line penetrated approximately 3 mm into the cavity. It was prevented from going any further by a length of

heat shrink tubing (3) which was wrapped around the outer conductor of the micro-coaxial line.

It was assumed that power drawn out of the cavity by this probe was proportional to the magnitude squared of the normal electric field at the cavity wall at the point of measurement. For the circular cylindrical cavity the component normal to the wall corresponds to the radial electric field. Experimental data presented later in this thesis confirms this conjecture by showing that the micro-coaxial field probe readings at the cavity wall predict the correct shape of the fields for known mode resonances. This was also shown previously by Rogers. 1

Under this assumption the micro-coaxial field probe power measurement is also proportional to the power dissipated in the cavity wall at the point of measurement. This is made clear by examining the boundary condition for tangential H at a conducting boundary:

$$\mathbf{n} \times \mathbf{H}_{\mathsf{t}} - \mathbf{j}_{\mathsf{s}} \tag{3.2}$$

where n is the vector normal to the conducting boundary and \mathbf{j}_{s} is the surface current density on the conductor. The power dissipated in the wall is ohmic loss which is proportional to the square of the surface current. Since the radial electric field at the wall is proportional to \mathbf{H}_{t} , and \mathbf{H}_{t} is proportional to the surface current, the power dissipated in the wall is proportional to the square of the radial electric field at the wall.

Temperature measurements of points inside the applicator were accomplished without disturbing the electromagnetic fields by using a Luxtron 750 fluoroptic probe optical temperature measurement system, shown

in Figure 3.3. The temperature probes were made of optical fibers of about 1 mm diameter which created a negligible perturbation of the cavity fields when inserted into the applicator. Phosphors at the tips of the temperature probes sent optical signals back to the temperature measurement module which output the temperature on a digital readout. The four channel Fluoroptic Probe system was capable of reading temperatures at up to four different locations inside the cavity at a time. This temperature measurement system is described in more detail by Wickersheim. 24

The final component of the measurement subsystem was a watch. Time parameters for experiments were commonly on the order of minutes, requiring accuracy of a few seconds, so no specialized time measurement instrumentation was necessary.

3.4 Seven Inch Applicator Experiments

The experiments with the seven inch applicator can be divided into two categories: the measurement of empty cavity parameters and fields, and the measurements of cavity parameters, material dielectric constants and temperatures, and field strengths at the cavity wall during the heating of materials in the applicator. The empty cavity experiments were performed to make sure the cavity operated properly, that its dimensions were close to theoretical values for given operating frequencies, and provided a calibration on resonant frequency and cavity Q for loaded cavity experiments. Experiments with materials in the cavity, when used in conjunction with the empty cavity calibration experiments, provided information on material dielectric constants as a function of coupled power and time, and served to demonstrate that for the small loads that

were used the radial electric field patterns at the cavity wall were the same shape as the empty cavity fields.

3.4.1 Empty Cavity Experiments

With the empty seven inch applicator three experiments were performed. These were measurement of cavity resonant length, determination of empty cavity Q, and testing of axial field patterns at the cavity wall with the microcoaxial field probe. The measured resonant length and cavity Q were compared to their theoretical values. ³⁹ Since the radial electric field at the cavity wall is theoretically sinusoidal in z, ie. in the direction from the cavity bottom toward the sliding short (see Figure 3.5), the measured radial electric field can easily be compared with theory.

3.4.1.1 Resonant Length Measurements

The expression for the empty circular cylindrical cavity resonant length is given by

$$L = \frac{q \pi}{\left[k^2 - (X_{pp}/r)^2\right]^{\frac{1}{2}}}$$
 (3.3)

where q is the third index in the mode designation number, X_{np} is the pth zero of the Bessel function J_n for TM_{npq} modes or J_n for TE_{npq} modes, k is the free space wave number, and r is the cavity radius.

Table 3.1 lists the experimentally measured eigenlengths (resonant lengths) for the nine lowest order modes. These eigenlengths were measured by sweeping the cavity frequency, using the oscilloscope as explained above in section 3.3.3, and adjusting the cavity length and probe position one at a time iteratively until the cavity was resonance

Mode	Ls(th.) (cm)	ls(ex.) (cm)	Lp (mm)	Q _{uo} (th.)	Q _{uo} (ex.)
TE111	6.686	6.634	2.24	12,359	2,692
- TM011	7.198	7.227	0.05	10,000	5,384
TE211	8.233	8.274	-3.27	14,512	8,596
TM111	11.257	11.226	3.09	13,463	7,904
TEO11	11.257	11.379	15.94	29,652	24,500
TE112	13.373	13.391	1.23	20,475	10,652
- TM012	14.397	14.473	0.79	15,523	10,000
TE311	15.645	15.981	-0.87	16,827	14,848
TE212	16.465	16.532	6.87	19,325	15,312

Table 3.1 Table of Resonant Lengths and Quality Factors For The Seven Inch Cavity With Collars At 2.45 GHz

matched at 2.45 GHz. As shown in Table 3.1, these measured lengths compare well with theoretical values calculated from equation 3.3.

It should be noted that the modes TM_{111} and TE_{011} are theoretically degenerate, but for the seven inch cavity they are not. This is because the seven inch cavity is not an ideal circular cylindrical cavity since it has a coupling probe, observation window, holes in the shorting plates, and finger-stock on the sliding short. In Table 3.1 the TM_{111} mode has been assigned to the measured 11.226 cm eigenlength and the TE_{011} to the measured 11.379 cm eigenlength because the respective measured Q_{uo} 's compare well with the theoretically calculated values for the corresponding modes.

3.4.1.2 Cavity Quality Factor Measurements

The quality factor of the cavity is a measure of the ratio of the energy stored in the cavity electromagnetic fields per unit time to the energy lost in the cavity walls per unit time. Hence it is a measure of the strength of the fields inside the cavity relative to the amount of power, $P_{\rm t}$, coupled into the cavity. The quality factor is given as

$$Q = \frac{2\pi f}{o} \times \text{energy stored in cavity}$$
average power dissipated (3.4)

where f is the resonant frequency of the cavity. 40

Since the cavity is part of a microwave circuit the quality factor of the cavity alone must be distinguished from the quality factor of the cavity loaded by the external circuit. The quality factor of the microwave circuit is defined similarly to the quality factor of the cavity as

$$Q_{L} = \frac{2\pi f_{o} \times \text{energy stored in circuit}}{\text{average power dissipated}}$$
(3.5)

where the subscript L indicates that the cavity is "loaded" by the external coupling circuit. It is important to remember that the term "loaded" does not imply that the cavity is loaded with a dielectric material. For purposes of notation Qu is defined as the quality factor of the cavity without the external circuit and Quo is defined as the quality factor of the special case of the empty cavity without the external circuit. The subscript "u" indicates that the quality factor referred to

is "unloaded". 41 The experimentally measured values of cavity Q listed in Table 3.1 are empty cavity unloaded quality factors.

The measurement of the cavity quality factor Q_u is done indirectly by measuring Q_L . The relationship between Q_L and Q_u is in general complicated. However, when the cavity is critically coupled to the circuit Q_u is given quite simply in terms of Q_L as,

$$Q_{11} = 2Q_{1}.$$
 (3.6)

Critically coupled means that there is no impedance mismatch at the junction between the cavity and the transmission line leading into the cavity, thus at critical coupling there is no reflection of incident power. Critical coupling for a particular mode is achieved by adjusting the cavity length and coupling probe penetration depth one at a time iteratively until the cavity impedance matches that of the rest of the circuit at the cavity-transmission line junction.

 $\mathbf{Q}_{\underline{\mathbf{L}}}$ can be determined from the frequency spectrum of the circuit. It can be shown that $\mathbf{Q}_{\underline{\mathbf{L}}}$ is given by,

$$Q_{I} = f_{O}/\hbar f \tag{3.7}$$

where f is the resonant frequency and I f is the half power bandwidth of the experimental power absorption curve. Therefore, when the cavity is critically coupled to the circuit, Q is given by,

$$Q_{ij} = 2x(f_0/\hbar f). \qquad (3.8)$$

The resonant frequency is found using the oscilloscope as described in section 3.3.3. The half power bandwidth is found in a similar manner except that frequencies are measured at the midway point between the zero reflected power line and the point of total reflection. These frequencies are referred to as half power frequencies, denoted f_1 and f_2 . The difference between these two frequencies is the half power bandwidth and is denoted Af,

$$\Delta f - f_2 - f_1$$
 (3.9)

Figure 3.6 shows the half power frequencies, f_1 and f_2 , the half power bandwidth, Af, and the center frequency, f_0 , on the sketch of a typical power absorption curve.

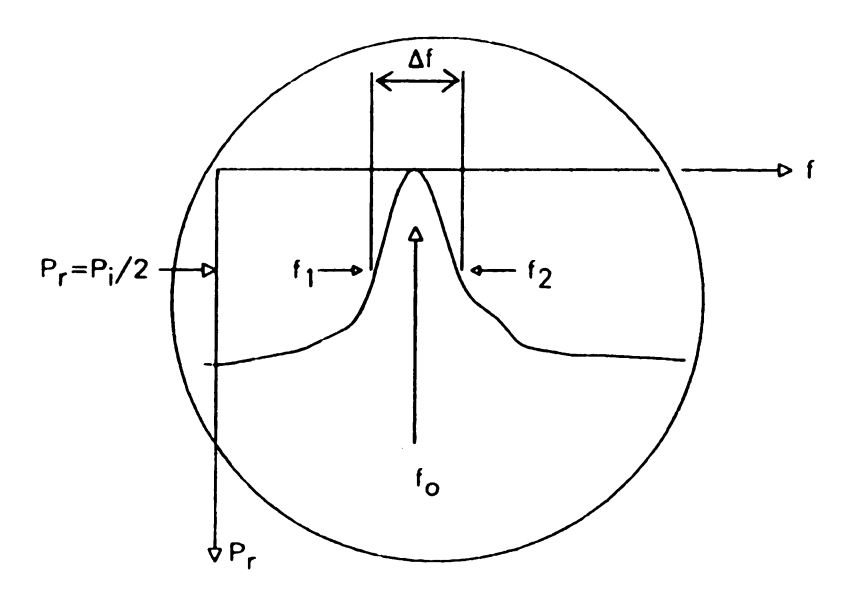


Figure 3.6 Using The Oscilloscope To Measure Q_{L}

Theoretical values for the empty cavity Q_{uo} can be obtained using perturbation techniques to calculate power lost in the cavity walls and energy stored in the fields. Table 3.1 lists the experimentally measured value of Q_{uo} and the corresponding theoretically calculated value for several modes.

The theoretical Q value is consistently higher since it is calculated for an ideal cylindrical cavity whereas the actual cavity has signal input ports, an input probe, finger-stock contacts for the sliding short, a screened observation window in the cavity wall, and holes in both the top and bottom shorting plates. All of these features increase the power lost in the cavity structure which reduces measured Q_u .

In particular, the holes in the shorting plates have a great effect on cavity Q and the existence of certain modes in general. When the brass collar which fits in the hole at the top is removed, the TM₁₁₁ and the

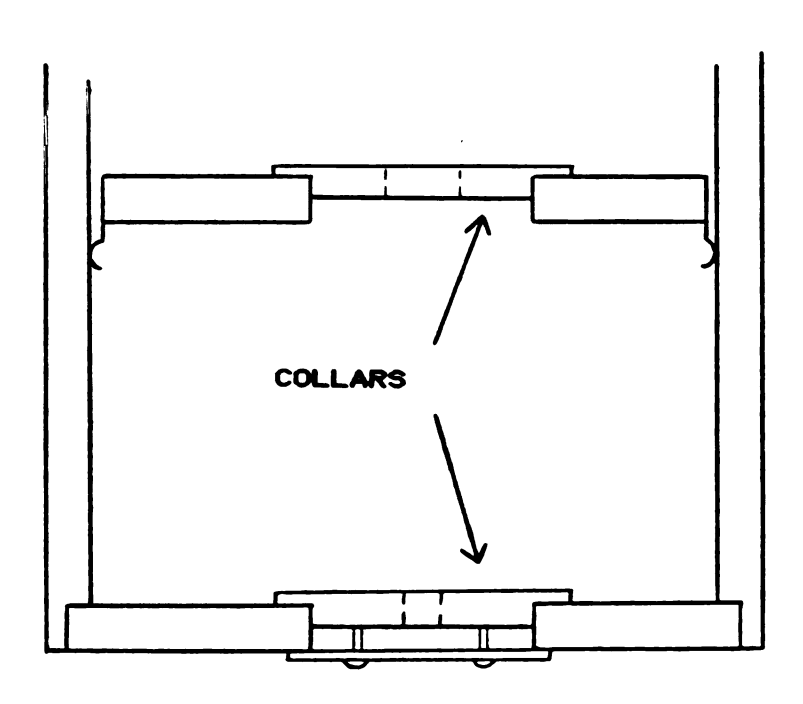


Figure 3.7 Collar Placement In Shorting Plate Holes

TE₁₁₂ modes are missing. If the bottom collar does not have a tight fit there is as much as an 80% drop in Q measurement. Since during the heating of materials the collars are in place, the values listed in Table 3.2 are for the cavity with collars. The bottom collar is solid brass with a 0.25 inch hole in the center while the top collar has a 0.5 inch diameter hole through its center which allows for materials of that diameter to be inserted into the cavity. Figure 3.7 is a sketch of the placement of the collars in the holes in the shorting plates. As shown, the bottom collar fits tighly in the bottom hole while the top collar simply rests on the top shorting plate.

3.4.1.3 Axial Field Pattern Measurements

Power measurements at the cavity wall were taken with the micro-coaxial field probe as described in section 3.3.3 and shown in Figure 3.5. An example of these measurements is shown in Figure 3.8. The cavity was resonant in the TM_{012} mode which has a radial electric field component at the cavity wall which is sinusoidal in the variable z of Figure 3.5.

The experimentally measured curve shown in Figure 3.8 is plotted as a solid line with data points indicated. A theoretical sine squared curve normalized to the maximum power measurement of the micro-coaxial probe is plotted as a dashed line for comparison. As expected, the general characteristics of the experimental and theoretical plots are similar. It is believed that the assymmetry seen in the plot of experimental points, viz. the higher powers measured in the lower half of the cavity, is due to the presence of the coupling probe in that region. The drop off in field intensity measured near the sliding short is probably due to the presence of the finger stock on the sliding short near the cavity wall.

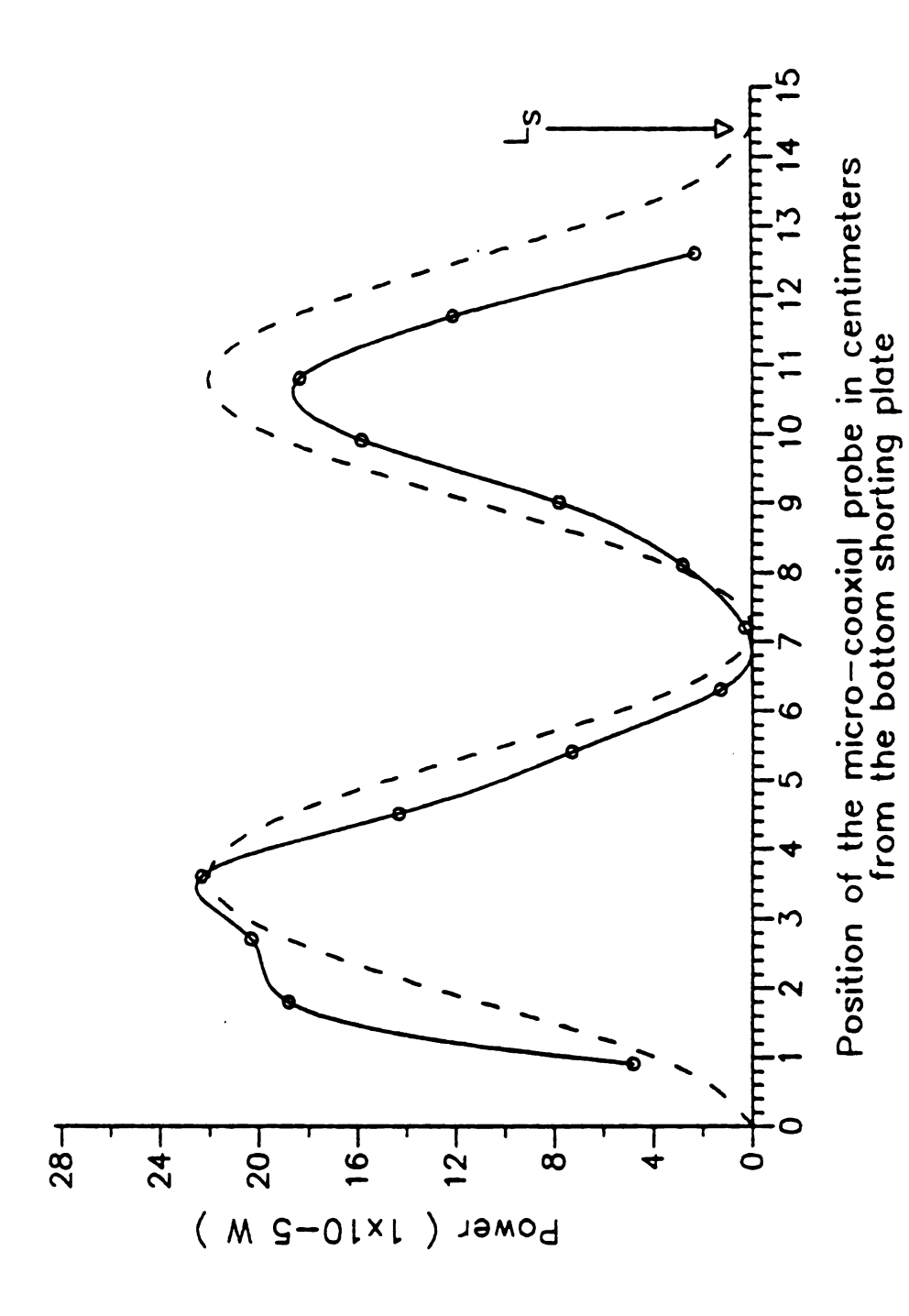


Figure 3.8 Micro-Coaxial Field Probe Measurements In The Empty Cavity Excited In The TM $_{
m 012}$ Mode

It should be noted that for similar experiments conducted with the six inch diagnostic cavity, described in section 3.5 and in L. Frasch's Ph.D. dissertation, 44 excellent agreement between theory and experiment was achieved by Frasch and is also demonstrated in section 3.7.2 of this thesis. Figure 3.23 for the six inch cavity may be consulted for comparison with Figure 3.8.

3.4.2 Loaded Cavity Experiments

Several different experiments were performed with materials positioned inside the cavity. Low power (less than 500 mW) swept frequency experiments were conducted using rods of nylon 66 and teflon 0.5 inches in diameter which were positioned coaxially in the cavity extending the entire cavity length as shown in Figure 2.9. Their dielectric constants were calculated using perturbation techniques and were compared with published data. A comparison between experimental eigenfrequencies, perturbation calculations of eigenfrequencies, and exact theoretical calculations of eigenfrequencies for this cavity configuration were also made.

Another experiment was performed with shorter cylindrical rods of material 2 to 3 cm in length. Cylinders of 0.5 inch diameter nylon 66 and 0.5 cm diameter quartz were suspended by cotton thread at various points along the cavity axis. The shift in resonant frequency and change in cavity quality factor from the empty cavity case were measured.

Higher power experiments (1 W to 8 W) consisted of time monitoring of cavity eigenlength and coupling probe position, load material temperature, and radial electric field intensity at a point on the cavity wall while heating the load material in the center of the cavity excited in the TM_{012} mode. Load materials consisted of cylinders approximately 0.5 inches in

diameter and 3 cm in length for nylon 66, water-soaked wood, and silicone rubber. Distilled water 4 cm in length and 4.5 mm in diameter held in a quartz tube was also heated in a similar fashion.

The measurements taken during the the experiments provided the means for calculating frequency shifts from the empty cavity case, cavity Q, material permittivities, and microwave coupling efficiencies. Weight before and after heating was measured for the cylinders of water and wet wood which provided information for the calculation of a drying efficiency or Specific Consumption (SC).

3.4.2.1 Low Power Sweeping Experiments

3.4.2.1.1 Rods of Length Equal to Ls

Rods of nylon and teflon 0.5 inches in diameter were placed coaxially in the cavity as shown in Figure 3.9. They extended through the top shorting plate through a collar with a 0.5 inch hole through its center.

The bottom of the rod rested on the bottom of the cavity on a collar with

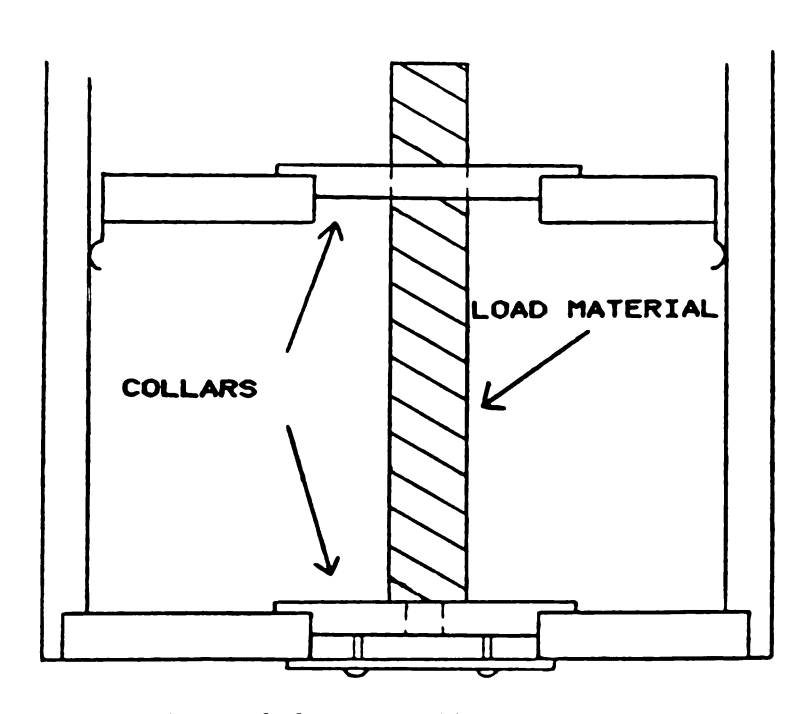


Figure 3.9 Coaxially Loaded Cavity

a 0.25 inch hole through its center, or extended through the cavity bottom through another 0.5 inch collar (not shown). Experiments were performed using both TM_{011} and TM_{012} modes at frequencies near 2.45 GHz.

In order to use perturbation equations to calculate the dielectric constants of the rods, measurements of frequency shift and change in cavity Q_u from the empty cavity values had to be made. This was done by first finding L_s , L_p , and Q_{uo} for the empty cavity at 2.45 GHz as the frequency was swept in a narrow range about 2.45 GHz. Then, without changing L_s , the rod was introduced into the cavity. L_p was adjusted for a match. The new resonant frequency and cavity Q_u were measured on the oscilloscope and recorded.

The frequency shifted down from the 2.45 GHz empty cavity resonant frequency by approximately 13.4 MHz for both TM₀₁₁ and TM₀₁₂ when the load material was nylon 66 and approximately 6.5 MHz when the load material was teflon. Since both nylon 66 and teflon have well known dielectric constants at this frequency, comparison can be made with expected values of the frequency shift using either perturbation theory or an exact theory relating dielectric constant to frequency shift. Tables 3.2 and 3.3 list values of expected resonant frequency shift for both a perturbation calculation and an exact calculation made by H. H. Lin, which did not take into account the coupling probe. The dielectric constants of nylon 66 and teflon used in the perturbation and exact calculations are given by the reference data in Table 3.4.

It is of interest to note that for nylon 66, which has a greater dielectric constant than teflon, the difference in predicted frequency shift between the perturbation calculation and the exact calculation is greater than the difference in predicted frequency shift for teflon. For

Nylon $f_0 = 2.4500 \text{ GHz}$

METHOD	TM ₀₁₁		TM ₀₁₂	
	f (GHz)	f _o -f (MHz)	f (GHz)	f _o -f (MHz)
Exact	2.4364	13.6	2.4364	13.6
Perturbation	2.4370	13.0	2.4370	13.0
Experimental	2.4370	13.0	2.4363	13.7

Table 3.2 Frequency Shift For Coaxially Loaded Nylon 66

Teflon $f_0 = 2.4500 \text{ GHz}$

METHOD	тм ₀₁₁		TM ₀₁₂	
	f (GHz)	f _o -f (MHz)	f (GHz)	f _o -f (MHz)
Exact	2.4427	7.3	2.4427	7.3
Perturbation	2.4429	7.1	2.4429	7.1
Experimental	2.4436	6.4	2.4435	6.5

Table 3.3 Frequency Shift For Coaxially Loaded Teflon

nylon 66, from Table 3.2a, the difference between exact and perturbation calculations is 0.6 MHz whereas for teflon, from Table 3.2b, the difference is only 0.2 MHz. This is as would be expected, since perturbation theory becomes more inexact as the dielectric constant of the load material increases.

The general form of the perturbation formula for a rod of radius c and length d suspended inside a cavity of radius a at a height h above the cavity floor for excitation in the TM_{0pq} mode is given in Appendix A. The material load of Figure 3.1 is positioned according to these parameters. For rods of length equal to L_s equations A.14 and A.15 can be used to calculate complex ϵ_r by setting d of equation A.16 equal to L_s .

An example of the use of equations A.14 and A.15 for perturbation permittivity calculations for 0.5 inch diameter rods of length equal to $L_{\rm s}$ is provided by the following equations:

$$L_s = 14.487 \text{ cm}$$
 $\epsilon_r' \approx 1 + 3.8003 \times 10^2 (f_o - f)/f$ $\epsilon_r'' \approx 1.90014 \times 10^2 (1/Q - 1/Q_o)$ $\epsilon_r'' \approx 1.90014 \times 10^2 (1/Q - 1/Q_o)$

$$L_s = 7.229 \text{ cm}$$

$$\begin{array}{c} \epsilon_r' \approx 1 + 3.8113 \times 10^2 \text{ (f_o-f)/f} \\ \epsilon_r'' \approx 1.90563 \times 10^2 \text{ (1/Q - 1/Q_o)} \end{array}$$
 TM_{011} (3.11)

Theoretically, the perturbation equations for the rod extending the entire length of the cavity should be the same for all the TM_{01q} modes $(q \neq 0)$, but because the experimental cavity is not an ideal circular cylindrical cavity, the experimental eigenlengths of the higher order modes $(q \geq 2)$ are not precise integer multiples of the TM_{011} eigenlength.

	Experiment		Reference Data ⁴⁵	
	nylon	teflon	nylon	teflon
ε _r '	3.033	1.998	3.03	2.1
$\epsilon_{\mathbf{r}^{''}}$	4.9x10 ⁻²	$-9.3x10^{-3}$	3.9×10^{-2}	3.0×10^{-4}
ε _r ' TM012	3.137	2.011		
ε _r ''	7.3x10 ⁻²	3.1x10 ⁻³		

Table 3.4 Perturbation Calculation Of Dielectric Constant For Coaxially Loaded Rods Of Length Equal To $L_{\rm g}$

Since the perturbation formula depends on the experimental eigenlength, the equations will differ slightly depending on $L_{\mathbf{g}}$ for each mode.

From the experimental frequency shift of Tables 3.2 and 3.3 the real part of the dielectric constants of nylon 66 and teflon were calculated using the perturbation equations 3.10 and 3.11. Using cavity $Q_{\rm u}$ measurements the imaginary parts were found as well. Table 3.4 compares the results of these calculations with reference data.

An explanation for the negative value of the imaginary dielectric constant measured for teflon in Table 3.3 is that the change in cavity Q is extremely small for such a low loss material as teflon. The measurement of a higher Q when teflon was inserted than when the cavity was empty may simply be experimental error. However, this phenomenon was

observed more often than not over a number of trials and it may be that losses in the cavity walls are less with teflon inside the cavity than when the cavity is empty. This could conceivably occur if the dielectric load caused more energy to be stored in the fields away from the cavity wall while not contributing to energy dissipation by dielectric loss mechanisms. More investigation is necessary before such a conjecture can be confirmed.

3.4.2.1.2 Rods of Length Less Than Ls

Experiments were also performed with shorter rod shaped materials. Small cylinders of nylon and quartz were suspended by cotton thread along the axis of the cavity as shown in Figure 3.1. The nylon cylinder was 2 cm in length and 0.635 cm in radius. The quartz cylinder was 3.1 cm in length and 0.25 cm in radius. The frequency was swept in a narrow range about 2.45 GHz and the cavity was in resonance in the TM₀₁₂ mode within that range. As the cylinders were lowered down the axis the absorption dip, similar to the ones shown in Figures 3.4 and 3.6, shifted down in frequency from the 2.45 GHz empty cavity resonance. As the rods passed through the region of maximum electric field along the axis the peak of the absorption dip began to move back towards 2.45 GHz. Figure 3.10 is a plot of the frequency shift versus the height, h, of the center of the rod above the cavity bottom for both the nylon 66 and quartz cylinders. As was expected the maximum frequency shift occured in the regions of the cavity with the greatest electric field.

The cavity Q also changed with varying height of the samples. Figure 3.11 is a plot of the cavity Q versus sample height for the nylon sample also using TM_{012} . The cavity Q was at its minimum in regions of high electric field and maximum where the field was small.

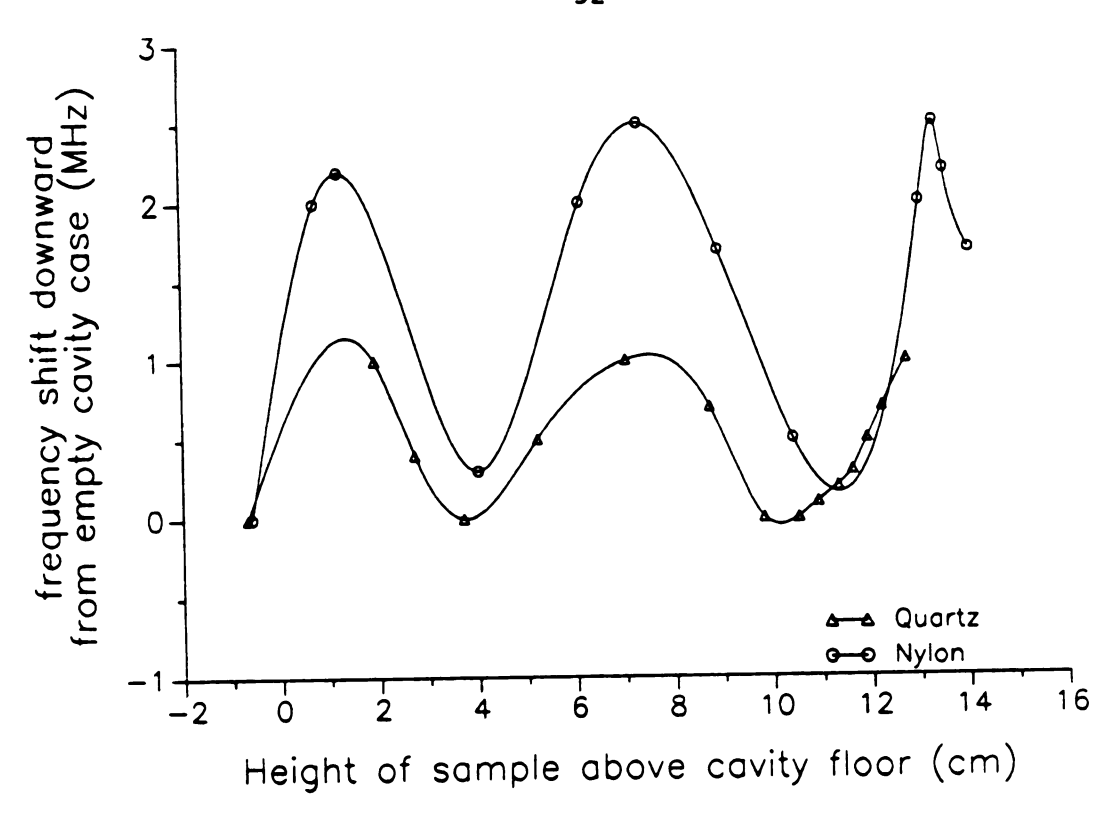


Figure 3.10 Frequency Shift Versus Sample Height

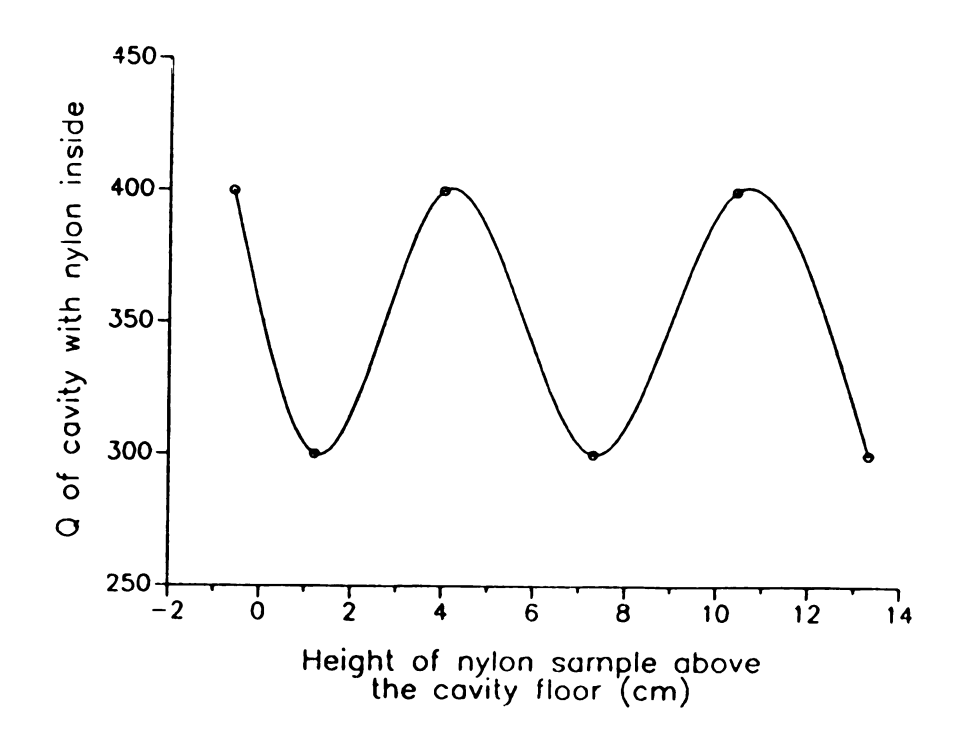


Figure 3.11 Cavity Q Versus Sample Height

3.4.2.2 Higher Power Heating Experiments

In order to heat load materials efficiently and to make accurate measurements of incident, reflected, and radial electric field powers experiments were performed in CW mode. Since the frequency was not being swept during heating, measurements of cavity Q could no longer be made using the oscilloscope as described previously. Instead, the micro-coaxial field probe was used to make the measurement in a manner similar to Rogers' method. Accordingly, the cavity Q was determined by:

$$Q_{u} = \frac{Q_{uo} P_{to}}{P_{po}} \times \frac{P_{p}}{P_{t}}$$
 (3.12)

Where Q_{uo} is the empty cavity unloaded Q, P_{to} is the low power empty cavity calibration input power, P_{po} is the micro-coaxial probe power reading from a particular port measured when P_{to} is the input power, P_{p} is the micro-coaxial probe reading during heating at the same port as previously, and P_{to} is the net input power during heating. P_{to} is defined in section 3.3.2 by equation 3.1 and P_{to} is similarly defined as:

$$P_{to} - P_{io} - P_{ro}$$
. (3.13)

where P_{io} and P_{ro} are the incident and reflected powers during empty cavity low power calibration.

This method of cavity Q measurement rests on the assumption that the change in the radial electric field patterns at the wall from the empty cavity case to the case when materials are introduced is negligible.

Under those conditions the ratio of the power dissipated in the wall to

the square of the radial electric field measured at a point on the wall is constant for both the loaded and the unloaded cavity. If P_b is the power dissipated in the wall for the loaded cavity and P_{bo} is the power dissipated in the wall for the unloaded cavity this relation can be expressed as,

$$P_b/P_p - P_{bo}/P_{po} - Const.$$
 (3.14)

For materials of large size or large dielectric constant, and for certain electromagnetic modes, this assumption may not hold. The materials used in the experiments presented here however, necessitated changes in L_s of no more than 3 mm for the lossiest material, water, and less than 1 mm for nylon. These shifts are only about 2% of the total cavity length. In addition, the empty cavity field pattern adjacent to the cavity wall for the TM₀₁₂ mode, which was the mode used for the heating experiments, is almost spatially identical to the field pattern adjacent to the cavity wall when coaxial material loads are present. Therefore, the z variation in the pattern of the radial fields for these material loads was assumed to be negligible.

It is important when measuring Q by this method not to move the micro-coaxial field probe between calibration and the measurement of the fields during the experiment. When the micro-coaxial field probe is moved between readings, it exhibits a variability which is probably greater than the actual radial field pattern variation due to a material load. Leaving it in one port eliminates that source of error.

All high power experiments were done using the TM_{012} mode. First, by sweeping the empty cavity Q_{10} was obtained. Then low power empty cavity

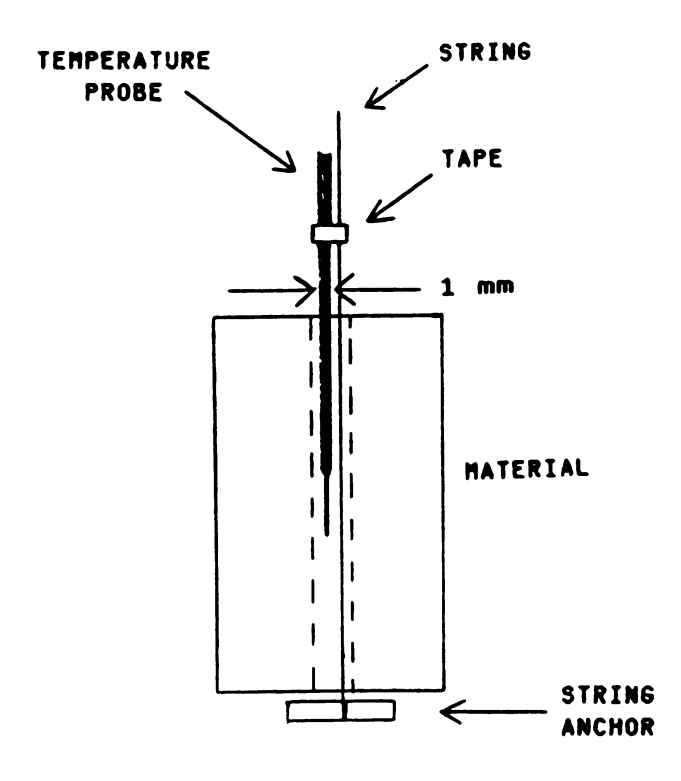


Figure 3.12 Temperature Probe Placement In Small Cylinders

CW measurements of P_{to} and P_{po} were made. P_{to} was typically on the order of 5 mW while P_{po} was typically on the order of 0.10 mW. The sample was then lowered into the cavity on a cotton thread which ran through a hole along the axis of the sample. Then the power was amplified by a TWT microwave amplifier to provide a P_{t} of 0.5 W to 10 W. Each heating experiment was performed with a constant incident power level and since the cavity was constantly adjusted to matched condition the power absorbed in the cavity, P_{t} , was held constant. As time was monitored, the temperature of the load material was measured using a Fluoroptic Temperature measurement system. As is shown in Figure 3.12, the optical probe was placed in the center of the material parallel to the thread used to suspend the sample.

During the experiment, L_s and L_p were manually adjusted to maintain minimum reflected power, indicating that the cavity was impedance matched to the external circuit. All data was recorded when the cavity was matched. After the heating was complete, the material was removed from the cavity. Then the empty cavity parameters L_s and L_p were adjusted back to each recorded setting and an empty cavity resonant frequency, f_o , was measured for each one. The measurements of f_o after heating and cavity Q during heating made it possible to calculate from perturbation theory both the real and imaginary parts of the dielectric constant of the material for each temperature recorded.

3.4.2.2.1 Nylon

The measured variation of complex dielectric constant of nylon 66 for two experiments of constant input powers of 3 W and 5 W is plotted in Figures 3.13 and 3.14. The nylon cylinder loads were 0.5 inches in diameter and 3 cm in length. The measurements are also compared in Figures 3.13 and 3.14 with published data. In these plots, as well as for those in the remainder of the seven inch cavity experimental results, each data point represents one minute elapsed time from the previous data point.

An explanation for the measured drop in the real part of the dielectric constant at higher temperatures seen in Figure 3.13 may be that the coupling probe had a greater effect on the empty cavity resonant frequency than expected. As the imaginary part of the nylon increases during heating, the coupling probe must be adjusted inward in order to maintain a match. Therefore, when $f_{_{\rm O}}$ is measured at the end of the experiment by returning the empty cavity to the various combinations of $L_{_{\rm S}}$ and $L_{_{\rm D}}$ that occured during heating, the input probe penetrates farther

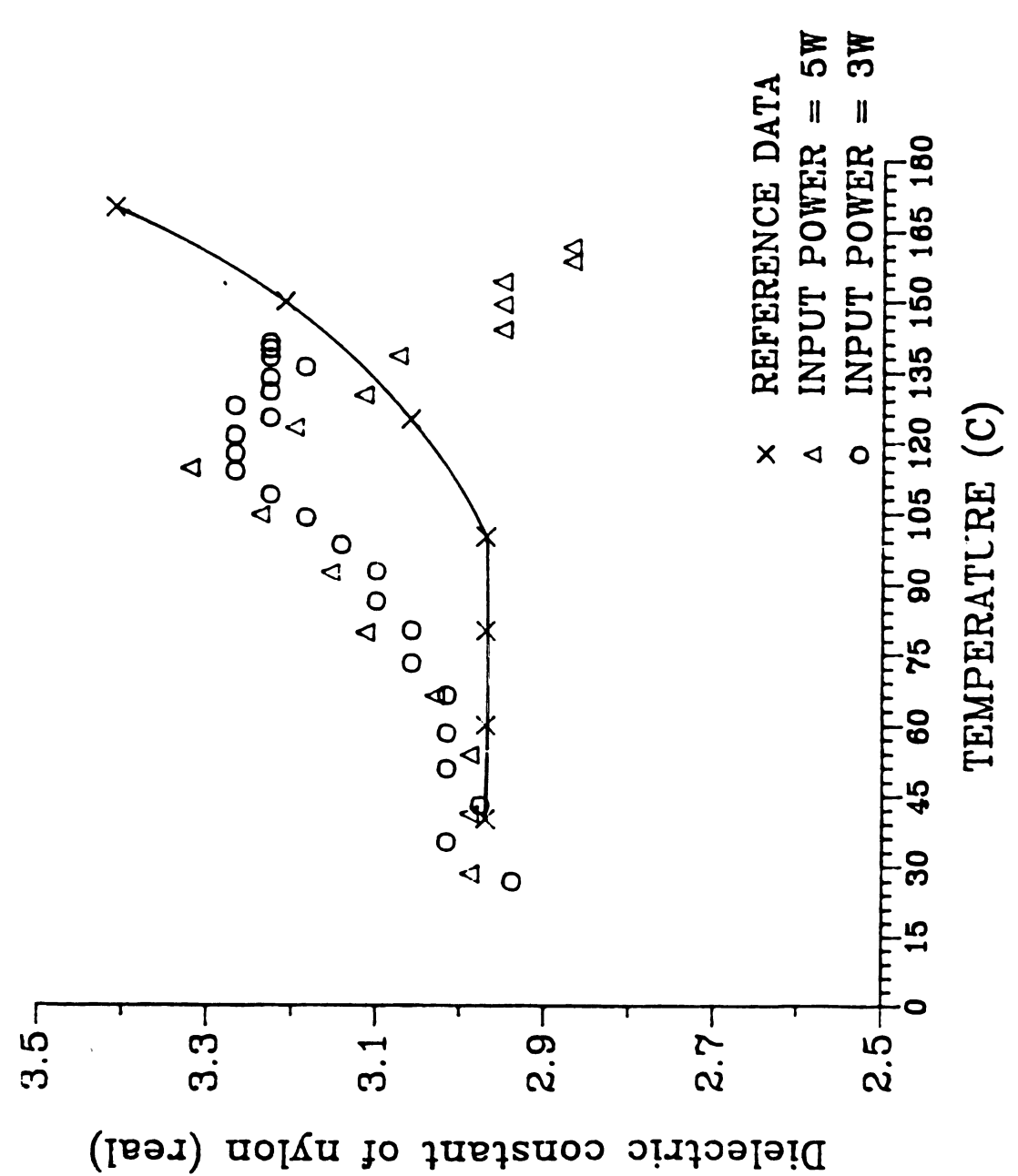


Figure 3.13 Real Dielectric Constant Of Nylon Versus Temperature

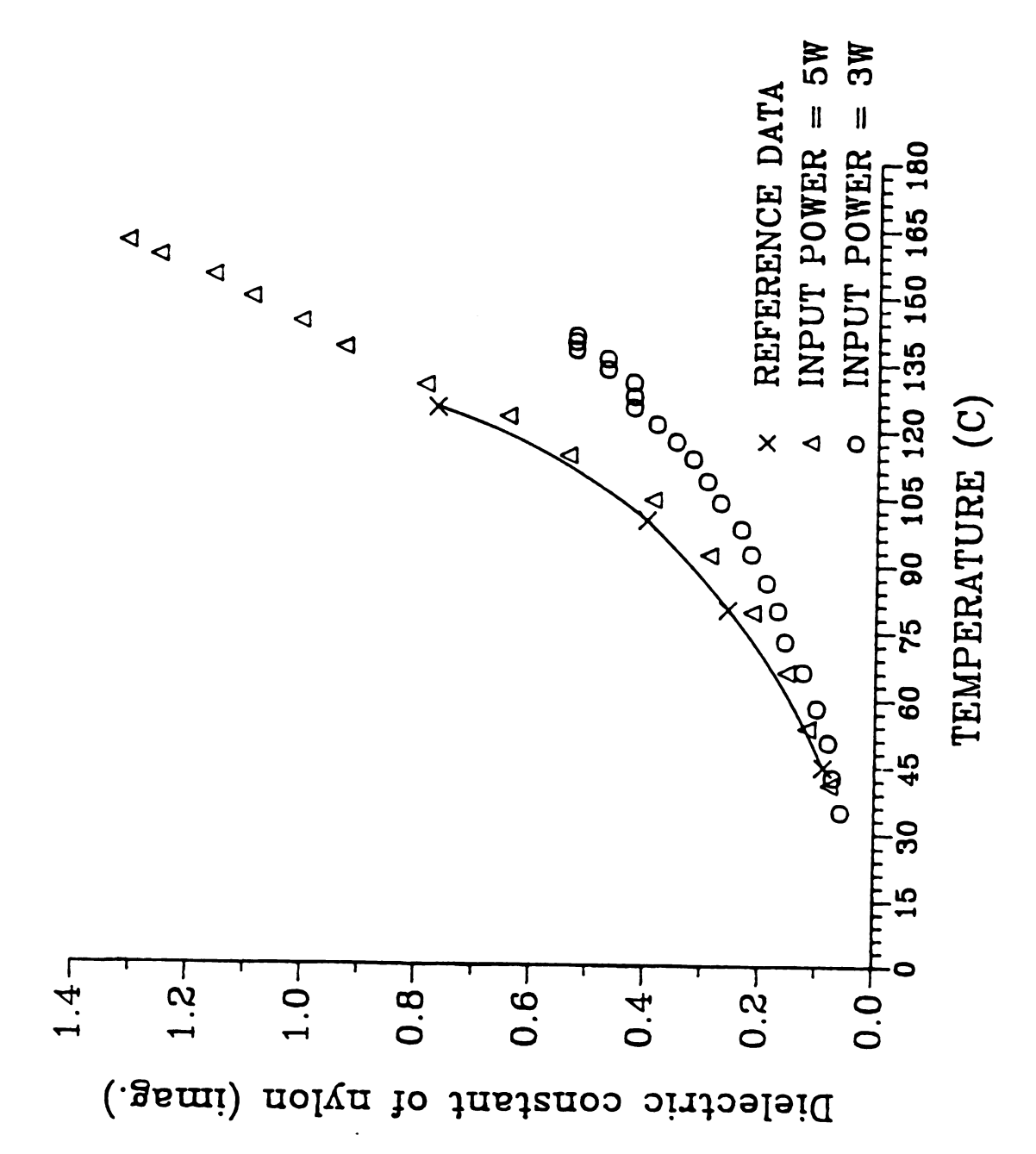


Figure 3.14 Imaginary Dielectric Constant of Nylon Versus Temperature

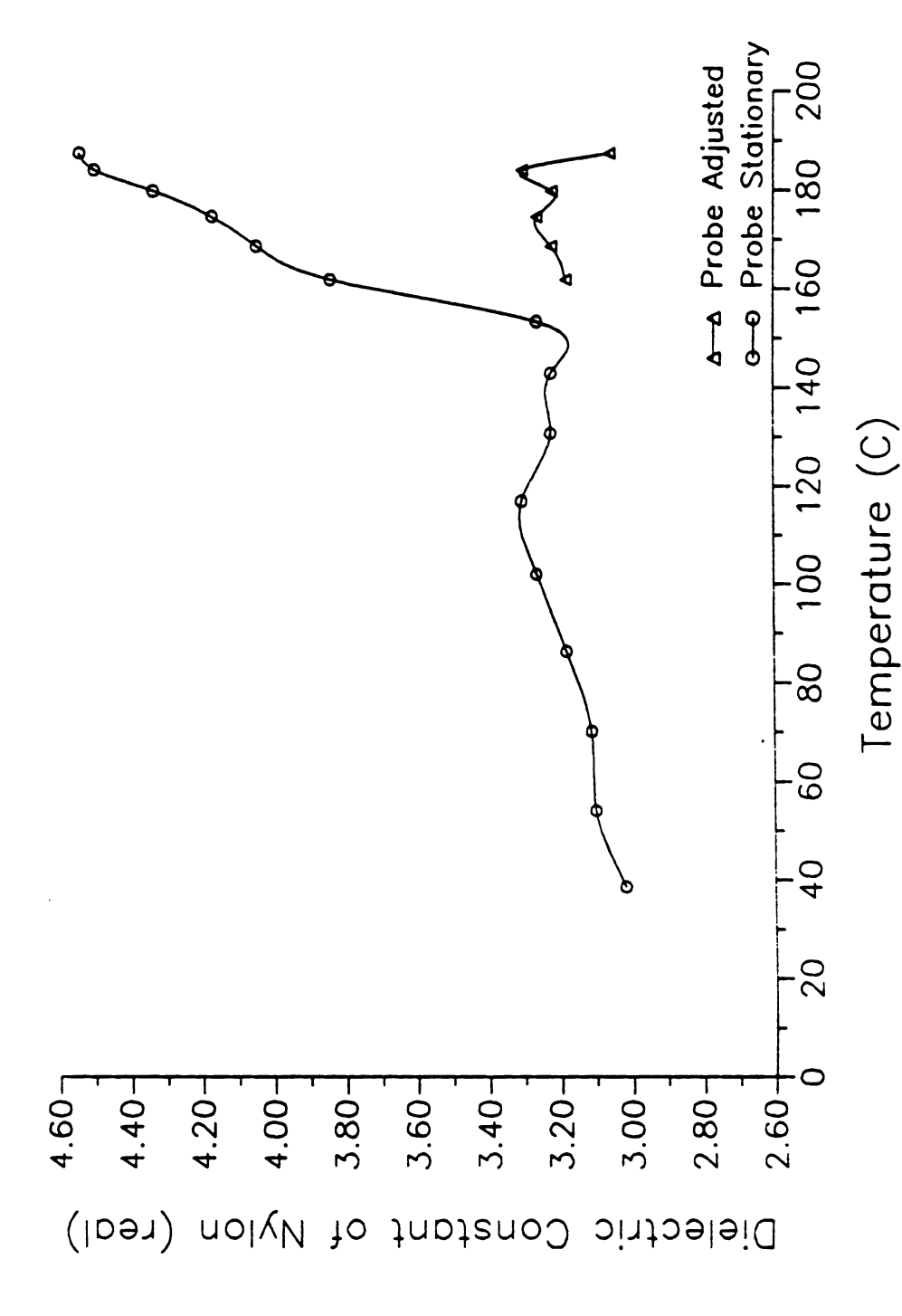


Figure 3.15 Real Dielectric Constant Of Nylon Measured With The Coupling Probe Stationary

into the cavity than it would if it were being adjusted for empty cavity match. Since the frequency dependence is strongly related to $L_{\rm g}$, small variation in the probe penetration should not affect the calculation of the dielectric constant. However, larger variations in the probe penetration may cause the drop that is observed in Figure 3.13 contrary to other published findings. 49

If the input probe is left at a median position during the final measurements of f_0 instead of being adjusted deeper and deeper as the warming of the material load requires, then the empty cavity resonant frequency gets larger with increasing temperature. The calculated dielectric constant would then get larger as well. Figure 3.15 demonstrates this effect. At the end of the heating period when the nylon was removed from the cavity, f_0 was measured as usual until the L_s , L_p combination corresponding to the reading at 9 minutes and a temperature of 150 °C was reached. After this point the input probe was left in place as L_s alone was adjusted to its former positions and f_0 was measured.

A perturbation analysis which takes into account the coupling probe during the heating and subsequent empty cavity frequency measurement, or an exact solution to the problem would provide a means of determining how the coupling probe affects the measurement of the dielectric constant.

Another calculation of interest is the coupling efficiency of the cavity-material system. The coupling efficiency is defined as the percent of P_{t} which is dissipated in the material load. The rest of the power is dissipated in the cavity walls or coupling probe. Since heating materials efficiently is always important, a high coupling efficiency is desireable.

If the energy dissipated in the material is defined as P_a and the power dissipated in the walls as P_b , then $P_t = P_a + P_b$. Therefore, the

coupling efficiency can be expressed as

Eff = 100% x
$$\frac{P_a}{P_a + P_b}$$
 = 100% x $[1 - \frac{P_b}{P_a + P_b}]$. (3.15)

Equation 3.15 can be related to the cavity quality factor in the following manner. Using equations 3.12 and 3.14, and remembering $P_{bo}-P_{to}$,

$$\frac{P_{b}}{P_{a} + P_{b}} = \frac{P_{p} \times P_{bo}/P_{po}}{P_{a} + P_{b}} = \frac{P_{p} \times P_{to}/P_{po}}{P_{a} + P_{b}} = \frac{P_{p}}{P_{t}} \times \frac{P_{to}}{P_{po}} = \frac{Q_{u}}{Q_{uo}}$$
(3.16)

Hence, the coupling efficiency is given by,

Eff = 100% x
$$[1 - \frac{Q_u}{Q_{uo}}]$$
. (3.17)

The measured coupling efficiency for nylon is shown in Figure 3.16.

Comparing Figure 3.15 with 3.16 shows that as the lossy part of the dielectric constant increases so does the coupling efficiency, as would be expected.

3.4.2.2.2 Wet Wood

Similar experiments were performed on cylinders of water-soaked wood dowels made of birch or poplar 0.91 cm in diameter and approximately 2 cm in length. These experiments were done exactly the same way as the nylon 66 experiments with the additional measurement of the initial and final weights of the wet wood to determine the amount of water driven from the samples during heating. Since water has a relatively high dielectric constant, ~77+j12, ⁵⁰ compared to dry birch, ~2+j0.2, ⁵¹ as the sample dried the dielectric constant decreased. Figures 3.17 and 3.18 are plots of the

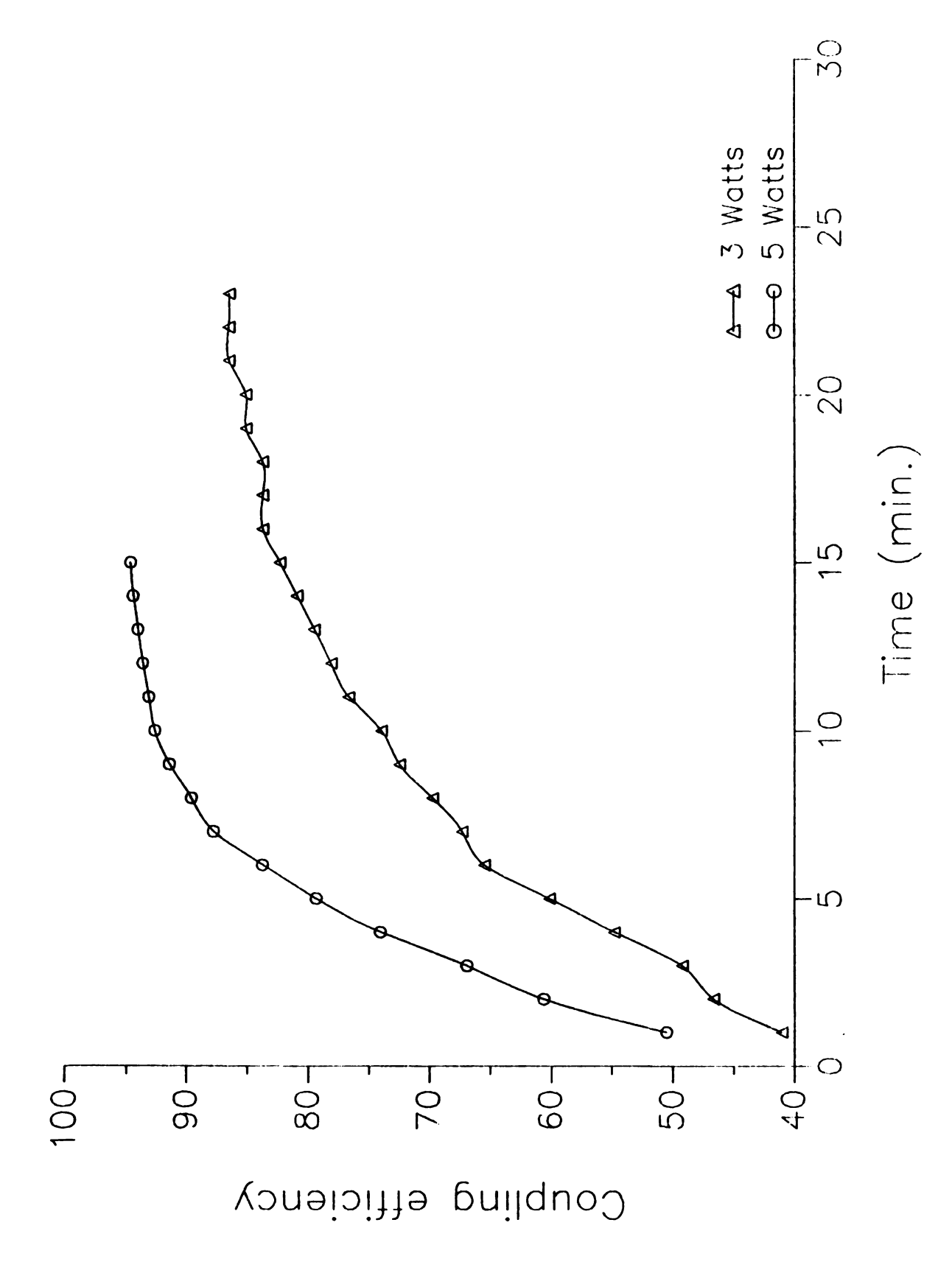


Figure 3.16 Coupling Efficiency Of Nylon Versus Temperature

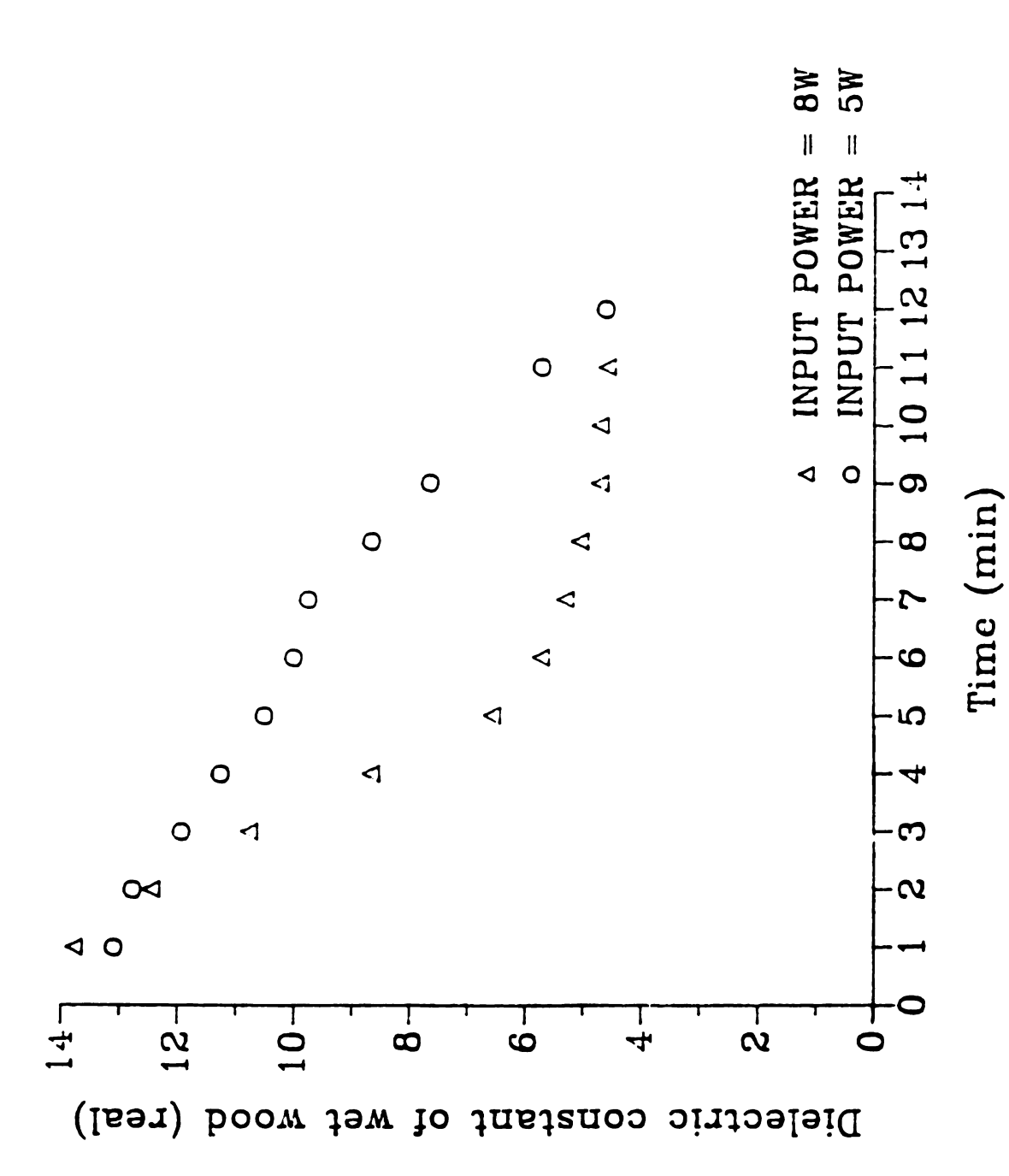


Figure 3.17 Real Dielectric Constant of Wet Wood Versus Time

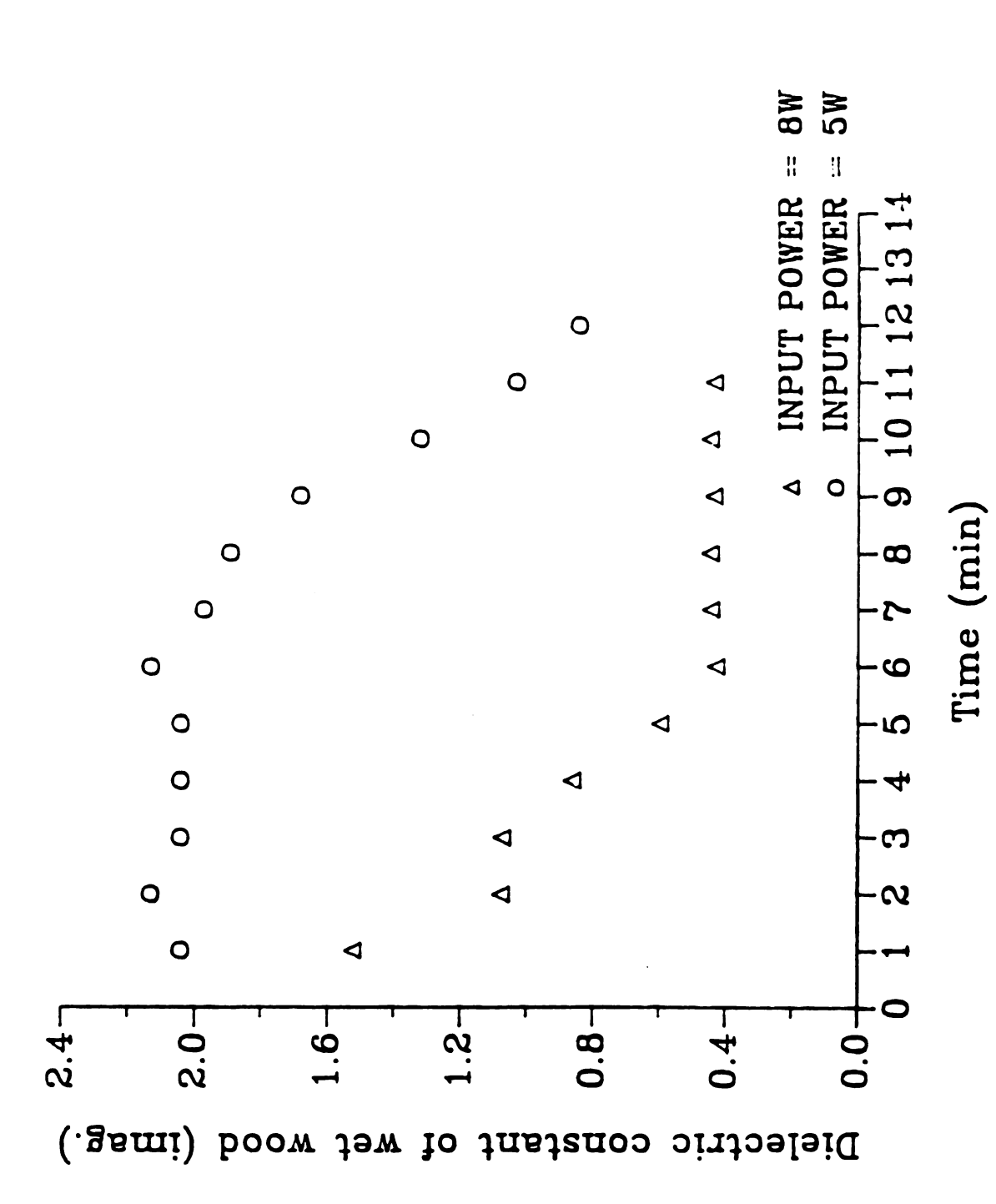


Figure 3.18 Imaginary Dielectric Constant Of Wet Wood Versus Time

complex dielectric constants of the wet wood versus time for two experiments using constant input powers of 5 W and 8 W respectively.

Using equation 3.17, the coupling efficiency for the wet wood was also calculated. Figure 3.19 is a plot of the coupling efficiency of the system for the wet wood samples. Both the experiments with nylon and wet wood show that coupling efficiencies of more than 90% are possible for even moderately low loss materials.

The measurement of the initial and final weights of the wet wood samples made it possible to determine the drying efficiency of heating the wet wood in the seven inch applicator. Knowing that it requires 4.177 J/gm-°C to heat water up to boiling and 2.257x10³ J/gm to vaporize it, the amount of energy absorbed by the water in the wet wood samples could be determined.

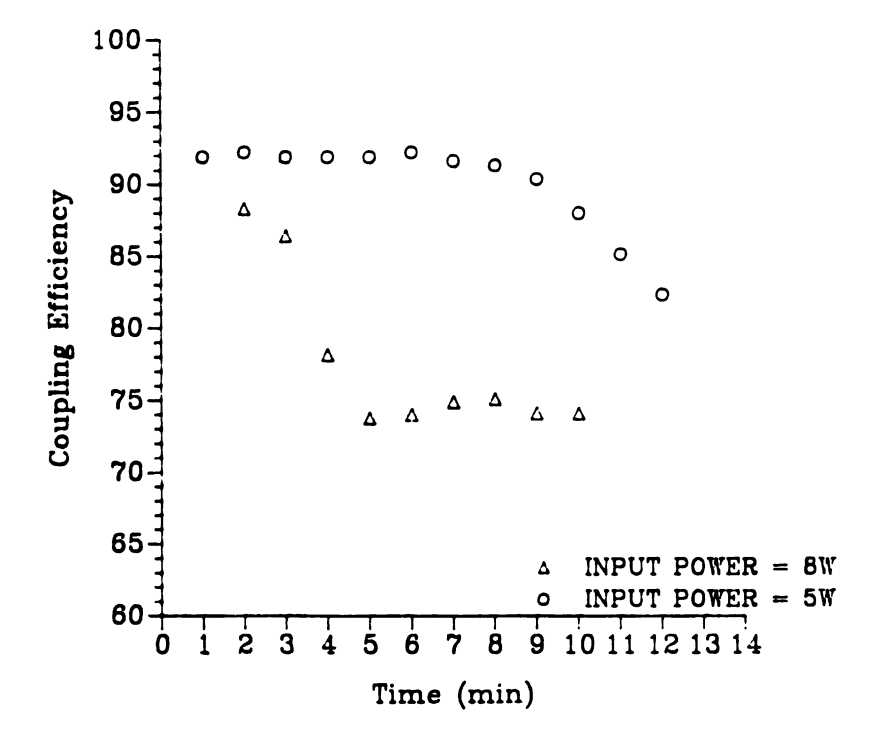


Figure 3.19 Coupling Efficiency Of Wet Wood Versus Time

The initial weight of the water-soaked piece used in the 5 W experiment was 2.102 gm while the final weight was 1.357 gm. From the graph of real dielectric constant versus time it appears that the wood in the 5 W experiment was dry after about 12 minutes. The average P_t during those 12 minutes was 4.97 W. Begining with a room temperature of 25 °C it required 1915 J to vaporize the 0.745 gm of water. The efficiency of drying the wood was then 53.5%. For the 8 W experiment the efficiency of vaporizing 0.720 gm of water from a sample which initially weighed 1.727 gm, assuming from the data on the dielectric constant that the wood was dry at the 6 minute mark, is 66.2%.

A conventional figure of merit for the drying efficiency of water extraction systems is the Specific Consumption (SC), which is defined as the amount of energy in kWh required to remove 1 kg of water from a sample. The 5 W experiment then demonstrated an SC of 1.33 kWh/kg while the 8 W experiment demonstrated an SC of 1.10 kWh/kg.

3.4.2.2.3 Water

Distilled water held in a quartz tube 5 cm in length, wall thickness 1 mm, and inside diameter 4.5 mm was suspended in the center of the cavity. The high dielectric constant of water, approximately 77-j12 at room temperature and 2.45 GHz, makes perturbation calculations for dielectric constants of samples of this size inaccurate. With much smaller samples, good measurements have been made using perturbation methods. Smaller sample size, however, requires accurate volume measurement instrumentation and very thin walled containers for the water in order for the container not to present a greater perturbation than the fluid it contains. Since our primary object was not to measure dielectric

constants, but to develop a controlled processing apparatus, these precision measurement capabilities were not explored.

Using input powers of 1 W, 1.5 W, and 2 W, three experiments were performed with water sample loads which filled the tube to approximately 4.15 cm, corresponding to measured weights of between 0.64 and 0.67 gm. The perturbation calculation of the dielectric constant revealed the disparity between actual values and perturbation results for such high permittivity materials. This difference is more apparent for our method in the measurement of the real part of the permittivity than for the imaginary part. This is probably due to the frequency shift perturbation introduced by the coupling probe as discussed in the results for nylon. As can be seen in Figure 3.20, the results for the real dielectric constant were in better accord with published data ⁵² in the latter part of the experiment when the coupling probe did not penetrate as far into the cavity. However, since the dielectric constant of water is so high, the disagreement between the perturbation measurement and the published data may simply be due to the inaccuracy of the perturbation method in this permittivity range.

The imaginary part of the permittivity measurement is dependent on micro-coaxial probe readings taken during heating and is more consistent with published data. Figures 3.20 and 3.21 are graphs of the real and imaginary parts of the measured relative dielectric constant of water versus temperature with reference data plotted for comparison.

3.4.2.2.4 Silicone Rubber

A cylinder of blue silicone rubber, RTV-664 cured at 120 °C for two hours, 1.1 cm in diameter and 2.94 cm in length was tested in the cavity in order to determine if it would be a good container for samples of epoxy

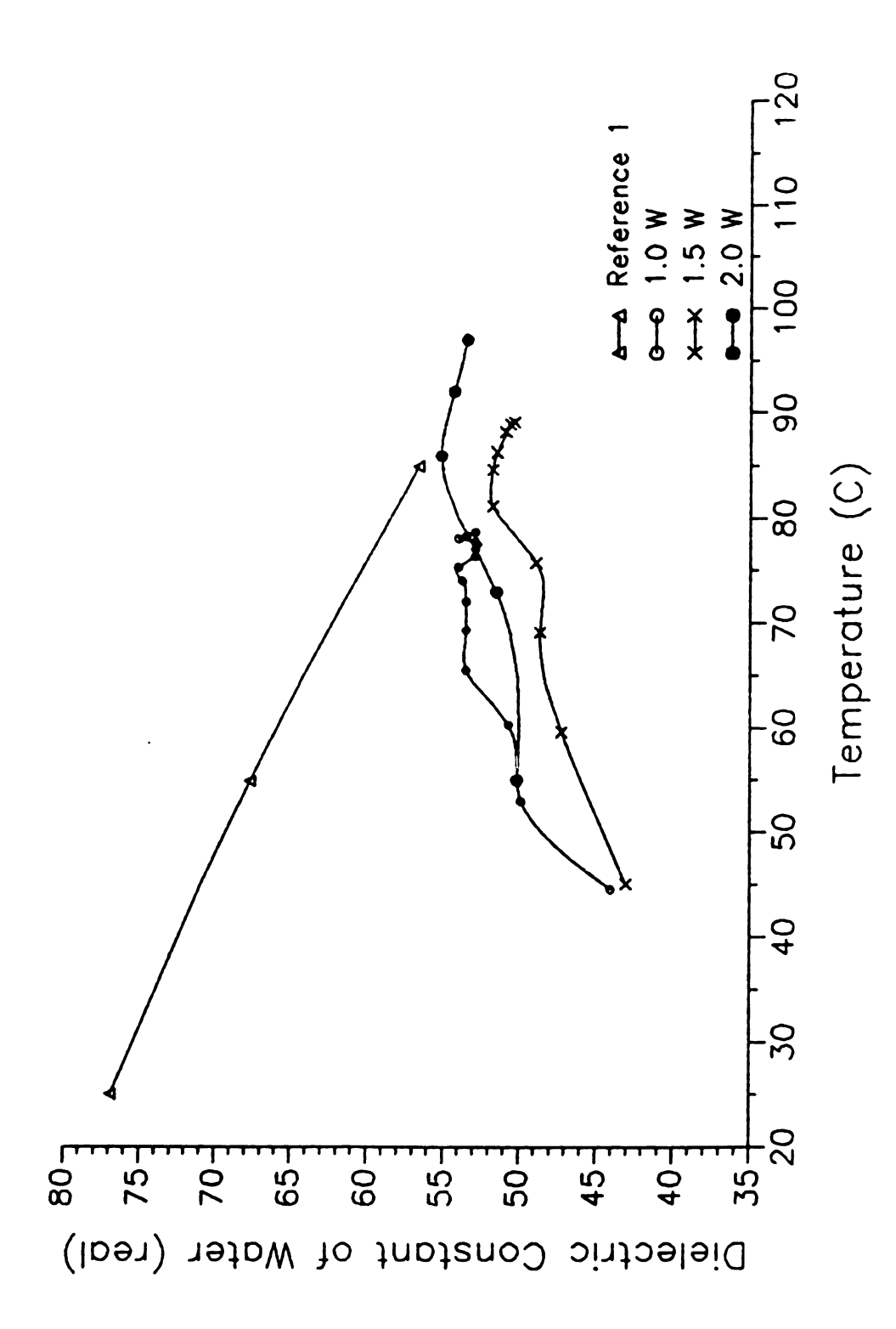
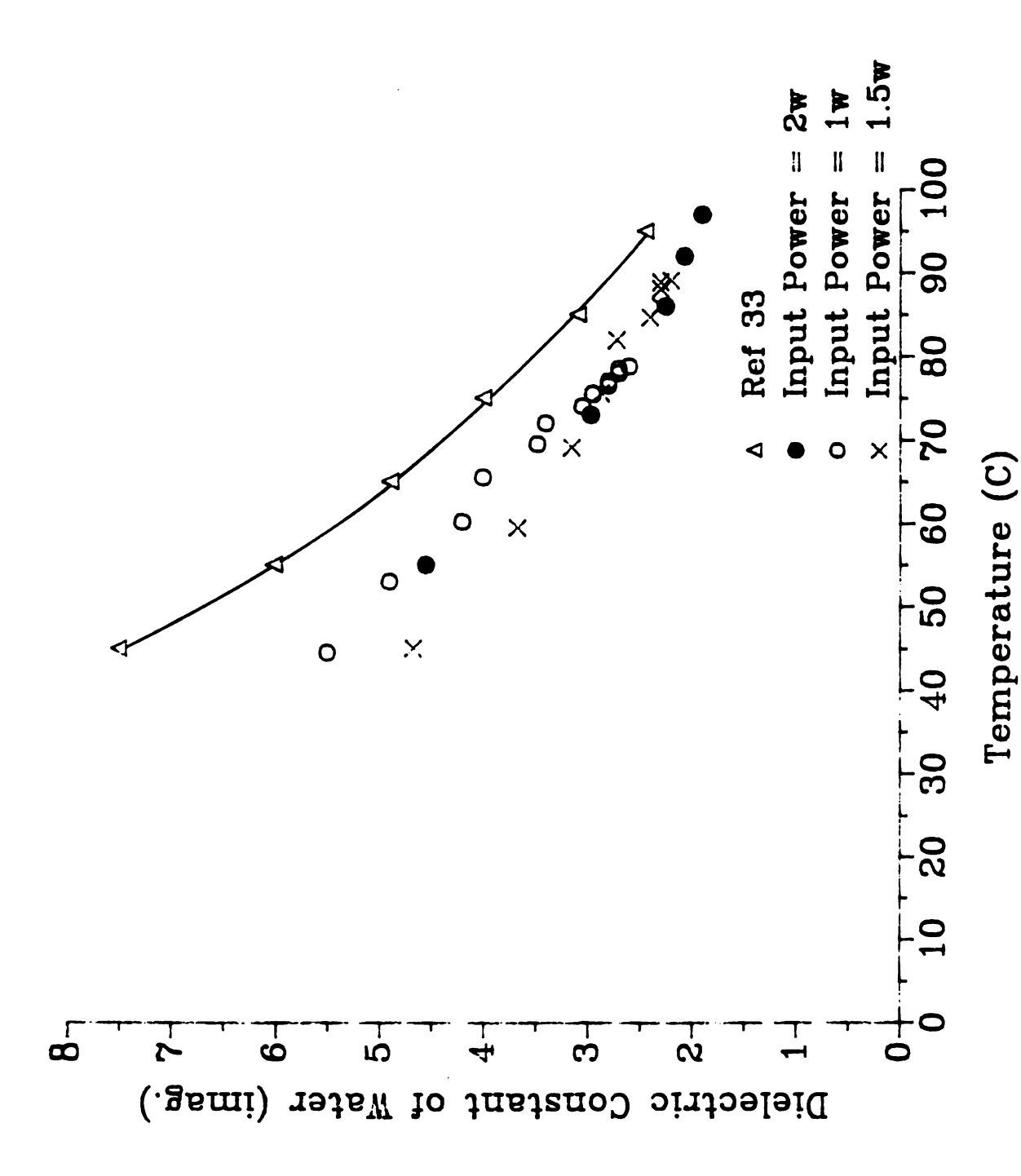


Figure 3.20 Real Dielectric Constant Of Water Calculated By Perturbation Methods Versus Temperature



Imaginary Dielectric Constant of Water Calculated By Perturbation Methods Versus Temperature Figure 3.21

undergoing microwave curing. Silicone rubber was chosen because it is pliable and cured epoxy samples can be easily removed by bending portions of the silicone rubber container away from the epoxy. The testing involved measurement of the complex permittivity versus temperature by perturbation methods. Figures 3.22 and 3.23 are plots of the results of those measurements.

These measurements reveal that silicone rubber is a good candidate for the epoxy molds. Although at room temperature both the real and imaginary parts of the permittivity are similar to nylon 66, as the temperature increases the permittivity of silicone rubber goes down, as opposed to nylon, whose permittivity goes up with increasing temperature. A material whose permittivity increases with temperature may exhibit thermal run away. That is, as the material's temperature increases it becomes lossier and therefore absorbs more and more energy which in turn gives rise to very great material temperatures in a relatively short time. These measurements indicate that silicone rubber molds are not likely to absorb much of the microwave energy as temperature increases. This property is important for microwave curing of the contained material in order that the container not absorb the microwave energy and heat the material by conduction instead of by the electromagnetic field in the cavity.

3.5 Six Inch Applicator Description

The six inch applicator is a resonant cavity very similar to the seven inch applicator described in Section 3.2. The six inch applicator, referred to as the diagnostic cavity by L. Frasch, was designed to minimize cavity imperfections due to the coupling probe, screened viewing

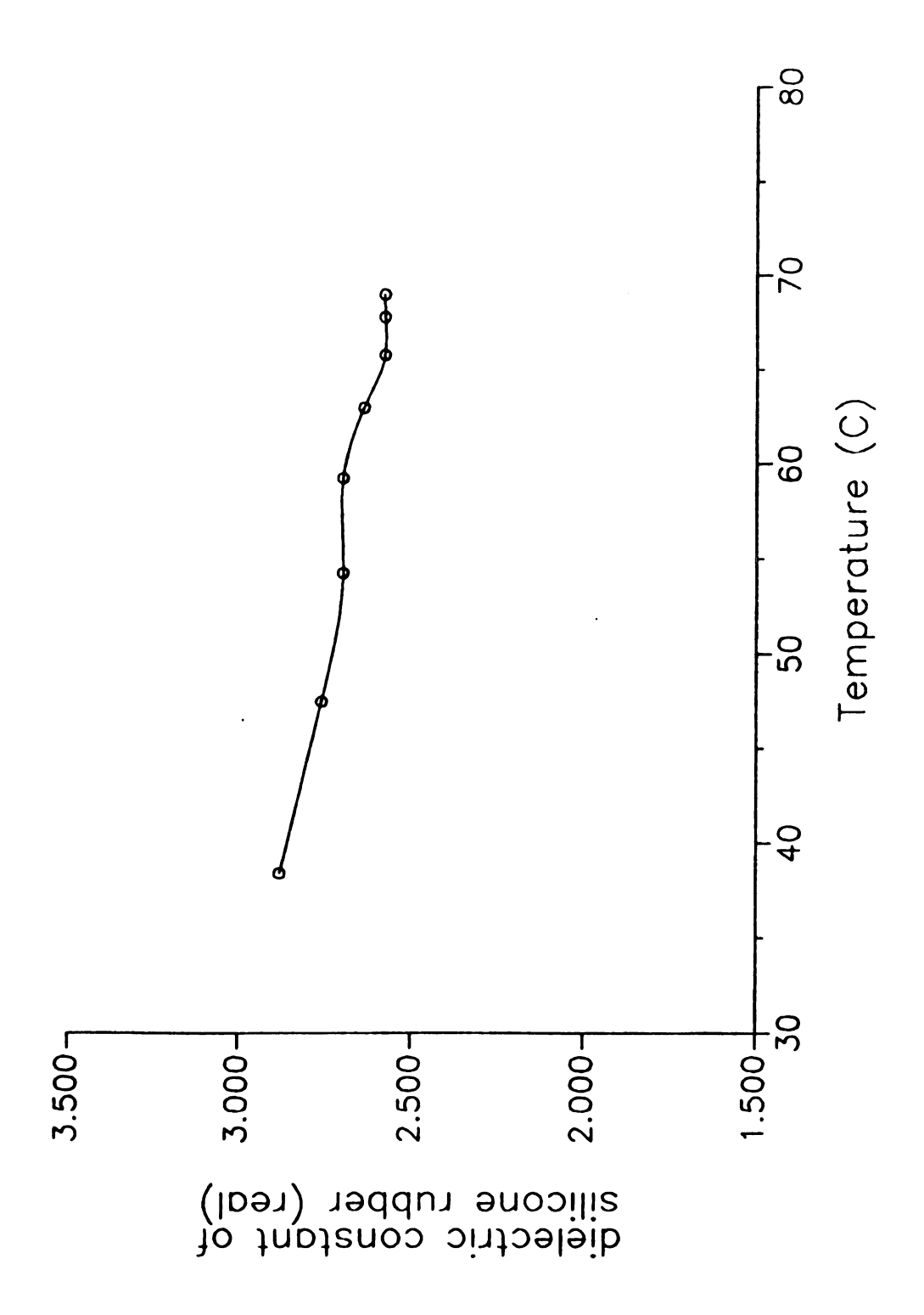


Figure 3.22 Real Dielectric Constant Of Silicone Rubber Versus Temperature

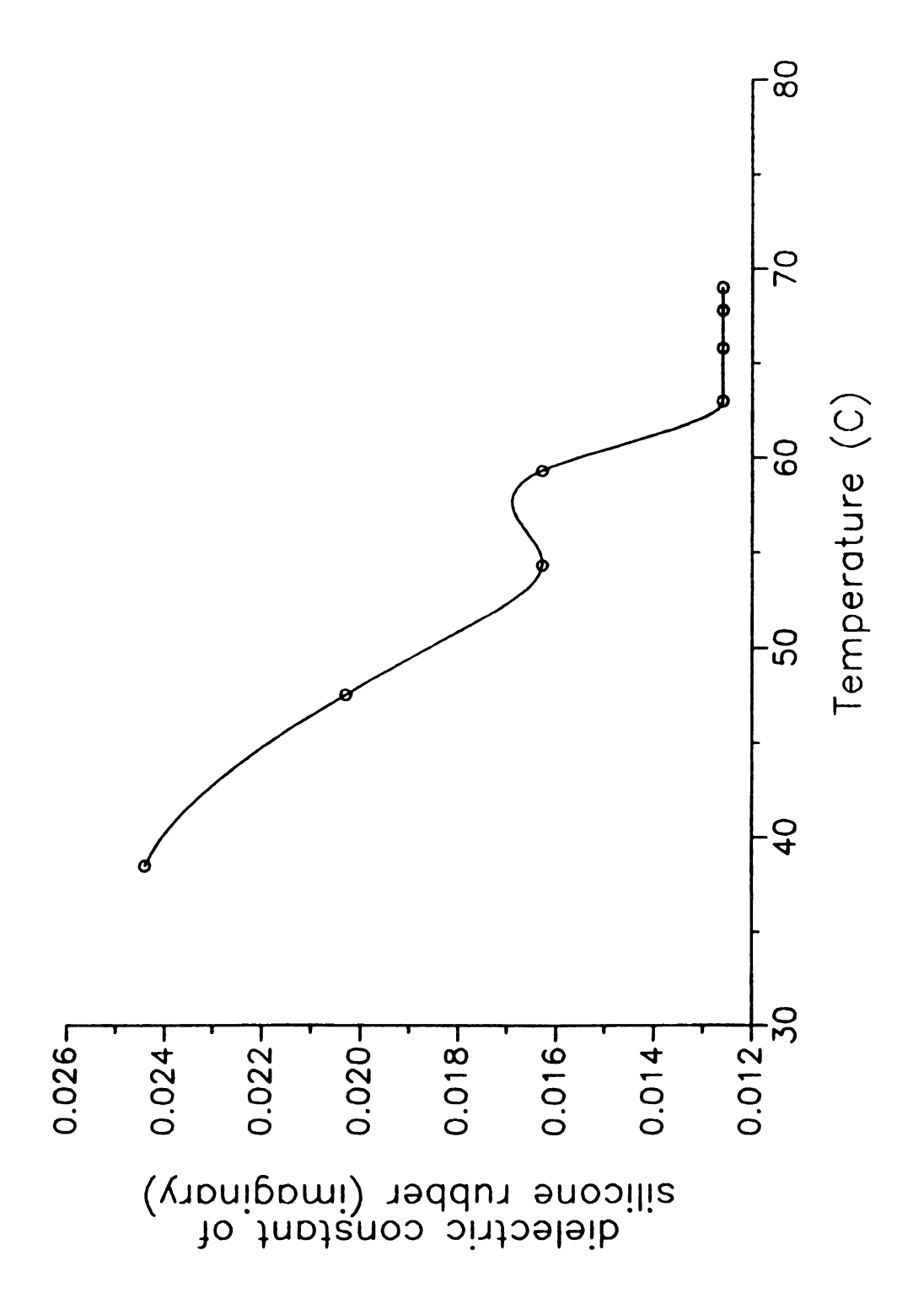


Figure 3.23 Imaginary Dielectric Constant Of Silicone Rubber Versus Temperature

window, and other holes in the cavity. With the diagnostic cavity measurements can be more carefully compared with theory. The cavity, designed by L. Frasch, is described in detail in his doctoral dissertation. 53 Thus, only a brief description will be given here.

The diagnostic cavity consists of a length of six inch diameter circular cylidrical waveguide with two shorting plates on either end. Both the waveguide and shorting plates are made of brass. The waveguide has a six inch inside diameter. One of the shorting plates, referred to as the cavity bottom, is fixed to the end of the waveguide with silver solder. The other shorting plate, referred to as the sliding short, is adjustable in a manner similar to the adjustment of the sliding short of the seven inch cavity, maintaining electrical contact with the waveguide by means of silver finger stock. These general features are similar to those illustrated in Figure 3.1 for the seven inch cavity. A detailed cutaway view of the diagnostic cavity is reproduced from L. Frasch's dissertation in Figure 3.24.

As shown in Figure 3.24, the diagnostic cavity differs from the seven inch cavity in a number of ways. The hole in the top shorting plate of the six inch cavity is only one inch in diameter. There is no large hole in the bottom shorting plate. In place of the hole in the bottom shorting plate are three very shallow concentric holes of diameters 0.25 inches, 0.5 inches, and 1.0 inches. These holes were used for the accurate coaxial positioning of the bottoms of rods in the cavity. Collars (not shown in Figure 3.24) with holes in the centers of diameters 0.25 inches and 0.5 inches were made to fit in the hole in the top shorting plate when rods of those diameters were inserted in the cavity.

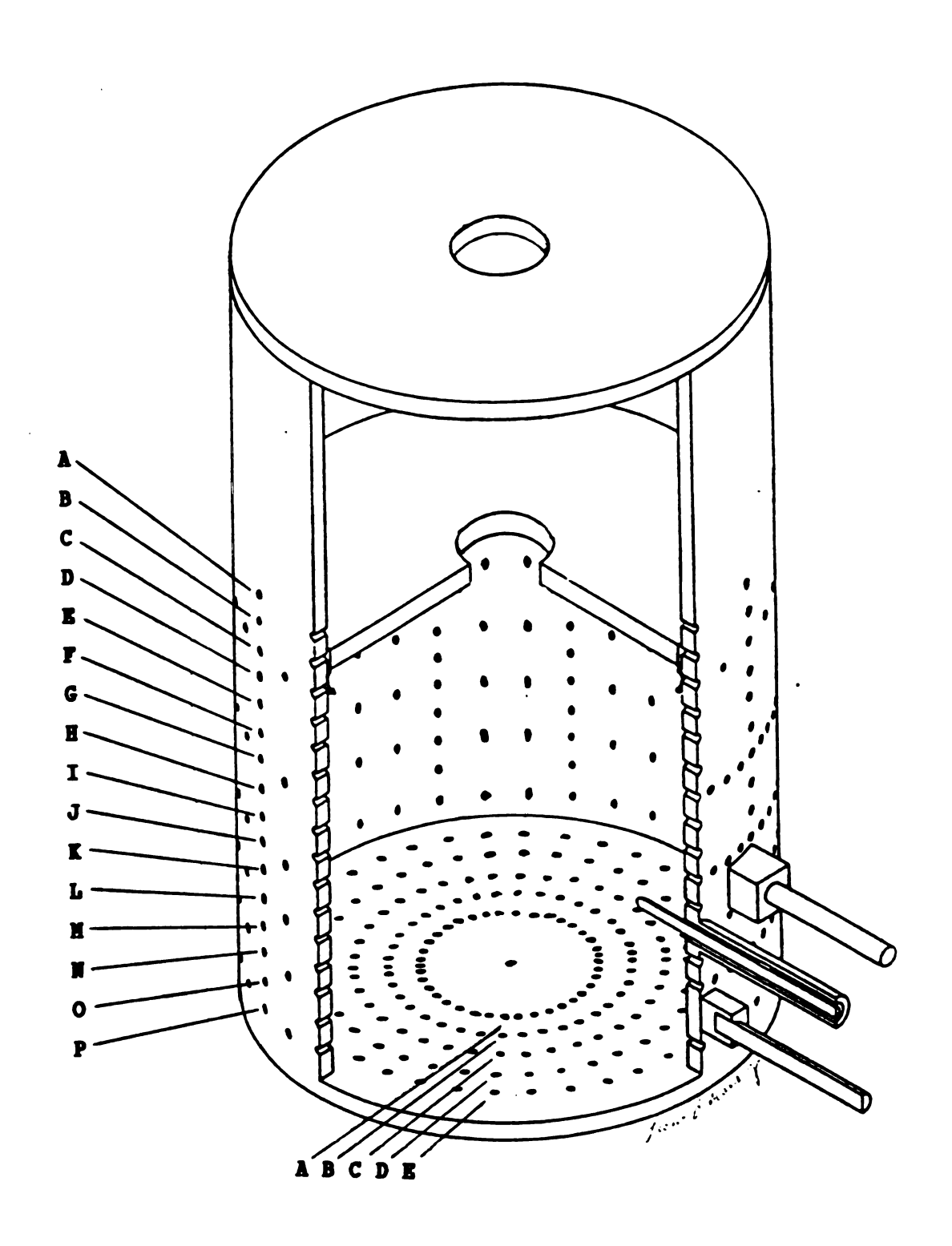


Figure 3.24 Cutaway Drawing Of The Six Inch Applicator

The input power coupling probe is smaller than the coupling probe for the seven inch cavity. It has a probe diameter of only 0.20 cm and an inside port diameter of 0.67 cm. There is no screened window in the cavity wall. As shown in Figure 3.24, diagnostic ports approximately 2 mm in diameter for the micro-coaxial field probe were drilled circumferentially around the cavity at 16 levels equally spaced at 0.953 cm apart beginning at 1.575 cm from the cavity bottom. As shown in Figure 3.24, The rows are labeled A through P with P being nearest the bottom. The port diameter is approximately 2 mm. To accommodate micro-coaxial field probe measurements without the use of field probe blocks all around the cavity, the cavity walls were made 0.25 inches thick. Diagnostic ports were also drilled in the cavity bottom in 5 rings labeled A through E at radii 2.225, 3.294, 4.445, 5.398, and 6.350 cm respectively. The ports were spaced 10° apart in each ring. A single diagnostic port was also drilled in the center of the bottom plate.

3.6 System Configuration For The Six Inch Applicator

The system configuration of the six inch applicator system was identical to the configuration of the seven inch system except that for experiments requiring powers of less than 1 W, the Varian VA-1356 TWT amplifier was replaced by an HP 491C TWT amplifier with a maximum power output of approximately 600 mW. In addition, a more extensive microcoaxial field measurement capability was incorporated. It provided the capability to make many more measurements at a variety of locations on the cavity wall, and these were measured with a more accurate HP 438A digital power meter equipped with an HP 8481H 0-3 W power sensor. The

micro-coaxial probe and measurement techniques are described in greater detail by Frasch. 54

Measurements of cavity parameters L_s and L_p using sensitive (0.01 mm accuracy) dial indicators, input and reflected powers, cavity Q measurements, and material load temperatures were made just as with the seven inch system as described in Section 3.3.

3.7 Six Inch Applicator Experiments

The low power (less than 1 W) experiments performed with the six inch applicator, in addition to the empty cavity calibration measurements of eigenlength and cavity Q for different modes, included measurements of the radial electric field at the cavity wall for the empty cavity, similar measurements for the cavity coaxially loaded with 0.5 inch diameter nylon rods of length equal to the cavity eigenlength, and permittivity measurements of 0.5 inch diameter coaxially loaded nylon and teflon rods of length equal to the cavity eigenlength using perturbation methods.

Higher power (1 W to 5 W) experiments were focussed on temperature measurements of load materials versus time for various input powers using the TM₀₁₂ mode. Load materials were cavity length rods of nylon of diameters 0.5 inches and 1.0 inches. Temperatures were measured at the centers of the samples for the 0.5 inch rods with the temperature probe located as shown in Figure 3.25. For the 1.0 inch rods temperatures were measured at the center, surface, and half-radius position of the rod with the temperature probe placed in the material through the holes shown in Figure 3.28. Temperature measurements of the input coupling probe at various distances from the tip were also taken.

Mode	Ls(th.)	Ls(ex.) (cm)	Lp (mm)	Q(th.)	Q(th.) Q(ex.)	
TM011	7.756	7.849	0.811	10,032	6,622	
TE211	9.789	9.908	0.537	15,110	10,889	
TE112	13.868	13.948	0.813	19,883	11,136	
TM012	15.513	15.659	0.868	15,001	10,208	

Table 3.5 Empty Cavity Measurements of L and Q For Several Modes In The Six Inch Cavity

3.7.1 Empty Cavity Experiments

Table 3.5 lists the measured eigenlength and cavity Q for various modes. Comparison is made with the theoretical eigenlength calculated using equation (3.3). The theoretical empty cavity Q^{55} is listed as well.

3.7.2 Loaded Cavity Experiments

Nylon rods of diameter 0.5 inches were place coaxially in the cavity excited in the TM₀₁₂ mode. Micro-coaxial field probe measurements were taken along the cavity wall at 90 away from the input power coupling probe for three different input powers, 127 mW, 184 mW, and 489 mW. Measurements were taken beginning at the point when the temperature of the nylon had reached steady state. The temperature was measured in the center of the rod with a temperature probe placed as shown in

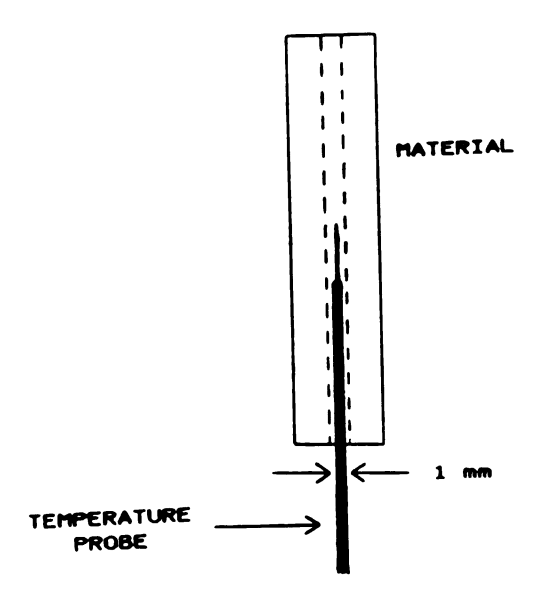


Figure 3.25 Positioning Of The Temperature Probe In The 0.5 Inch Diameter Cavity Length Nylon Rods

Figure 3.25. The temperature probe was inserted through the diagnostic port in the center of the cavity bottom and extended through the coaxial hole in the rod to a position where the tip was half way between the cavity shorting plates.

For the 127 mW experiment, the initial temperature at the center of the rod at the time readings were begun was 26.1 °C which was the final temperature as well. For the 184 mW experiment the initial temperature was 27.5 °C with the final temperature at 27.7 °C. For the 489 mW experiment the initial temperature was 33.0 °C with a final temperature of 33.2 °C. Figure 3.26 below is a plot of the results of these experiments. Referring to Figures 3.13 and 3.14, changes in the field patterns are not expected for these relatively low temperatures since the

dielectric constant of nylon is constant in this range. As Figure 3.26 demonstrates, the electromagnetic field in the cavity is a well defined standing wave under these material loading conditions.

Figure 3.26 also includes an empty cavity radial electric field pattern measurement for comparison. It can be seen in Figure 3.26 that the cavity eigenlength is less for the loaded cavity than for the empty cavity.

The dielectric constants of nylon and teflon were also calculated using perturbation theory. Rods of nylon and teflon 0.5 inches in diameter were loaded coaxially in the cavity. Frequency shift and change in cavity Q were measured in sweep mode. Measurements were taken for both TM₀₁₁ and TM₀₁₂ modes. From appendix A, equations A.14 and A.15 with d equal to L_s in equation A.16 yielded the results tabulated in Table 3.6. Comparison can be made with Table 3.4 which gives results for a similar experiment conducted in the seven inch cavity. In general, since the six inch cavity is smaller, perturbation calculations would be expected to be slightly worse for experiments done in it than for experiments done in the seven inch cavity on materials of the same size. However, since the six inch cavity is more like an ideal cavity, agreement between theory and experiment is good for the six inch system, as can be seen by examining Table 3.6.

Exploratory high power experiments were run with the same cavity loading as for the experiments which were performed for the the results of Table 3.6. Q_u was between 2500 and 3000 for the material loaded cavity at room temperature so that, from equation 3.17, 70% to 75% of input power was coupled into the material at the beginning. Although Q_u was not monitored during heating, it is sure that coupling efficiencies increased

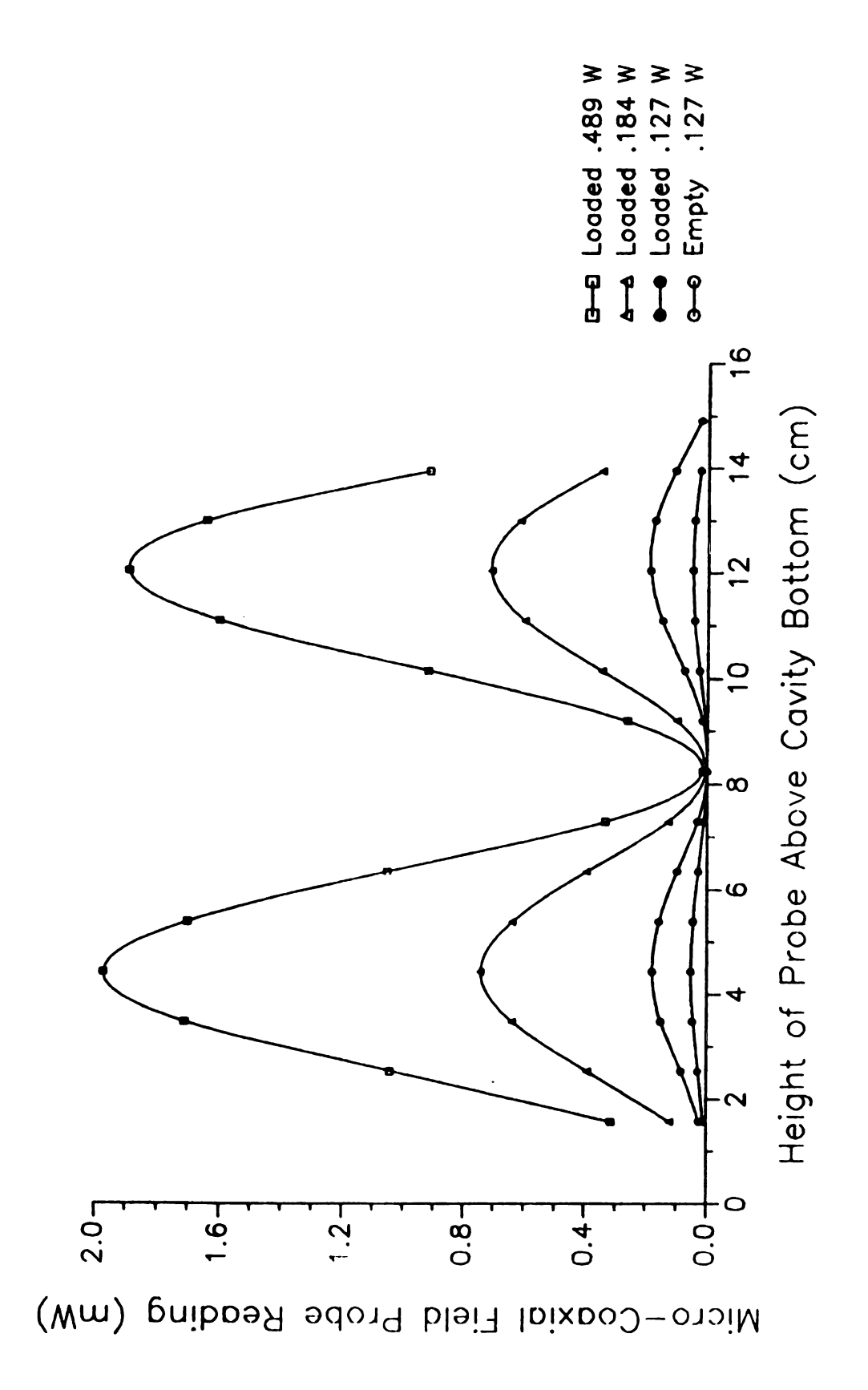


Figure 3.26 Axial Field Patterns Of Nylon Loaded Cavity Excited In The TM $_{012}$ Mode For Various Input Powers

		Experiment		Ref. Data 45		
		nylon	teflon	nylon	teflon	
ε _ι ΤΜΟ11	r'	3.121	2.046	3.03	2.1	
	r"	2.7E-2	1.9E3	3.9E-2	3.0E-4	
TM012		3.124 2.6E-2	2.065 6.3E-4			

Table 3.6 Perturbation Calculation Of Permittivities Of Nylon And Teflon For ${
m TM}_{011}$ And ${
m TM}_{012}$ Modes

during the experiment, similar to the experiments on nylon in the seven inch cavity. This, again, is due to the increase in imaginary dielectric constant of nylon with temperature. See Figures 3.14 and 3.16.

Figure 3.27 is a plot of the temperature of the nylon rod in the six inch cavity versus time. The temperature probe was in the center of the nylon rod half way between the two shorting plates as described above.

Input powers were 600 mW and 1.00 W respectively. Each data point in Figure 3.27 and in the remaining Figures in this chapter represents 30 seconds elapsed time from the previous data point.

In order to guage heating uniformity along the radius of rod shaped loads, the heating cross section of a 1.0 inch diameter nylon rod in the cavity was measured. In order to measure temperatures across the cross

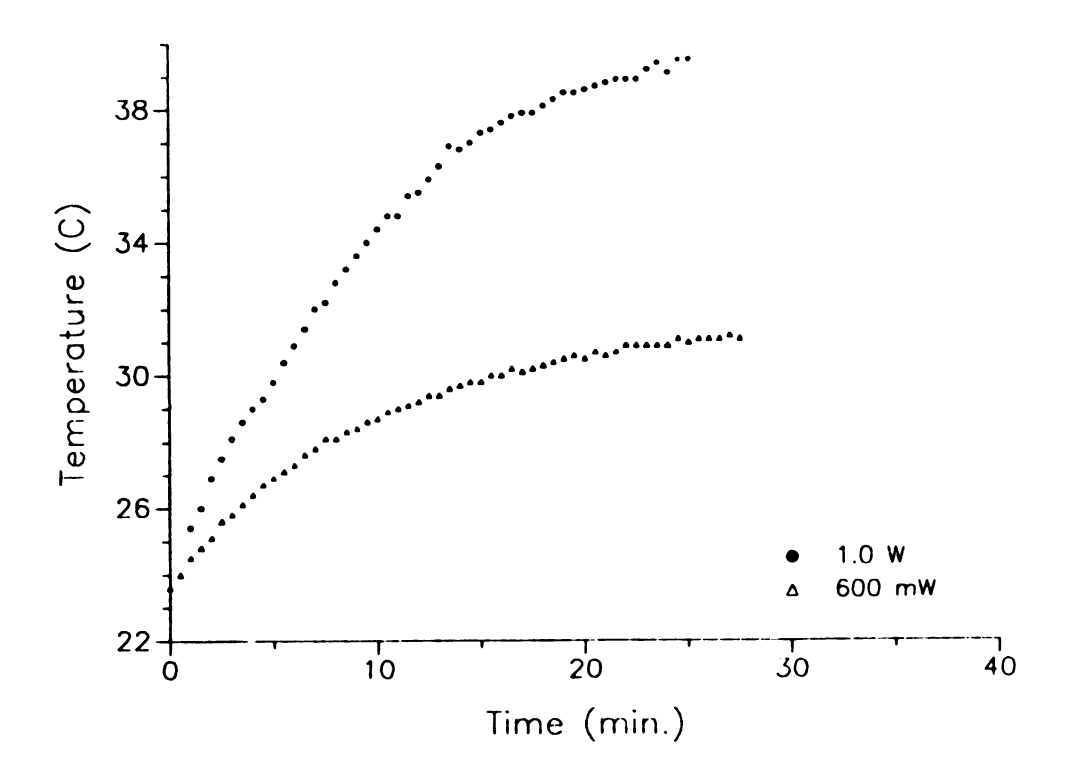


Figure 3.27 Nylon Temperature Versus Time For Input Powers Of 600 mW And 1.00 W

section of the nylon rod three holes were drilled in the rod into which fiberoptic probes were inserted. Figure 3.28 is a drawing of the rod with the holes drilled in it. A hole was drilled along the axis of the rod a distance equal to half the eigenlength of the cavity when loaded coaxially with the rod. Another hole was drilled perpendicular to the first one at the same distance from the end of the rod as the terminal point of the first hole. This second hole was 0.25 inches long, half of the radius of the rod. A third very shallow hole was drilled opposite the second hole in order to lodge a fiberoptic probe there for surface temperature measurement.

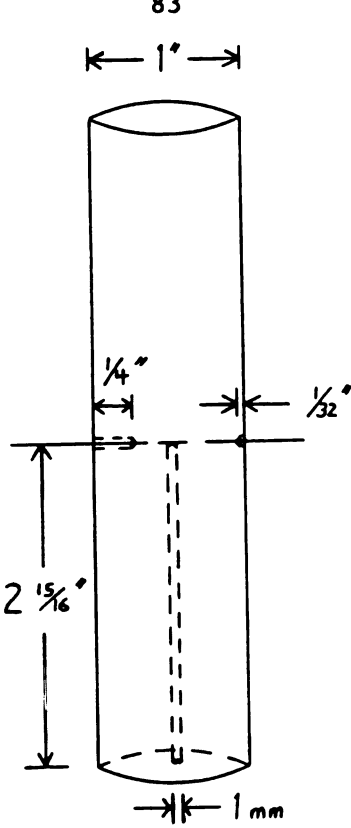


Figure 3.28 One Inch Diameter Nylon Rod With Holes For Temperature Cross Section Measurement

The fiberoptic probes were inserted through diagnostic ports in the cavity wall in order to reach the placement holes in the side of the rod. The center temperature measurement probe was inserted through the center diagnostic port in the cavity bottom into the material. The Q_u of the material loaded cavity was 961 as opposed to an empty cavity Q_{uo} of 10,208. Input power of 5.0 W was applied while temperatures and cavity Q_v by means of a micro-coaxial field probe, were monitored. Figure 3.29 is a plot of the temperature profile at the hottest part of the rod.

Figure 3.29 shows that heating is fairly uniform out to the midradius point. The final temperatures of the center and midradius point differ by only 3.6 $^{\circ}$ C at an average temperature of 66.7 $^{\circ}$ C. The final temperature

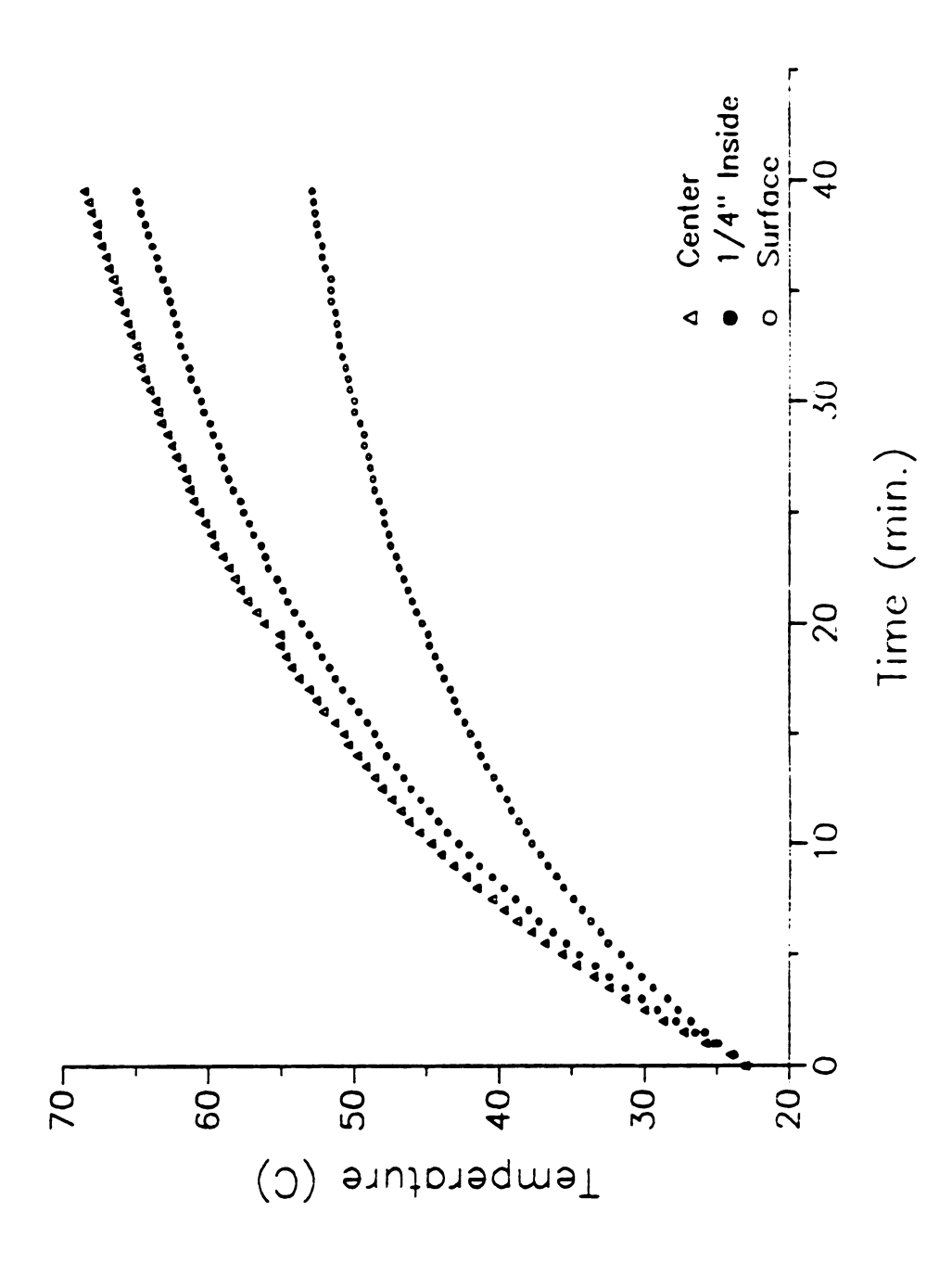


Figure 3.29 Temperature Profile Of One Inch Nylon Rod Versus Time For 5 W Input Power

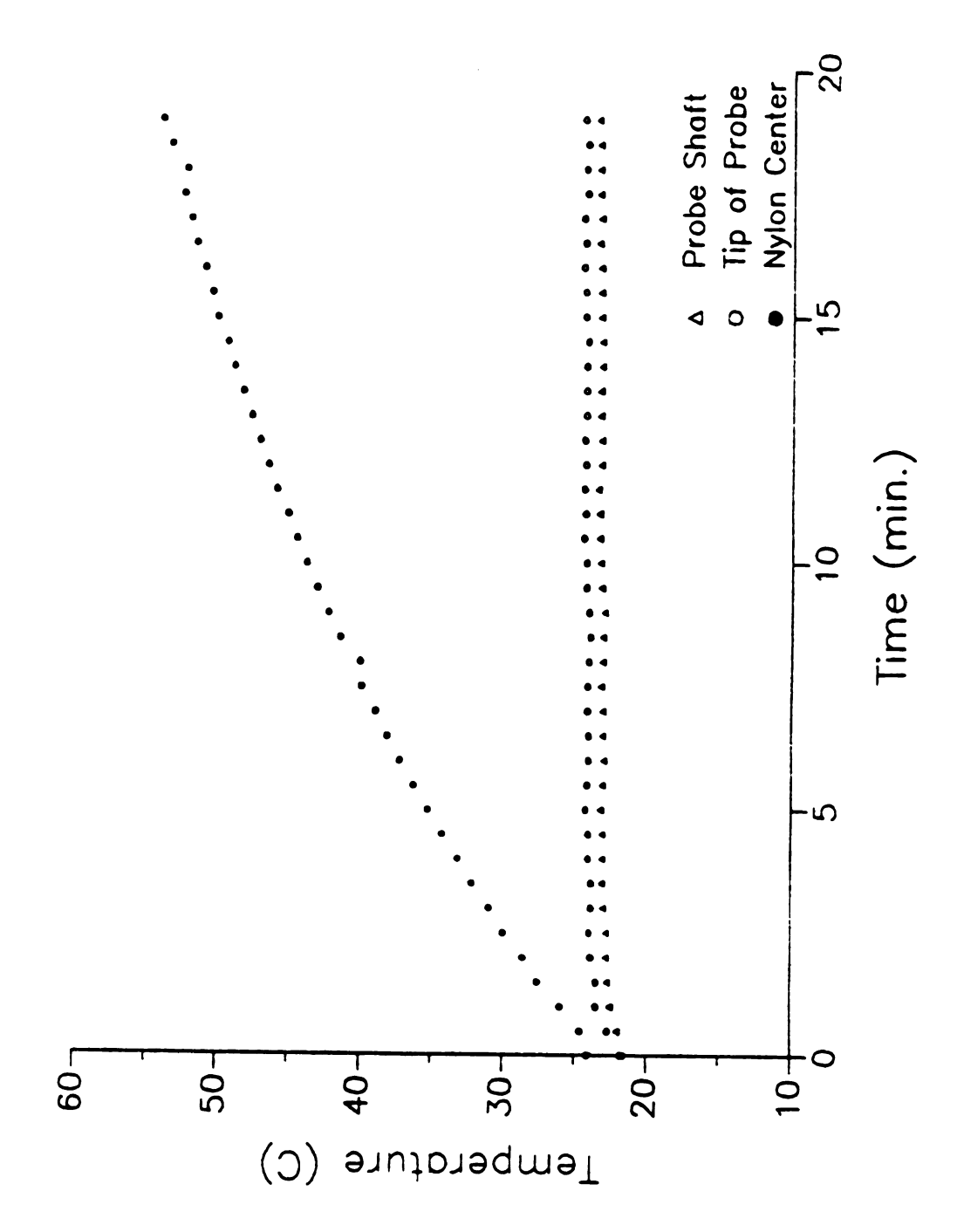
of the surface is 53.9 $^{\circ}$ C, a difference of 14.6 $^{\circ}$ C from the center temperature.

A final experiment, consisting of measurements of the coupling probe temperature, was conducted to determine if a significant amount of power was being dissipated in the coupling probe structure. If power into the cavity were being dissipated in the coupling probe it would make energy balance analysis on materials being processed in the cavity inaccurate since mico-coaxial field probe readings would not yield accurate Q measurements.

Two temperature probes were attached to the input power coupling probe, one 2.5 mm from the tip, one 2.5 cm from the tip. A third temperature probe was put in the center of the 1 inch diameter nylon rod load as in the experiment done for Figure 3.29. Input power was 5.0 W. The results of this experiment are plotted in Figure 3.30.

Figure 3.30 shows that even in a coupling probe as small as the one used in the six inch applicator there is no significant temperature rise. The initial temperature of the coupling probe was 21.8 °C while after 19 minutes the final temperature of the tip was 24.6 °C with the shaft 2.5 cm back from the tip at 23.6 °C. In a probe of larger mass even less temperature rise would be expected for similar power coupled in. These small temperature rises indicate that there is probably not much power being dissipated in the coupling structure.

In conclusion, it is possible to carefully monitor and control heating of rod samples with high microwave coupling efficiencies using variable heating times and input powers in the six inch diagnostic cavity. It is also possible to study heating uniformity in samples using a fluoroptic probe optical temperature measurement system.



Temperature Measurement Of The Input Power Coupling Probe For 1 Inch Diameter Nylon Load At 5.0 W Figure 3.30

CHAPTER IV

A CAVITY DESIGN EXAMPLE

4.1 Overview

The considerations involved in designing a single-mode circular cylindrical microwave cavity are illustrated by reviewing the design process of a new larger 915 MHz cavity. The design considerations presented here, along with the sketching of plans and the oversight of the construction of a 915 MHz cavity were included as part of the research for this M.S. Thesis. The finished product of this design is shown in the photograph of Figure 4.6.

Like 2.45 GHz, the frequency used in the experiments presented in this thesis, 915 MHz is one of the two FCC standard heating frequencies. The primary advantage of using the 915 MHz excitation frequency is that it will allow larger cavity volumes at single-mode resonance than a 2.45 GHz excitation will. In scaling up in size and down in frequency from 2.45 GHz, the volume of the 915 MHz cavity is approximately the volume of the 2.45 GHz cavity multiplied by the cube of the ratio of the free space wavelengths of the excitation signals. That means as a rough estimate on the dimensions of the larger cavity the radius and the cavity height may be calculated by multiplying the corresponding dimensions of the smaller cavity by \(\lambda_{larger} \text{ cavity} \) \(\lambda_{smaller} \text{ cavity} \)

The larger cavity size means that larger samples can be cured and larger plasma discharges can be achieved. Larger plasma discharges are useful in attaining higher thrust in plasma engines, or for providing an ion beam or plasma with a larger cross sectional area. For materials

processing, in addition to making the treatment of larger samples possible, it means that smaller samples may be processed more uniformly. One other benefit of larger cavity volume is that larger objects undergoing processing may be analysed more accurately by perturbation theory than if they were in a smaller cavity.

4.2 <u>Cavity Dimensions - Empty Cavity Resonances</u>

Maximization of cavity volume for a particuar mode and frequency is not possible. The cavity radius may approach infinity while the resonant length approaches a half-integer multiple of the free space wavelength. The expression for the empty cavity resonant length is given by equation 3.3. Examining this equation, it can be seen that as $r \to \infty$, $L \to q\pi/k$ for a TE_{npq} or TM_{npq} mode.

For f=915 MHz this means L_s is approximately $(q \times 6.5)$ inches for very large values of r. It is apparent then that the volume may increase indefinitely. At these large r values, however, the resonance would not be single-mode. All of the non cut-off modes would be crowded together around the asymptotic value of L_s .

Where the modes lie with regard to L_s is in fact the most important consideration when determining the cavity dimensions. If several modes have nearly the same empty cavity resonant length then the cavity is no longer a good single-mode cavity. While processing near this mode cluster more than one mode may be involved in the heating and it may be impossible to determine which mode is doing the primary heating or how the heating is divided between the modes. The ability to control and understand the processing is then lost. On the other hand, if the modes are too far apart more work is involved in retuning the cavity for a new mode, and,

more importantly, unless the cavity length is adjustable over a very wide range, there will be only a few modes available for use. These would be the lower order ${^{TE}}_{111}$, ${^{TM}}_{011}$, and the ${^{TE}}_{211}$ modes. The higher order double-lobed ${^{TE}}_{np2}$ or ${^{TM}}_{np2}$ modes would be at eigenlengths too large to reach.

One consideration, although not as important as the first one, is that the ratio of the cavity surface area to the cavity volume be minimized. This is because cavity Q values are roughly proportional to some power of the inverse of this ratio. Q is a measure of the ratio of stored energy in the cavity to the power dissipated in the walls for a given frequency, and is defined by equation 3.4. A higher Q means that the fields inside the cavity are stronger per unit of cavity input power.

Since L_g and r are related by equation 3.3, one may attempt to minimize the ratio of the cavity surface area to the cavity volume, A/V, for a particular mode by taking the derivative of A/V with respect to r with equation 3.3 as a constraint. This would yield an r_{min} and corresponding eigenlength for the minimal A/V for a particular mode. It is important to note that A/V would be minimal for only one mode.

The cavity surface area, cavity volume and the ratio of the surface area to the volume are given below in equations 4.2.

$$A = 2\pi r^{2} + 2\pi r L_{s} \qquad V = \pi r^{2} L_{s}$$

$$A/V = (2/L_{s}) + (2/r)$$
(4.2)

Taking the derivative of the ratio of cavity surface area to cavity volume with respect to the cavity radius gives

$$d(A/V)dr = (-2/L_g^2)dL_g/dr + (-2/r^2)$$
 (4.3)

where dL_s/dr is obtained using equation 3.3. Setting the derivative of A/V with respect to r to zero gives us a value for r which is above the cutoff radius.

$$r = (X_{np}/k)[(X_{np}/q\pi)^2 + 1]^{\frac{1}{2}}$$
 (4.4)

This is, however, a maximum for A/V instead of a minimum. Since the derivative of A/V has no other roots for which r is positive or finite there is no way to minimize A/V subject to the constraint of equation 3.3. Fortunately it is not necessary to do so.

Therefore only the consideration concerning the spacing of the modes is conclusive and it is sufficient to base the cavity dimensions on desired mode spacings. Since the well tested seven inch cavity modes are properly spaced, an upscaling of the diameter of the seven inch cavity by a factor of 2.45 GHz/915 MHz = 2.68, or to a value of 18.7 inches, should provide adequate mode spacings for the 915 MHz cavity. The following Figures 4.1, 4.2, and 4.3 are plots of the resonant frequency of several modes versus their eigenlengths, L_S, for cavity radii of 17, 18, and 19 inches. This is a plot of equation 3.3 for each mode. 915 MHz has been highlighted and appears as a horizontal line through 915 MHz on the ordinate. Where this line intersects the plot of the mode is the eigenlength for that mode at 915 MHz.

For Figures 4.1 and 4.3 not all the modes in the space are represented, some of the modes at 915 MHz with $L_{_{\rm S}}$ above 50 cm being omitted. Comparison can be made with Figure 4.2 for a cavity diameter of 18 inches in which all of the modes in the space have been included.

It can be seen that, in general, as the radius gets larger the eigenlength gets smaller. As is evident by examining equation 3.3 and

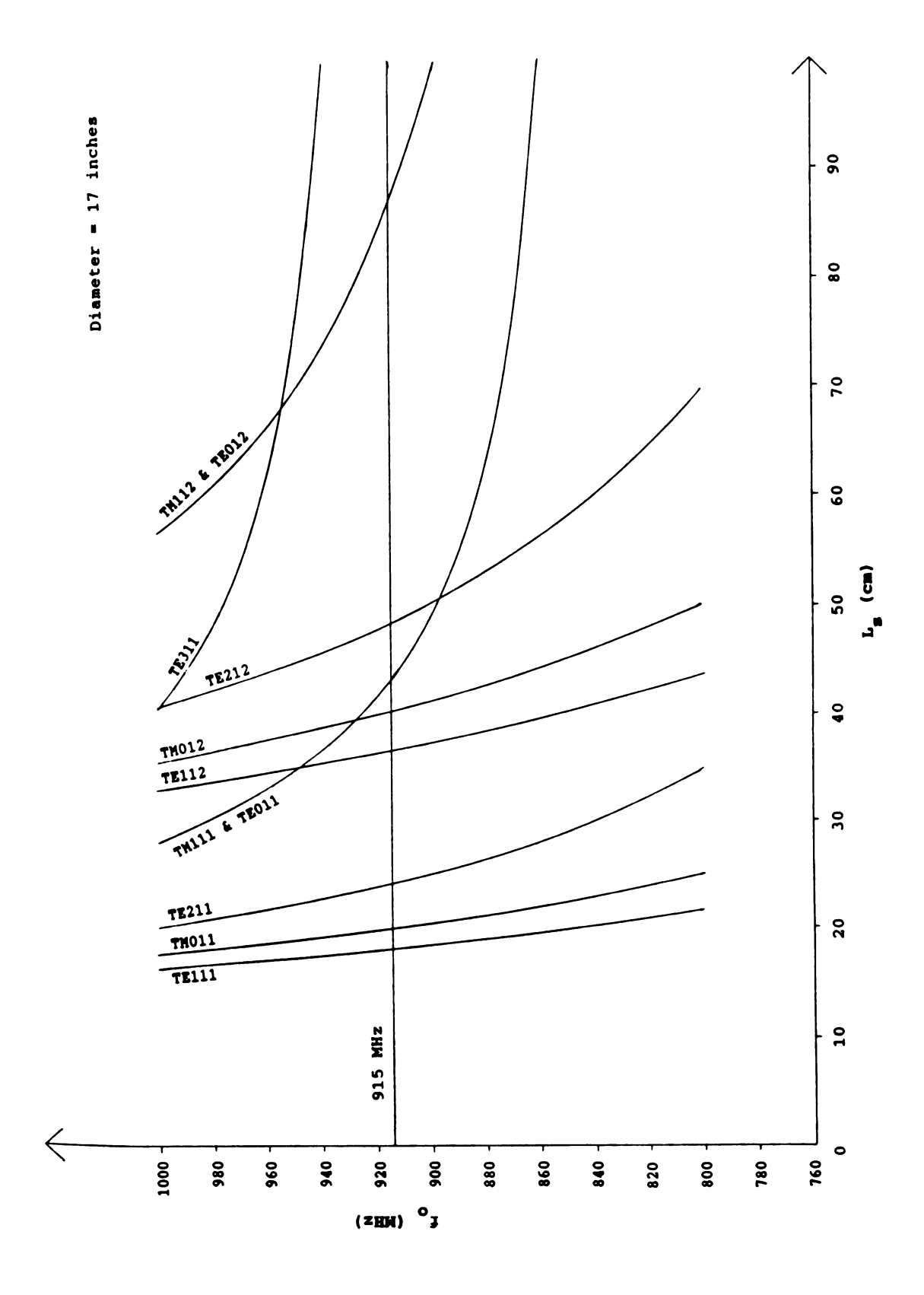


Figure 4.1 Mode Chart For 17" Diameter Cavity

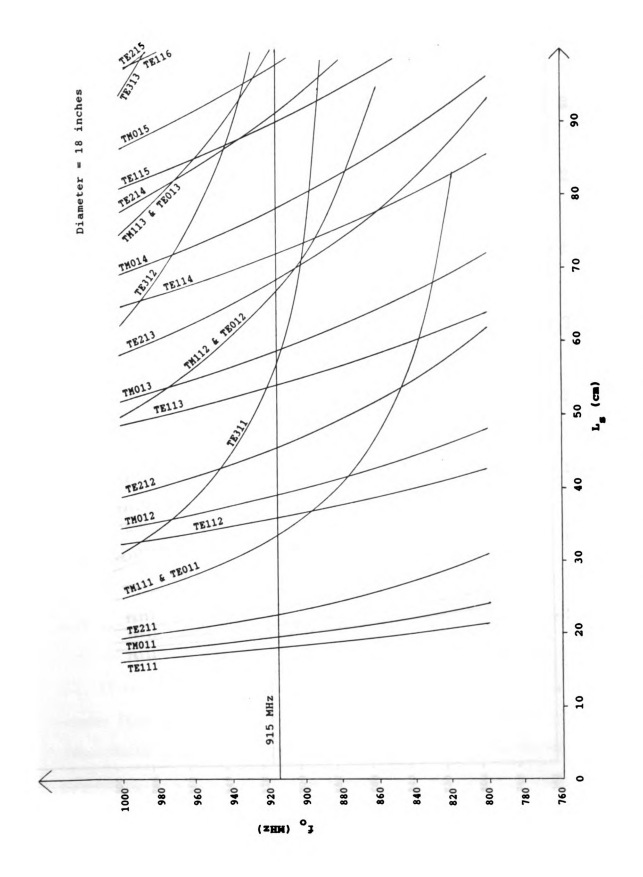


Figure 4.2 Mode Chart For 18" Diameter Cavity

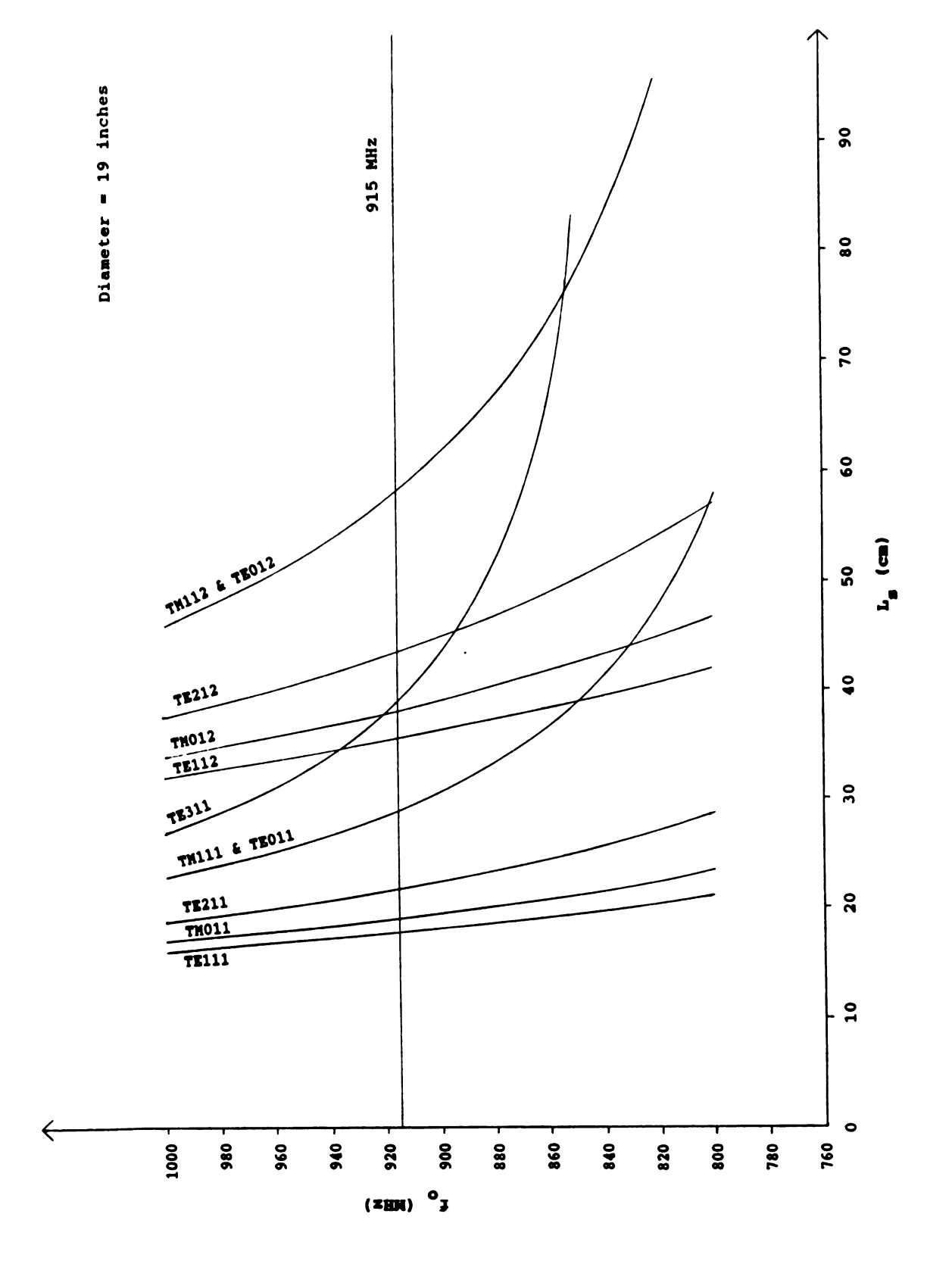


Figure 4.3 Mode Chart For 19" Diameter Cavity

these figures, the relationship of the radius to the eigenlength is by no means linear. Furthermore, it is very mode dependent. Notice in particular the dramatic sweep downward of the ${\rm TE}_{311}$ mode as the radius increases. Compare this with the stability of the ${\rm TE}_{111}$ mode.

For each of the three cavity radii of Figures 4.1, 4.2, and 4.3 each mode, apart from the degenerate TM_{111} - TE_{011} mode, has its own unique eigenlength. Hence there is no 915 MHz empty cavity degeneracy inherent in cavities of these radii. For heating in only single-mode resonance, that is good. For degenerate mode heating it will be necessary to use either the TM_{111} - TE_{011} mode or change the excitation frequency.

A problem remains in designing for degenerate mode heating. Although a degeneracy may occur in the empty cavity for a given frequency, when the cavity is loaded the degeneracy may become uncoupled in the presence of the load material. Or, it may happen that new degeneracies appear in the loaded cavity case whereas they were absent in the empty cavity. This sort of heating, then, will be highly dependent on the individual experimental conditions, specifically the loading material shapes, sizes, and dielectric properties, and where in the cavity the material is located.

4.3 Cavity Materials

Having decided approximately what the ideal cavity dimensions should be, it now becomes a question of how to construct such a cavity. This means finding comercially available parts and pieces of the proper size from which to build the applicator, since it is too expensive and time consuming to start building the cavity from unmachined solid raw materials. First of all, then, it is necessary to determine what sort of metals are allowable building materials for this application.

The most commonly used metals for electomagnetic wave-guide applications are copper, aluminum, and brass. All three are very good conductors and have other desirable properties. Copper and brass are easy to work with and aluminum weighs very little. They are available in a variety of forms. They are also only mildly corrosive.

The difficulty with these materials is finding them in the form of tubing or pipe with inner diameter anywhere near 18 inches. Since most industrial applications which require copper tubing are for the transmission of water or natural gas, it generally comes in much smaller sizes. Furthermore, copper is very soft and will not easily retain its shape at such a radius if there is any strain on it. Since the cavity bears a rather heavy L adjustment mechanism on top, this problem could be significant. Copper is also extremely heavy and is expensive. For these reasons it was not considered.

Brass, in addition to being a good conductor, is non-paramagnetic, non-corrosive, sturdier than copper, and is easily machineable. Furthermore, experience in using it on the seven inch cavity has demonstrated its viability. However, it is nearly as heavy as copper, heavier than iron, and it is not commercially available in the large diameter required for the 915 MHz applicator.

Iron tubing can be found at inner radii of the required magnitude.

Iron, however, presents several difficulties which rule it out as a possibility. First of all is its weight. The finished cavity, if made from iron, would weigh several hundred pounds. Secondly, iron rusts very readily and would require constant care to maintain the cavity as a high Q

device. Finally, most iron is paramagnetic and therefore would present problems in case magnets were used as a part of an experiment with the cavity. For instance, if a plasma discharge were contained by an array of permanent magnets, the presence of the magnetic material would magnetize the cavity walls, altering the magnetic field patterns to an even greater extent than the permanent magnets by themselves would.

Stainless steel is also a consideration. It is commercially available in the right form, but it is just as heavy as iron, it is not as good a conductor as any of the other materials considered here, and it is prohibitively expensive.

That leaves aluminum. Fortunately, aluminum proves to be available in the right form. Some standard wave-guide, used for transmission of microwave power to the top of radio antennas, was purchased. Its inner diameter is 18 inches. All things considered, aluminum is probably the best material for the application. Its light weight is a great advantage. This advantage offsets to some extent the problem that might arise in having things welded to the aluminum cavity walls since not all machine shops are equipped to weld aluminum.

Table 4.1 assimilates the information on building materials given above.

4.4 Cavity Description

It is assumed that the top shorting plate is adjustable. This plate is similar to earlier descriptions in section 3.2 for the 2.45 GHz case and is not really a design parameter because there are very few ways to build it. The following things, however, are amenable to design changes.

	Copper	Aluminum	Iron	Stainless Steel	Brass
Resistivity (A-cm)	1.7	2.8	9.5	89.8	6.6
Density (gm/ccm)	8.9	2.7	7.8	7.9	8.5
Corrosiveness	moderate	moderate	high	none	moderate
Rigity	low	moderate	high	high	moderate
Cost	high	moderate	low	very high	moderate
Paramagnetic	no	no	yes	no	no
Commercially Available in proper size	no	yes	yes	yes	no

Table 4.1 Summary Of Cavity Material Properties

4.4.1 Removeable Bottom

If it is desired to process slabs of material as they sit on the cavity bottom, or if very large materials need to be introduced into the cavity without removing the sliding short at the top, then it is necessary to design the cavity bottom to be removeable. An example of such a design is shown in Figure 4.4.

The bottom is in the shape of a disk with the central portion raised to fit up inside the cavity. It must make good electrical contact with the cavity walls. This may be accomplished by the use of finger-stock (1) as on the sliding short.

The blocks (2) on the outside of the cavity contain holes through which screws may be put to fasten the cavity bottom to the rest of the cavity. The top portion of the cavity, which includes the walls, needs to be suspended in some way. The cavity bottom and material to be processed (3) can then be lifted up to fit into the walls using a lab jack (4).

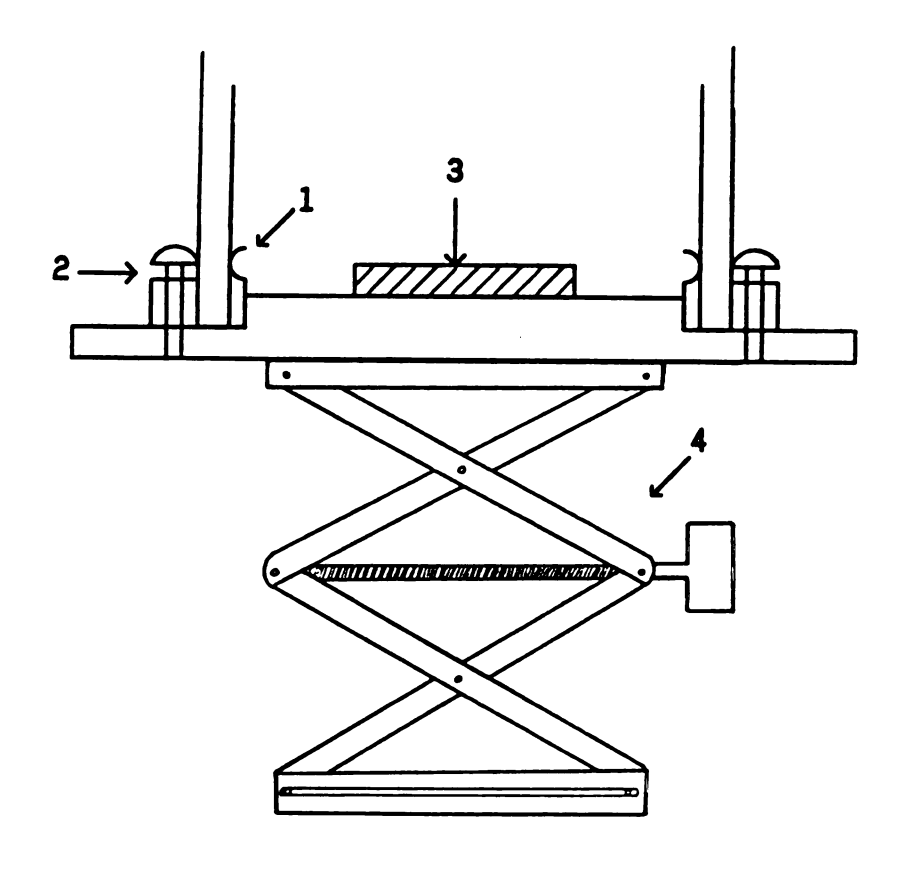


Figure 4.4 Removeable Bottom Shorting Plate

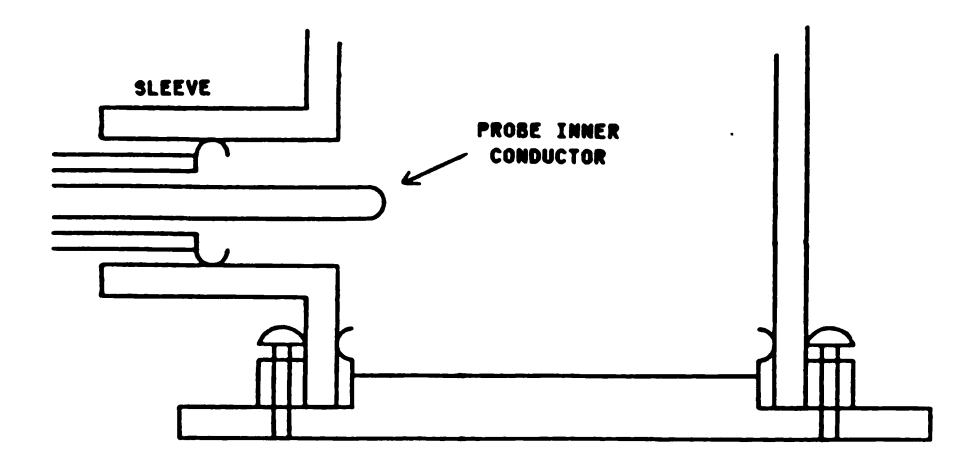


Figure 4.5 Input Port And Coupling Probe

4.4.2 <u>Input Ports And Power Coupling Probes</u>

In order to get microwave power into the cavity it is necessary to have a coupling port in the cavity wall through which the coaxial input probe is inserted. Figure 4.5 is a sketch of the input coupling port with the probe inserted. The port consists of a sleeve on the outside of the cavity which butts up to a hole in the cavity wall. This sleeve provides mechanical support for the probe while allowing the outer conductor of the coaxial probe to maintain contact with the port as the inner conductor penetration depth is adjusted. This configuration also allows the coupling probe to be removed from the port altogether and prevents power from being coupled out of an empty port when power is input through a port located elsewhere on the cavity.

The location of the input ports is very important. If the port is located at a position on the cavity wall where the normal electric field for a particular mode is zero, it will be very difficult to excite that mode with a probe in that port. If the probe is located at a place of very high normal electric field for a mode, the best coupling to the cavity mode is achieved. Since all the modes have different field configurations, any one place is not optimum for all modes, but a fairly good compromise is to place the input port about one quarter of a waveguide wavelength up from the cavity bottom.

There is also the question of how many ports to have. One port is probably sufficient to excite and match all the desired modes. However, with some discharge loads perfect matching cannot be achieved with the iterative variation of sliding short and coupling probe. Therefore it is desireable to have two ports, one slightly above one-quarter of a wavelength from the bottom, and one slightly below the one-quarter

wavelength mark. That way if excitation and matching from one port are not achieved, a match may be obtained with excitation from the other port. If two modes are to be excited at once, or if it is desired to attempt to circularly polarize the fields inside the cavity, i.e. excite two modes of the same kind 90 out of phase, then two ports will be needed. For the circularly polarized case, the ports will have to be 90 apart and at the same level.

The input probe dimensions will determine the size of the ports. Two considerations are in order with regard to input probe dimensions. First is the characteristic impedance of the coaxial probe. The probe characteristic impedance needs to be such as to match the coaxial feed from the power source. This is generally 50Ω . The characteristic impedance of a coaxial transmission line is given by

$$Z_{o} = \frac{\eta}{2\pi} \ln(b/a) \tag{4.5}$$

where η is the wave impedance in the media between the inner and outer conductors, $376.72\,\Omega$ in free space, b is the inner diameter of the outer conductor, and a is the diameter of the inner conductor. In order to have a $50\,\Omega$ characteristic impedance when the media between the inner and outer conductors is free space, the ratio of the radius of the inner conductor of the probe to the inner radius of the outer conductor must be 2.30.

The second consideration is the amount of power that will be transmitted through the probe. The heat dissipated in a coaxial transmission line is proportional to the attenuation constant of the transmission line. ⁵⁶ For a coaxial cable, the attenuation constant is

Α,

proportional to the square root of the frequency of the transmitted power and inversely proportional to the diameter of the coaxial cable. 57

Therefore, a coaxial transmission line of given diameter can transmit 1.64 times as much power at 915 MHz as at 2.45 GHz. An outer conductor diameter of 7/8 inch is sufficient to transmit a kilowatt average power at 2.45 GHz without causing undue heating of the probe components. 58 For the 915 MHz cavity an equal probe size permits powers of 1700 W to be transmitted to the cavity. Arcing in the 7/8 inch diameter coaxial line does not occur until peak powers of 44 kW have been achieved. 59 For actual power transmission, the cable leading from the power source to the cavity may be the limiting factor on power transmission. If powers of 1.7 kW are transmitted to the 915 MHz cavity, the connecting cable will have to be at least 7/8 inch in diameter.

4.4.3 Observation Windows

Finally, it may be desirable to include in the design an observation window in the cavity wall. A window of large enough size to make observation possible will have to be covered with screen to prevent radiation from leaking through the window. A window of 5 or 6 inches square covered by a conducting screen with a grid of 10 squares to the inch of 24 guage wire is sufficient to meet those requirements.

4.5 Finished Cavity

As was stated in section 4.1, the object of these design considerations was to construct an actual 915 MHz single-mode resonant applicator. A photograph of the finished cavity is shown in Figure 4.6.

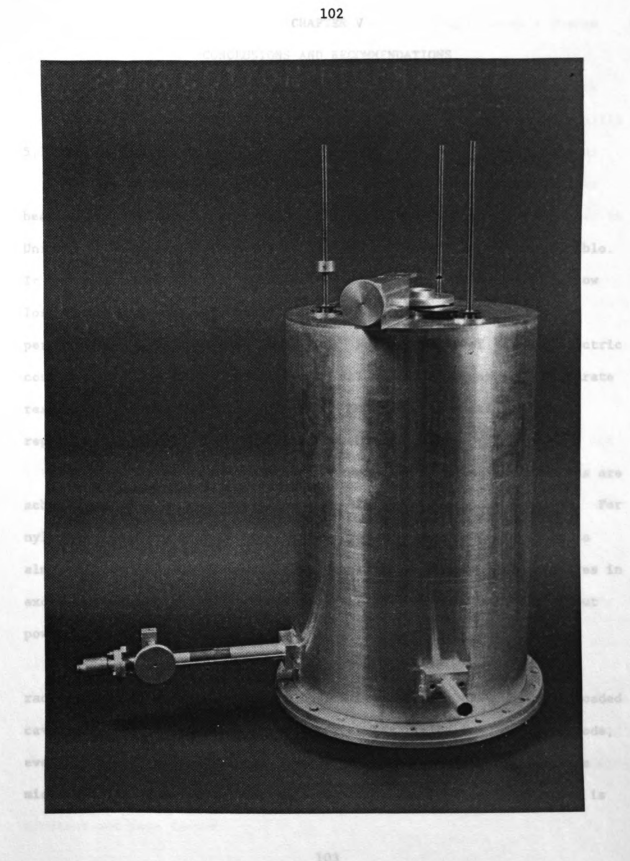


Figure 4.6 Photograph Of The 915 MHz Cavity

CHAPTER V

CONCLUSIONS AND RECOMMENDATIONS

5.1 Conclusions

The experiments presented in this thesis have demonstrated that heating and on-line diagnosis of materials in the Michigan State

University single-mode circular cylindrical resonant cavity are possible.

It has been shown that for materials of low dielectric constant and low loss factor perturbation theory can be used to accurately measure the permittivity as the material is heated. For materials of large dielectric constant and loss factor, perturbation calculations do not yield accurate results for permittivity measurements. However, the heating cycle is repeatable and controlable for these materials.

These experiments have also shown that high coupling efficiencies are achievable, even to relatively low loss dielectrics such as nylon 66. For nylon 66, coupling efficiencies ranged from 40% at room temperature to almost 95% at 165 °C. Wet wood (35% water) shows coupling efficiencies in excess of 90% and specific consumptions of 1.1 kWh/kg with 8 W of input power.

Experiments in the six inch diagnostic cavity demonstrated that radial electric field patterns at the cavity wall for the coaxially loaded cavity are axially similar to the empty cavity fields for the TM₀₁₂ mode, even for one inch diameter rod loads of nylon 66. This means that the micro-coaxial field probe Q measurement technique developed by Rogers is

viable for these load types as long as the cavity length doesn't change appreciably when the load is introduced.

Other low power experiments in the six inch diagnostic cavity show that coaxially loaded rods of one inch diameter nylon 66 are heated fairly uniformly out to one-quarter of an inch from the center while the outer portions of the rod are cooler. It was also shown that the input power coupling probe does not heat up significantly for the power levels used in the experiments reported here. Thus the power loss to the coupling structure was small compared to the power coupled to the material load.

5.2 Recommendations

The chief recommendation to arise in the course of these experiments concerns the matter of an adequate theory to calculate the dielectric constant and loss factor of materials with large dielectric constants and loss factors in the resonant cavity. As discussed in Chapter II, perturbation calculations of high complex permitivities of materials in cavities have been made using calibrating materials to normalize the resonant frequency shift and quality factor for large perturbations. 18,21-22 This method is not accurate when the permittivity of the material load is much different from the permittivity of the calibration material. This problem is especially great for materials whose dielectric properties change substantially during the heating cycle. Futhermore, the calibration method relies on other methods for determining the permittivity of the calibrating material and cannot be used as a standalone measurement of permittivities of materials of high dielectric constant and loss factor.

If the explanation of the behavior seen in Figure 3.15 is correct, it does not seem as if an exact soultion which does not consider the effect of the coupling probe will yield much better results than perturbation theory for loads placed near the coupling probe. This problem may be overcome by positioning loads in the upper half of the cavity, away from the coupling probe. Another solution might be to account for the presence of the probe using perturbation theory. A correction factor could then be added to perturbation or exact analysis to yield better results. Finally, an exact theory which takes the presence of the coupling probe into account could be formulated. An exact analysis including the effects of the coupling probe is, however, a formidable problem.

A second recommendation has to do with the stability of the microwave power source. For careful measurements of frequency shift, and for input power stability, a phase-locked loop system or a synthesized microwave power source would be useful. If power levels need to be adjusted during the course of an experiment, the frequency may shift slightly with the present system. Also long term stability is needed in order that the frequency not drift with time.

For high power experiments the signal would need to be amplified. In that case, the amplifier would need to amplify the power without adding much noise to the signal. A noisy amplifier would negate the benefit of the frequency stability. For experiments performed to confirm the results of the work recommended above, a stable source would be especially useful.

APPENDIX A

DERIVATION OF A PERTURBATION FORMULA FOR CALCULATING
THE DIELECTRIC CONSTANT OF A ROD COAXIALLY SUSPENDED
IN A CIRCULAR CYLINDRICAL RESONANT CAVITY EXCITED IN THE TMODE

Given a resonant cavity filled with a dielectric material of dielectric constant E it can be shown that its resonant frequency differs from the empty cavity resonant frequency according to the relationship

$$\frac{\mathbf{f}_o - \mathbf{f}}{\mathbf{f}} = \frac{\int_{\mathbf{v}} \mathbf{\Delta} \boldsymbol{\epsilon} \, \mathbf{E} \cdot \, \mathbf{E}_o^* \, d\mathbf{v}}{\int_{\mathbf{v}} \left[\mu_o \, \mathbf{H} \cdot \, \mathbf{H}_o^* + \boldsymbol{\epsilon}_o \, \mathbf{E} \cdot \, \mathbf{E}_o^* \, \right] \, d\mathbf{v}}$$
(A.1)

where E and H are the fields in the dielectric filled cavity, E_o and H_o are the fields in the empty cavity, ϵ_o is the free space dielectric constant which is equal to 8.85418 x 10⁻¹⁴ F/cm, and $\Delta \epsilon = \epsilon - \epsilon_o$. 60

For a partially filled cavity, A \(\) is a function of space, being zero for areas outside the dielectric and a constant inside the dielectric for a homogeneous material. Also, at resonance, the denominator on the right hand side of the equation can be expressed by either the electric fields alone or the magnetic fields alone since the energy is divided equally between them. To simplify the calculations, the E field term is doubled while the H field term is neglected. The field in the dielectric in the denominator can be approximated by the empty cavity field. This gives

$$\frac{\mathbf{f_0} - \mathbf{f}}{\mathbf{f}} = \frac{\int_{\mathbf{v}'} \Delta \in_{\mathbf{r}} \mathbf{E} \cdot \mathbf{E_0}^* d\mathbf{v}'}{\int_{\mathbf{v}} 2 |\mathbf{E_0}|^2 d\mathbf{v}}$$
(A.2)

where v' is the space occupied by the dielectric material and $\Delta \in r^{-\Delta \xi/\xi_0}$.

For the cavity partially filled with a rod shaped material, E in the numerator is approximated at resonance by the relationship that obtains for a dielectic rod in a static field. This is referred to as a quasi-static approximation. If the length of the rod is large compared with the diameter, or, if the ends of the rod are in a region of low electric field inside the cavity, the end effects of the rod can be neglected. The z component of E, E, is approximated by the z component of E, E_0 , and the radial component of E, E, is given by

$$E_r \approx 2E_{or}/(1+\epsilon_r). \tag{A.3}$$

For the case that the dielectric material is lossy, f, f_o , and ϵ_r are replaced as follows:

$$f \longrightarrow f + jf/2Q$$
 (A.5)

$$f_0 \longrightarrow f_0 + jf /2Q_0$$
 (A.6)

$$\epsilon_r \longrightarrow \epsilon_r' - j\epsilon_r"$$
 (A.7)

where Q is the quality factor of the cavity system with the material inside, and Q_0 is the empty cavity quality factor. $\in_{\mathbf{r}}$ and $\in_{\mathbf{r}}$ are the real and imaginary parts of the dielectric constant respectively.

Finally the field equations for the TM_{0pq} modes are needed for substitution into equation A.2. They are given by equations A.8 as

$$E_{r} = \frac{-2\pi \chi_{0p} J_{o}'(X_{0p} r/a) \sin(q\pi z/L_{s})}{j \ 2\pi f \epsilon_{o} a L_{s}}$$
(A.8a)

$$\mathbf{E}_{\mathbf{p}} = \mathbf{0} \tag{A.8b}$$

$$E_{z} = \frac{(X_{0p})^{2} J_{o}(X_{0p} r/a) \cos(q\pi z/L_{s})}{j 2\pi f \in a^{2}}$$
 (A.8c)

where a is the cavity radius, L_s is the cavity eigenlength, and X_{0p} is the pth zero of the zeroth order Bessel function of the first kind.

Substituting the quasi-static approximations to the actual field inside the dielectric, the transformations to the lossy case, and the field equations for TM_{0pq} modes into equation A.2, equations A.9 and A.10 for ϵ_r ' and ϵ_r " are obtained as given below:

$$\frac{f - f_{o}}{f} = \frac{(1 - \epsilon_{r}') \int_{\mathbf{v}'} |\mathbf{E}_{oz}|^{2} d\mathbf{v}' + \frac{1 - \epsilon_{r}'^{2} - \epsilon_{r}''^{2}}{(1 + \epsilon_{r}')^{2} + \epsilon_{r}''^{2}} \int_{\mathbf{v}'} |\mathbf{E}_{or}|^{2} d\mathbf{v}'}{2 \int_{\mathbf{v}} |\mathbf{E}_{o}|^{2} d\mathbf{v}}$$
(A.9)

$$\frac{\epsilon_{\mathbf{r}} \int_{\mathbf{v}'} |\mathbf{E}_{oz}|^{2} d\mathbf{v}' + \frac{4\epsilon_{\mathbf{r}}}{(1+\epsilon_{\mathbf{r}}')^{2}+\epsilon_{\mathbf{r}}^{2}} \int_{\mathbf{v}'} |\mathbf{E}_{or}|^{2} d\mathbf{v}'}{\int_{\mathbf{v}} |\mathbf{E}_{o}|^{2} d\mathbf{v}}$$

$$(A.10)$$

where the integrals are given by

$$\int_{\mathbf{V}'} |\mathbf{E}_{oz}|^{2} d\mathbf{V}' = \frac{\mathbf{c}^{2} (X_{0p}/a)^{4} [J_{o}^{2} (X_{0p} \mathbf{c}/a) + J_{1}^{2} (X_{0p} \mathbf{c}/a)]}{8\pi \mathbf{f}^{2} \epsilon_{o}} \times [\mathbf{d} + (\mathbf{L}_{s}/q\pi) \cos(2q\pi h/\mathbf{L}_{s}) \sin(q\pi d/\mathbf{L}_{s})]$$
(A.11)

$$\int_{\mathbf{v'}} \left| \mathbf{E}_{or} \right|^2 d\mathbf{v'} = \frac{\pi(qc) \left[\mathbf{J_o^2} \left(\mathbf{X_{0p} c/a} \right) + \mathbf{J_1^2} \left(\mathbf{X_{0p} c/a} \right) - (2a/\mathbf{X_{0p} c}) \mathbf{J_1} \left(\mathbf{X_{0p} c/a} \right) \mathbf{J_0} \left(\mathbf{X_{0p} c/a} \right) \right]}{8 \left(\mathbf{f} \in_{\mathbf{o}} \mathbf{L_s} \mathbf{a} \right)^2}$$

$$\times X_{0p}^{2} \left[d - (L_{s}/q\pi) \cos(2q\pi h/L_{s}) \sin(q\pi d/L_{s}) \right]$$
(A.12)

$$\int_{\mathbf{v}} |\mathbf{E}_{o}|^{2} dv = \frac{X_{0p}^{2} J_{1}^{2} (X_{0p}) [(X_{0p}/a)^{2} L_{s} + (\pi q)^{2}/L_{s}]}{8\pi f^{2} \epsilon_{o}^{2}}$$
(A.13)

where c is the radius of the rod, d is the length of the rod, and h is the height of the center of the rod above the cavity floor.

In most cases the second term in the numerators of equations A.9 and A.10 can be neglected. Even for the case of the rod running the entire length of the cavity with a ratio of rod radius to cavity radius of 1:6 the second term is on the order of 10^{-2} of the first term. If the ratio of the integral of $|\mathbf{E}_0|^2$ over the cavity volume to the integral of $|\mathbf{E}_{0z}|^2$ over the dielectric volume is given by some constant R, then the complex permittivity can be expressed explicitly by equations A.14 and A.15.

$$\epsilon_{r}' = 1 + \frac{2R (f_0 - f)}{f}$$
 (A.14)

$$\epsilon_r$$
" = R (1/Q - 1/Q₀) (A.15)

with R =
$$\frac{\int_{v} |E_{o}|^{2} dv}{\int_{v'} |E_{oz}|^{2} dv'} = \frac{[1 + (q\pi a/X_{0p}L_{s})^{2}] \times \frac{(a/c)^{2} J_{1}^{2}(X_{0p})}{J_{o}^{2}(X_{0p}c/a) + J_{1}^{2}(X_{0p}c/a)}}{(d/L_{s}) + (1/q\pi)\cos(2q\pi h/L_{s})\sin(q\pi d/L_{s})}$$

(A.16)

It is useful to have the Bessel functions J_0 and J_1 tabulated for some common arguments for use in these equations. Since the experiments in this thesis were performed using rods of radii 0.55, 0.5, 0.25, 0.225, and 0.125 inches in cavities of both 3 and 3.5 inch radii using TM_{01q} modes, the Bessel functions appropriate to the various combinations of cavity and rod radii are tabulated below in Table A.1.

$$J_0(X_{01} \text{ c/a}) \text{ and } J_1(X_{01} \text{ c/a})$$

$$X_{01} = 2.4048255577$$

$$J_1(X_{01}) = 0.51914750$$

1,01, -0.31,14,30	
7 inch Cavity (a-3.5")	6 inch Cavity (a-3")
c - 0.125"	c - 0.125"
$J_0 = 0.99815672$ $J_1 = 4.29037292 \times 10^{-2}$	$J_0 = 0.99749151$ $J_1 = 5.00376805 \times 10^{-2}$
c = 0.225"	c - 0.25"
$J_0 = 0.99907049$ $J_1 = 3.04181796 \times 10^{-2}$	$J_0 = 0.98998492$ $J_1 = 9.96988835 \times 10^{-2}$
c - 0.25 cm	c - 0.5"
$J_0 = 0.99263708$ $J_1 = 8.55702443 \times 10^{-2}$	$J_0 = 0.96024042$ $J_1 = 0.19640480$
c = 0.55 cm	
$J_0 = 0.99447378$ $J_1 = 7.41843494 \times 10^{-2}$	

Table A.1 Values of Bessel Functions Used in the Perturbation Equations for Experiments Presented in This Thesis

REFERENCES

- [1] J. Rogers, Ph.D. dissertation, Michigan State University, 1982.
- [2] Jes Asmussen, Jr., Raghuveer Mallavarpu, John R. Hamann, and Hee Chung Park, "The Design of a Microwave Plasma Cavity," Proc. IEEE, 62(1) January 1974, pp.109-117.
- [3] R. M. Fredricks and J. Asmussen, Jr., "High Density Resonantly Sustained Plasma in a Variable-Length Cylindrical Cavity," Applied Physics Letters, 19(12) December 1971, pp.508-510.
- [4] S. Whitehair, J. Asmussen, S. Nakanishi, "Microwave Electrothermal Thruster Performance in Helium Gas," J. Propulsion and Power, 3(2) March-April 1987, pp.136-144.
- [5] Joseph Root and Jes Asmussen, "Experimental Performance of a Microwave Cavity Plasma Disk Ion Source," Rev. Sci. Instrum., 56(8) August 1985, pp.1511-1519.
- [6] T. Roppel, D. K. Reinhard, and J. Asmussen, "Low Temperature Oxidation of Silicon Using a Microwave Plasma Disk Source," J. Vac. Sci. Technol. B, 4(1) Jan./Feb. 1986, pp.295-298.
- [7] J. Hopwood, M. Dahimene, D. K. Reinhard, and J. Asmussen, "Plasma Etching With a Microwave Cavity Plasma Disk Source," J. Vac. Sci. Technol. B, 6(1) Jan./Feb. 1988, pp.268-271.
- [8] L. Mahoney, M. Dahimene, and J. Asmussen, "Low Power, 3.2 cm, Efficient Microwave Electron Cyclotron Resonant Ion Source," Rev. Sci. Instrum., 59(3) March 1988, pp.448-452.
- [9] J. Asmussen, H. H. Lin, B. Manring, and R. Fritz, "Single-mode or Controlled Multimode Microwave Cavity Applicators for Precision Materials Processing," Rev. Sci. Instrum., 58(8) August 1987, pp.1477-1486.
- [10] Jinder Jow, Martin Halley, Mark Finzel, Jes Asmussen, Jr., Haw-Hwa Lin, and Ben Manring, "Microwave Processing and Diagnosis of Chemically Reacting Materials in a Single-Mode Cavity Applicator," IEEE Trans.

 Microwave Theory Tech., MTT-35(12) December 1987, pp.1435-1443.
- [11] George H. Brown, Cyril N. Hoyler, and Rudolph A. Bierwirth, <u>Theory And Application of Radio Frequency Heating</u>, D. Van Nostrand Company, 1947, p.iii.
- [12] ibid. pp.234, 307, 328.
- [13] E. F. Labuda and R. C. LeCraw, "New Technique for Measurement of Microwave Dielectric Constants," Rev. Sci. Instrum., 32(4) April 1961, pp.391-392.
- [14] Norman L. Conger and Shao E. Tung, "Measurement of Dielectric Constant and Loss Factor of Powder Materials in the Microwave Region," Rev. Sci. Instrum., 38(3) March 1967, pp.384-386.
- [15] H. Altschuler, "Dielectric Constant," Handbook of Microwave Measurements, Vol. 2, M. Sucher, J. Fox ed., Brooklyn, N.Y., Polytechnic Press, 1963, quoted in Rzepecka, cited below.
- [16] Maria A Rzepecka, "A Cavity Perturbation Method for Routine Permittivity Measurement," J. Microwave Power, 8(1) 1973, pp.3-11.
- [17] D. Couderc, M. Giroux, and R. G. Bosisio, "Dynamic High Temperature Microwave Complex Permittivity Measurements on Samples Heated Via Microwave Absorption," J. Microwave Power, 8(1) 1973, pp.69-82.
- [18] C. Akyel, R. G. Bosisio, R. Chahine, and T. K. Bose, "Measurements of the Complex Permittivity of Food Products During Microwave Power Heating Cycles," J. Microwave Power, 18(4) 1983, pp.355-365.

- [19] Shuh-han Chao, "Measurements of Microwave Conductivity and Dielectric Constant by the Cavity Perturbation Method and Their Errors," IEEE Trans. Microwave Theory Tech., MTT-33(6) June 1985, pp.519-526.
- [20] M. E. Brodwin and M.K. Parsons, "New Approach to the Perturbation of Cavity Resonators by Homogenous Isotropic Spheres," J. Appl. Phys., vol. 36, 1980, p.272.
- [21] R. C. Jain and W. A. G. Voss, "Dielectric Properties fo Raw and Cooked Chicken Egg at 3 GHz, 23-140 C," J. Microwave Power, 22(4) 1987, pp.221-227.
- [22] P. O. Risman and N. E. Bengtsson, "Dielectric Properties of Foods at 3 GHz as Determined by a Cavity Perturbation Technique," J. Microwave Power, 6(2) 1971, pp.101-124.
- [23] P. O. Risman and Th. Ohlsson, "Brief Communication: Dielectric Constants for High Loss Materials, A Comment on Earlier Measurements," J. Microwave Power, 8(2) 1973, pp.185-188.
- [24] K. A. Wickersheim, "Fiberoptic Thermometry Based on Measurement of Fluorescent Decay Time," J. Microwave Power, 21(2) 1986, pp.105-106.
- [25] S. Shridhar and W. L. Kennedy, "Novel Technique to Measure the Microwave Response of High T Superconductors between 4.2 and 200 K," Rev. Sci. Instrum., 59(4) April 1988, pp.531-536.
- [26] D. M. Bolle, "Eigenvalues for a Centrally Loaded Circular Cylindrical Cavity," IRE Trans. Microwave Theory Tech., MTT-10(3) March 1962, pp.133-138.
- [27] Kawthar A. Zaki and Ali E. Atia, "Modes in Dielectric-Loaded Waveguides and Resonators," IEEE Trans. Microwave Theory Tech., MTT-31(12) December 1983, pp.1039-1044.
- [28] S. Vigneron and P. Guillon, "Mode Matching Method for Determination of the Resonant Frequency of a Dielectric Resonator Placed in a Metallic Box," IEEE Proc., vol. 134, Pt. H, No. 2, April 1987, pp.151-155.
- [29] G. Roussy and M. Felden, "A Sensitive Method for Measuring Complex Permittivity with a Microwave Resonator," IEEE Trans. Microwave Theory Tech., MTT-14(4) April 1966, pp.171-175.
- [30] Shihe Li, Cevdet Akyel, and Renato G. Bosisio, "Precise Calculations and Measurements on the Complex Dielectric Constant of Lossy Materials Using TM010 Cavity Perturbation Techniques," IEEE Trans. Microwave Theory Tech., MTT-29(10) October 1981, pp.1041-1047.
- [31] W. C. Hahn, "A New Method for Calculation of Cavity Resonators," J. Applied Phys., vol. 12, January 1941, p.62, quoted in Bolle, cited below.
- [32] J. Rogers and J. Asmussen, "Standing Waves Along a Microwave Generated Surface Wave Plasma," IEEE Trans. Plasma Sci., PS-10(1) March 1982, pp.11-16.
- [33] S. Burkhart, "Coaxial E-Field Probe for High Power Microwave Measurements," IEEE Trans. Microwave Theory Tech., MTT-33(3) March 1985, pp.262-265.
- [34] L. C. Maier and J. C. Slater, J. Appl. Phys. 23, 1952, p.68, quoted in Amato and Hermann cited below.
- [35] Laurent-Guy Bernier, Thomas Sphicopoulos, and Fred E. Gardiol, "An Automatic System for the Measurement of the Field Distribution in Resonant Cavities," IEEE Trans. Instrum. Meas., IM-32(4) December 1983, pp.462-466.

- [36] J. C. Amato and H. Hermann, "Improved Method for Measuring the Electric Fields in Microwave Cavity Resonators," Rev. Sci. Instrum., 56(5) May 1985, pp.696-699.
- [37] Georges Roussy, Anne Mercier, Jean-Marie Thiebaut, and Jean-Pierre Vaubourg, "Temperature Runaway of Microwave Heated Materials: Study and Control," J. Microwave Power, 20(1) 1985, pp.47-51.
- [38] Hua-Feng Huang, "Temperature Control in a Microwave Resonant Cavity System for Rapid Heating of Nylon Monofilament," J. Microwave Power, 11(4) 1976, pp.305-313.
- [39] R. F. Harrington, <u>Time-Harmonic Electromagnetic Fields</u>, McGraw-Hill Book Company, 1961, pp.214, 257.
- [40] ibid., p.29.
- [41] Rogers, op. cit., p.28.
- [42] Harrington, op. cit., p.257.
- [43] Rogers, op. cit., p.39.
- [44] Lydell L. Frasch, Ph.D. dissertation, Michigan State University, 1987.
- [45] Harrington, op. cit., p.453.
- [46] Rogers, op. cit., p.66.
- [47] ibid., pp.65-66.
- [48] Huang, op. cit., p.306.
- [49] ibid.
- [50] Harrington, op. cit., p.455.
- [51] W. R. Tinga and S. O. Nelson, "Dielectric Properties of Materials for Microwave Processing Tabulated," J. Microwave Power, 8(1) 1973, pp.3-11.
- [52] A. R. Von Hippel, <u>Dielectric Materials and Applications</u>, MIT, Cambridge, MA, 1954, p.361.
- [53] Frasch, op. cit., pp.137-152.
- [54] ibid., pp.155-157.
- [55] Harrington, op. cit., p.257.
- [56] ibid., p.66.
- [57] Pender and McIlwain, <u>Electrical Engineers Handbook</u>.

 <u>Communication-Electronics</u>, 4th Ed., 1950, pp.10.6-10.9.
- [58] Andrews Catalog, 1988
- [59] ibid.
- [60] Harrington, op. cit., p.322.

